Department of Chemical Engineering

Heat Transfer Mechanisms in an Indirectly Heated Rotary Kiln with Lifters and Its Role in Scaling

Iwan Harsono Hwan

This thesis is presented for the Degree of
Doctor of Philosophy
of
Curtin University of Technology

April 2009

Declaration

To the best of my knowledge and belief this thesis contains no material previously published by any other person except where due acknowledgment has been made.

This thesis contains no material which has been accepted for the award of any other degree or diploma in any other university.

Signature : ……

Date : ……

Dedications

To my wife, Nancy, my children, Kenzo - Keiko, my cheerleaders

Abstract

This present research aims to obtain a fundamental understanding on solid transport, solid mixing and the complex heat transfer mechanisms related to the important installed segmented lifter in an indirectly heated rotary kiln. To accomplish these objectives in a systematic manner, the experimental and modelling studies on solid transport and mixing were first carried out in pilot-scale cold kilns at Curtin University of Technology, Perth, Western Australia then followed by heat transfer study in a pilot-scale hot kiln system available at ANSAC Pty Ltd, Bunbury, Western Australia.

For design and scaling purposes, dimensional analysis was carried out. A series of experiments in cold kilns were also carried out, considering lifter design, lifter configurations, helix, a wide-range of solid and various kiln designs under different kiln operating conditions. The results showed that a flat bed depth profile can be achieved using purposely-designed segmented lifters at favourable practical low Re_ω values (less energy input to drive the kilns and more throughputs), with a low total kiln filling fraction and a high degree of axial mixing ($Pe < 50$ or $D_z = 10^{-5}$ - 10^{-3} m^2/s). This is essential to good heat transfer performance. The effects of helix, *L/D*, *Fr* and *d/D* have relatively insignificant differences on solid transport and mixing under the current experimental conditions. These findings demonstrate the unique advantages of the purposely-designed segmented lifters compared to other conventional lifters (e.g. single throughout lifters), providing important information for scaling criteria and modelling work.

A preliminary DEM simulation, as an emerging simulation tool at a particle level, confirmed that axial displacement is mainly due to the function of the folded lifter sections of the segmented lifters. The folded lifter sections push the solids towards the kiln discharge end along the bed arc length and such effect increases as Re_ω increases. This finding leads to the development of a transport model, limited to underloading regimes, to predict the average bed depth in this type of kilns. The

model predictions are in good agreement with experimental data. A set of global power-law dimensionless empirical correlations on solid transport and mixing, applicable to all three (over-, design-, underloading) regimes, were also developed based on the data obtained from our systematic experiments. The validity was tested with data presented in selected previous studies. It is found that the developed correlations are largely specific to the present lifter design and configurations.

A steady-state axial heat transfer model has also been developed for a kiln with segmented lifters. The model predicts the temperature profiles at inner heat tube, in the freeboard gas, in the bed, on the tube wall and the outer heat tube in the flue gas. The model incorporates developed solid transport and mixing correlations, as well as suitable heat transfer modes and reaction model. It takes the form of ordinary differential equations which were solved numerically. The input data necessary for the model were obtained by our own experiments and/or extracted from the literature. The model was validated by the temperature profiles obtained from the hot kiln. Among the heat transfer modes considered, it is found that the limiting step of heat transfer in the kiln is the heat transfer from covered inner kiln wall to covered bed, which is highly influenced by solid transport and mixing. Under the current experimental conditions, the typical overall heat transfer coefficient was found to be 31 - 35 $W/m^2.K$.

The present research advances the fundamental understanding on solid transport, solid mixing and the complex heat transfer mechanisms in an indirectly heated rotary kiln with segmented lifters. The obtained data and knowledge are important to improve the kiln energy efficiency, reduce kiln manufacture and operation costs and widen the kiln applications at different scales.

Due to nature of this thesis, chapter 6 is confidential for the first three-year based on a confidentiality agreement with industrial partner.

Acknowledgments

Completing a PhD is truly a marathon event and would not be possible if it is an individual task. I would not have been able to complete this journey without the tireless assistance, encouragement and contributions of the following individuals and organizations:

Associate Professor Hongwei Wu, as my supervisor, for his unstinting commitment to helping see this project through to its final completion. He provided me with direction to follow, technical support, perceptive feedback and especially for the enthusiasm which he invoked within me. Again, thank you for giving me examples how to become a truly good researcher in the academic world and caring my future career. My hope is that in future we will be able to keep regular contact and strengthen the friendship we have established here.

From the industrial partner, special thanks to Matthew Martella, Managing Director, ANZAC Pty Ltd, for providing me with pilot-scale experimental rigs. I would like to thank for his contribution for the fruitful discussions on the industrial perspective in this project. The support and assistance of Aron Abolis, Engineering Manager and Gavin de Bres, Projects Manager, ANSAC Pty Ltd during the hot kiln test is also gratefully acknowledged.

My deepest appreciation is given for those who have contributed in either the experimental, data processing and/or preliminary modelling work for both cold and hot kilns. Firstly to the Faculty and Department workshop staff, Karen Haynes, John Murray, David Collier and Michael Ellis, for help with the construction of helixes and lifters at different configurations; and modification of cold kilns. To Dr Huiling Wee, Dr Hamzah Fansuri, Syamsuddin Yani, Gunawan Wibisono and Henny Yap, who assisted in part of the lab work and/or image processing. To 4th year students under ChE49x research project units, Steven Rule, Sandi Ma, Shunyin Chng, Chin Yen Pui, Ahmad Badarani, Moiz Alibhai, Young L. Pang, Kee L. Pau, Mohd A.M.

Sabri and Tasha A. Yahya, for their assistance in the lab and image processing work, Edward Ee in the solid transport modelling work, Andrew Barycki in the DEM simulation work, Jonathan Khoo and Jonathan Chi Yong Teoh in the heat transfer modelling work and William Hendrawinata and Xiangpeng Gao in setting up the data takers.

My PhD period in the Chemical Engineering Department is one of the best times in my life, and I would like to thank all my colleagues who have shared it with me: Johan Utomo, Agus Saptoro, Dr Richard R. Gunawan and Dr Kong Vui Yip for being my partners in the academics and spiritual discussion; Shariff Ibrahim, Pradeep K. Shukla, and Nurul Widiastuti for being good partners in the laboratory; Jann Bolton and Naomi Tokisue for the administrative support.

Perth is a city with a large population of Indonesia community. Some of them have shared their best time with me: Herman Yapeter, Dani Pranoto, Uras T. Palis, Iman Faskayana, Hanny H. Tumbelaka, Johan Utomo and their families for the best cell group I ever had; Christian friends, especially Pastor Paulus Surya, at WPC in Bull Creek and my friendly neighbours at Toledo in East Victoria Park.

I must acknowledge my wife (Nancy Hendradjaja), my children (Kenzo and Keiko), Papa and Mama, my mother- and father-in-law for the strong continuous moral support, encouragement, understanding and immeasurable love during my 3.5 years of PhD study overseas. I hope I have done something which makes you proud.

Financial and other supports received for this research from the Australian Research Council, ANZAC Pty Ltd through the ARC Linkage Projects Scheme and CIRTS scholarship from Curtin University of Technology is gratefully acknowledged.

Thank you Christ Jesus as Lord over all things for guiding me the way of life You would have me to go.

Table of Contents

List of Figures

List of Tables

Chapter 1
Introduction

1.1 Background

Rotary kilns play an important role in diverse industrial applications, especially in the processing of coarse or free-flowing solid in the chemical, metallurgical ores, mineral, pharmaceutical, ceramics, cement, polymers, food, fertilizer and waste process industries. They are used in operations such as mixing, heating, cooling, reacting and drying of solid or combination of theses operations. The wide use of kilns can be attributed to major factors such as the ability to handle an extensive range of feed physical properties and the flexible adjustment of residence time in a continuous operation mode involving heterogeneous reactions.

Rotary kilns used in industry vary greatly in heating modes, kiln axis slopes and lifter types. The kilns can be either directly or indirectly heated. In a directly heated kiln, fuel (coal, gas or oil) goes through combustor or burner where it is mixed with oxygen to generate high temperature gas. The hot gas is then introduced into the kiln in a direction either co-current or counter-current to the solid flow. However, in an indirectly heated kiln, the heat tube is housed in casing and the combustion occurs with the case but external to the kiln while the solid is processed inside the kiln. Therefore, indirect heating of kilns provide clean heating and flexible in controlling the heat transfer for solid.

ANSAC is a wholly owned Australian company engaged in the development, design, manufacture and supply of quality engineered thermal process equipment for applications in the industrial and mining markets. ANSAC's core competencies are

in the specialised engineering fields of combustion, heat transfer, high temperature materials engineering, solids and materials handling, mechanical component design and horizontal rotating elements.

The ANSAC indirectly heated rotary kiln typically operates at 873-1073°K. This kiln is not inclined, achieving excellent mechanic performance. Compared to most conventional single throughout lifters, the ANSAC lifters consist of a number of segments. These lifters may provide three key functions, enhancing solid transport, mixing and heat transfer inside the kiln.

The heat transfer inside and outside the ANSAC kiln occurs via the following series of modes (Figure 1.1):

1. $Q_{f\text{-}iw}$, from flue gas to exposed inner kiln wall;
2. $Q_{cw\text{-}cb}$, from covered inner kiln wall to covered bed;
3. $Q_{ew\text{-}g}$, from exposed inner kiln wall to freeboard gas;
4. $Q_{g\text{-}eb}$, from exposed bed to freeboard gas;
5. $Q_{g\text{-}fp}$, from falling particles to freeboard gas and
6. $Q_{f\text{-}a}$, from flue gas to ambient.

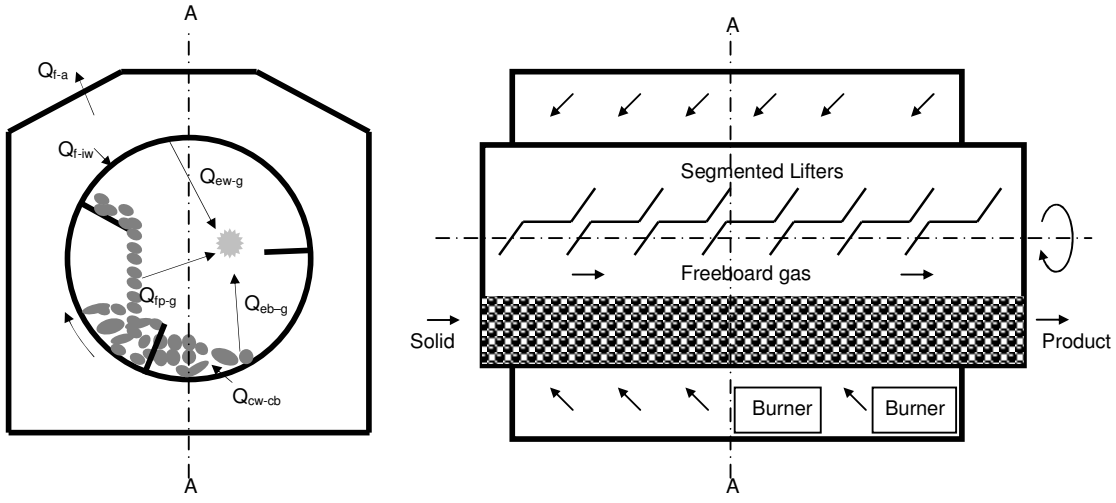

(a) (b)

Figure 1.1. Heat transfer modes inside and outside in an ANSAC indirectly heated rotary kiln at (a) transversal and (b) axial directions. (do not scale)

Each mode may involve one or more heat transfer mechanisms. The relative importance of these modes determining the overall heat transfer which is function of the solid thermo-physical properties, kiln designs, operating and process conditions. Among the abovementioned heat transfer in an ANSAC kiln, steps b), d) and e) play crucial role. This is determined by the complex motion and mixing of the solid which is known to be one of the major challenges facing the kiln designing and scaling.

A good understanding of the complex heat transfer mechanisms in the ANSAC kiln potentially will lead to energy efficiency improvement, reduction in costs of kiln manufacture and operation as well as widen its applications at different scales. However, the controlling steps in heat transfer have not been fully understood. Moreover, no suitable simple, quick and reliable predictive tools as well as scaling criteria have been developed for this kiln, as a foundation for the purpose of process design, development and operation of any practical utilisation of this kiln.

1.2 Thesis Objectives and Structure

1.2.1 Thesis Objectives

This research is jointly developed by the collaborating partners between Curtin University of Technology, Perth, Western Australia and ANSAC Pty Ltd, Bunbury, Western Australia. This present research aims to obtain a fundamental understanding of the complex heat transfer mechanisms in an indirectly heated rotary kiln with segmented lifters and its role in scaling through experimental and modelling studies. Following the understanding of the heat transfer mechanisms, semi-empirical models and criteria will be developed to serve as a predictive tool for simple, quick and reliable kiln designing and scaling. The study focuses on the influences of the solid transport and mixing as well as heat transfer modes where appropriate.

1.2.2 Thesis Structure

Including this chapter, there are a total of 7 chapters in this thesis. Each chapter is outlined as follows:

- Chapter 1 gives an overview of the thesis.

- Chapter 2 reviews the current state of knowledge on this subject in literature, including solid transport, mixing and heat transfer through experimental and modelling studies. Chapter 2 then identifies the key research gaps and specific objectives for the present research.

- Chapter 3 describes the overall methodology employed in this study, along with the explanations of the experimental and modelling techniques used.

- Chapter 4 presents the results of the experimental and modelling studies on solid transport in cold kilns. Effects of segmented lifter design configurations and helix on transport prediction equations and axial bed depth profiles are investigated. The data shows that the segmented lifters enhance axial solid transport and lead to flat bed depth profiles. Chapter 4 also shows results from the preliminary DEM simulation and development of a transport model as well as dimensionless empirical transport correlations. Attempts have also been made to compare the results in this study with those in relevant previous studies.

- Chapter 5 reports the results of the effects of segmented lifter design, lifter configurations and helix on solid mixing. The data show that the segmented lifters enhance axial solid mixing and transport, leads to the development of a dimensionless empirical mixing correlation. Attempts have also been made to compare the results in this study with those in relevant previous studies.

- Chapter 6 offers a fully integrated steady state axial heat transfer model in an indirectly heated rotary kiln with segmented lifters. The model incorporates developed solid transport and mixing correlations, as well as suitable heat transfer modes and reaction rate model for a low-rank coal pyrolysis case. The model has been validated by hot kiln experimental data. The controlling steps in heat transfer, overall heat transfer coefficient and heat transfer efficiency are then determined.

- Chapter 7 presents the conclusions over the whole study and outlines recommendations for future research and development.

Chapter 2
Literature Review

Extensive experimental and modelling efforts have been made in order to understand heat transfer mechanisms in rotary kilns. It is necessary to establish a solid knowledge base for the present study by examining the information available on this subject. This chapter reviews the previous work on the fundamentals of the solid transport, mixing and heat transfer in continuous systems. Through a critical evaluation of the previous work, the key research gaps in these areas are then identified, assisting in defining the specific objectives of the present study.

2.1 Solid Transport

There are two components in the transport of the granular solid through the kiln, the transport that occurs in a transverse section, perpendicular to the kiln axis, and the transport taking place along the kiln axis. While the first is important to the homogeneity of the solid bed, the second is critical in determining the bed profile and the mean residence time of the solid in the kiln.

The prevailing form of solid transversal motion in rotating kilns without lifters is rolling motion (see in Figure 2.1). This type of motion is characterized by a uniform, static flow of a particle layer on the surface (active layer), while the larger part of the bed (passive layer) is transported upwards by solid body rotation with the rotational speed of the wall (Mellmann, 2001).

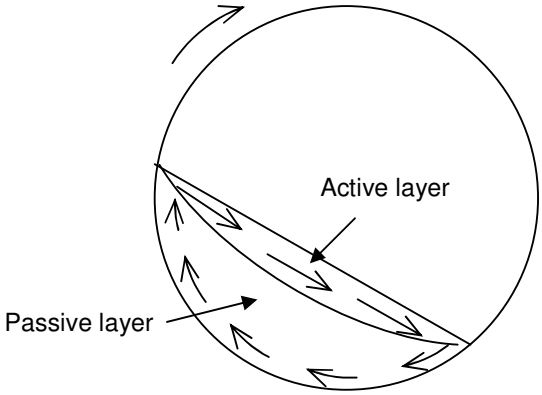

Figure 2.1 Schematic of the bed cross-section under rolling bed motion in rotary kilns without lifters.

2.1.1 Modelling

Four different approaches are commonly used (1951-2006) for the quantification of axial solid transport variables, e.g. axial bed depth profile, total hold-up, mean residence time and axial velocity with or without considering the effect of freeboard gas and end restriction:

1. Dimensionless empirical correlations, typically in the case of kilns without lifters (Chaterjee et al., 1983a, 1983b; Vahl and Kingma, 1952);
2. Mechanistic models using geometrical deduction and calculations, firstly proposed by Saeman (1951) and then used in other studies in kilns without lifters (Austin and Flemmer, 1978; Gupta et al., 1991; Hehl et al., 1978; Kohav et al., 1995; Kramers and Crookckewit, 1952; Lebas et al., 1995; Roger and Gardner, 1979; Spurling, 2000; Vahl and Kingma, 1952) and with lifters (Afacan and Masliyah, 1990; Hogg et al., 1974; Li et al., 2002b);
3. Semi-dimensionless empirical models in kilns with lifters using definition of the underloaded, design loaded and overloaded kilns (see in Figure 2.2) and related

to airborne and dense phases, which was firstly proposed by Matchett and Baker (1987, 1988) and subsequently used in other studies (Matchett and Sheikh, 1990; Sherritt et al., 1993, 1994, 1996; Pan et al., 2006), in kilns without freeboard gas, with lifters (Abouzeid and Fuerstenau, 1980; Karra and Fuerstenau, 1978) or without lifters (Perron and Bui, 1990);

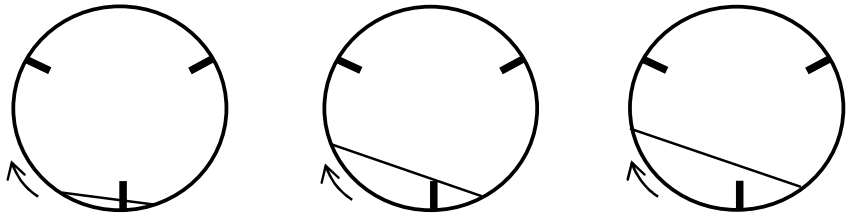

(a) (b) (c)

Figure 2.2 A discrete slice of a rotary kiln showing the definition of the (a) underloaded, (b) design loaded and (c) overloaded kilns.

4. Discrete Element Method (DEM) simulations, considering flow patterns and velocity distribution in the axial direction devices (Pandey et al., 2006; Gyenis et al., 1999; Laurent, 2006). DEM simulation data give a good chance to give insight and get reasonable explanations on the particle level for the practical observations quantitatively and qualitatively.

The second approach is often favoured because it is possible to extrapolate outside the operating conditions with reasonable confidence using measurable physical and operational properties. The second and third approaches have not been widely used in practical applications due to its complexity. In addition, the required depth and quality of experimental data for model development in practical applications is often difficult to obtain, such as initial angle of lifter discharge, lifter hold-up and dynamic angle of repose (Matchett and Baker, 1987).

This has led to the emergence of more pragmatic approaches such as empirical correlations. Empirical correlations are more practical solutions to express global outcomes as a function of the various key measurable engineering parameters. However, the number of dimensionless groups and the parameters within the groups differed among different studies (Abouzeid and Fuerstenau, 1980; Chaterjee et al., 1983a, 1983b; Karra and Fuerstenau, 1978; Perron and Bui, 1990; Vahl and Kingma, 1952). Dimensionless correlations may be used for scaling-up purpose. However, empirical correlations in terms of the dimensionless groups were fitted to experimental data and demonstrated to give a good fit to the data for the specific granular solid, and the range of kiln designs and operating conditions under study.

2.1.2 Experimental

The common basis for all experimental studies is the measurement of the total hold-up and axial bed depth, mainly by varying kiln operating conditions and kiln axis slope. A considerable amount of experimental studies (1927-2006) were carried out on axial bed depth (Table 2.1) and total hold-up (Table 2.2) measurements of the solid in rotating kilns with or without lifters and end restrictions, commencing with the work of Sullivan et al (1927). Table 2.1 and 2.2 list the key studies which are relevant to this topic and provided sufficient process details. The devices in all studies were operated at room temperature under steady-state conditions using dry and free-flowing solid without freeboard gas. A wide-range of granular solid was used, considering differences in particle size (0.19 mm - 15 mm), bulk density (225 kg/m^3 - 2500 kg/m^3) and angle of repose (27.4° to 48.5°), but in all cases the physical and chemical properties of solid were unchanged when the solid passed through the kilns.

The kiln size varied between the laboratory- and pilot-scales; the minimum kiln diameter studied was 0.0515 m and the maximum 0.6 m, and the ratio of the kiln length to diameter was between 2.61 and 40. The typical kiln diameter was between 0.1 m and 0.3 m and the ratio of length to diameter between 5 and 10. The devices

were operated at total kiln volumetric filling fractions of 1-30%. A wide range of rotational Froude numbers of 2.01×10^{-5} – 9.09×10^{-1} was investigated, resulting in cascading and cataracting motions in the transverse plane of the granular bed, as described by Mellmann (2001). The slope of the kiln axis was small (0-6°).

For open-end kilns, the bed cross-section decreases along the axial kiln length, i.e. the axial solid velocity increases and residence time decreases along kiln. In Table 2.1, some kilns deployed with end restrictions to increase the total hold-up by reducing the slope of the granular solid bed (Chaterjee et al., 1983a, 1983b; Hogg et al., 1974; Li et al., 2002a; Sai et al., 1990, 1992; Spurling, 2000). A flat bed depth profile along the kiln with end restriction, which is necessary for good heat transfer performances, may be achieved by varying the kiln rotational speed and axis slope (Chaterjee et al., 1983a; Sai et al., 1990, 1992).

As shown in Table 2.2, in all cases the rotary kilns except those in two experimental studies (Vahl and Kingma, 1952; Li et al., 2002a) are slightly inclined without lifters (Kramer and Croockewit, 1952; Chaterjee et al., 1983a, 1983b) or horizontal positioned with inclined lifters (Pan et al., 2006) or lifters parallel to the axis of the kiln (Afacan and Masliyah, 1990; Hogg et al., 1974). It was found that a horizontal kiln with slightly inclined lifters can transport solid in a similar matter to an inclined kiln without lifters (Pan et al., 2006).

In sum, the literature data in Table 2.2 suggests that:

1. An increase in the kiln axis slope, lifter slope or the kiln rotational speed force the material inside the kiln to move toward the exit end, cause a decrease in the mean residence time and total hold-up also an increase in the axial velocity.
2. The feed rate has a minor effect on the mean residence time; a rapid increase of mean residence time can be achieved by decreasing the kiln rotational speed.
3. The residence time of the charge and the total hold-up decrease with increasing kiln axis slope at fixed kiln rotational speed and also with increasing kiln rotational speeds at any fixed kiln axis slope.

4. The residence time of the charge decreases with increasing kiln diameter at a constant feed rate.
5. An increase in filling degree because of an increase in feed rate reduces the residence time, whereas any increase in the filling degree as a consequence of changes in other operational variables increases the residence time.

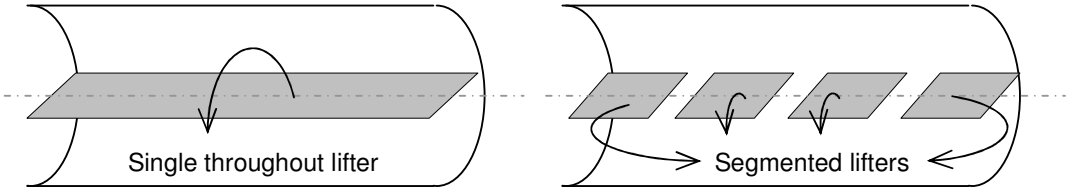

(a) (b)

Figure 2.3 Schematic of attached (a) single throughout lifter and (b) segmented lifters in an axial slice of rotary kilns.

Typically, in the past study, single throughout lifters were considered (see in Figure 2.3, compared to segmented lifters). Depending on the flow characteristics of the particles, the lifter shapes vary from straight to folded or more complex shapes, such as square, spiral, circular. Moreover, the lifter height plays a major role in the solid transport (Li et al., 2002a). Most lifters are fitted to scoop, lift the solid out of the bed and spill it into the freeboard gas. In general, these lifters provide two common tasks. The other is to improve heat transfer between the solid and freeboard gas by falling curtains and to improve solid mixing along the kiln.

2.2 Solid Mixing

A particle travelling in a rotating kiln moves in both transverse and axial directions. Mixing in the transverse plane is much more rapid and is a combination of convective (macro) and diffusive (micro) mixing. Mixing in the axial direction is

generally much slower, characterised as purely diffusive caused by the random collisions of particles in the active region (Clement et al., 1995; Khakhar et al., 1997; Metcalfe et al., 1995; Santomaso et al., 2005; Sherritt et al., 2003; Van Puyvelde, 1999). Generally, lifters can be installed to enhance axial mixing. The key mechanism is an overall convection causing the bulk movement of the material from the inlet of the kiln to the outlet at an average velocity equal to the plug flow velocity (Marias et al., 2005; Mujumdar et al., 2006, Patisson et al., 2000).

2.2.1 Modelling

The velocity field in a rotating kiln is very complex and it is not possible to describe it theoretically. In order to depict a mixing's flow behaviour, one relies on empirical models. The axial dispersion model is the classical one. The most common method of describing diffusive particle mixing in the axial direction of a rotating kiln treats the bed of particles as a continuum (Sherritt et al., 2003). Dispersion corresponds to diffusion in bulk flow liquid mixtures. It is assumed that there is no heterogeneity in a radial direction. Compared to the multi-parameter model (Adler and Hovorka, 1961; Dinesh and Sai, 2004; Mu and Perlmutter, 1980), the axial dispersion model, also referred as one-parameter model, provides the best combination of simplicity, interpretability and integrity therefore useful in kiln design and scaling.

The axial dispersion model is based on the solution to a partial differential equation with specific assumptions to suit a particular system. The equation can be written as

$$\frac{\partial C}{\partial t} = D_z \frac{\partial^2 C}{\partial z^2} - u \frac{\partial C}{\partial z} \quad \text{.....} \quad (2.1)$$

where D_z is the axial-dispersion coefficient, m^2/s; C is the (physical or non-reactive) tracer concentration,-; z is the axial distance, m; t is the time, s and u is the mean axial velocity, m/s. Equation (2.1) can be rewritten in a generalized dimensionless form and solved using closed-closed boundary conditions where tracer is injected

into the system at a short distance downstream from the entrance (Levenspiel, 1999). The cross-sectional area is constant along the kiln length. The dimensionless standard deviation from the mean residence time is related to the Peclet number and can be written as

$$\sigma_\theta^2 = \frac{\sigma^2}{\bar{t}^2} = \frac{2}{Pe} - \frac{2}{Pe^2}\left(1 - \exp(-Pe)\right) \quad \text{..... (2.2)}$$

with $\bar{t} = \dfrac{\sum t_i C_i \Delta t_i}{\sum C_i \Delta t_i} = \sum t_i E_i \Delta t_i$, $\sigma^2 = \dfrac{\sum t_i^2 C_i \Delta t_i}{\sum C_i \Delta t_i} - \bar{t}^2 = \sum t_i^2 E_i \Delta t_i - \bar{t}^2$, $Pe = \dfrac{uz}{D_z}$

where σ_θ^2 = dimensionless standard deviation, -; σ^2 = variance, s^2; $\bar{t}$ = mean residence time, s, i = n^{th} data, E_i = exit age distribution, s^{-1} and Pe = Peclet number, dimensionless. The variance represents the square of the spread of the distribution. Peclet number is a dimensionless parameter that describes deviations from the ideal continuous stirred tank reactor (CSTR) or the plug-flow reactor (PFR). A small Peclet number means large dispersion, hence mixed flow, conversely, a big Peclet number (Pe > 50) means small dispersion, hence plug flow. With the instantaneously introduction of tracer (kg) into the solid entering the kiln, the tracer concentration C_i versus time t_i leaving the kiln can then be recorded at regular intervals Δt_i. The mean residence time can be calculated from the measured data on total hold-up and feed rate.

Several attempts (Moriyama and Suga, 1974; Sai et al., 1990; Sze, 1995) have also been made to correlate experimental values of axial dispersion coefficients at the kiln discharge end in continuous rotating kilns without lifters. Moriyama and Suga (1974) reported the axial dispersion and Residence Time Distribution (RTD) of spherical particles, in the form of dimensionless correlations. Sai et al. (1990) developed empirical correlations using two tracer materials which were substantially different than the bulk material. Sze (1995) reported the axial dispersion of coal in a kiln using a mixture of coal (-3.35 + 2.0 mm) and zircon (-180 + 125 μm) as feed in an 140 x 1800 mm inclined kiln.

Sherritt et al. (2003) proposed empirical design equations for the axial dispersion coefficient in terms of kiln rotational speed, degree of fill, kiln and particle diameter. A total of 179 data points from the literature, encompassing both batch and continuous operational modes without lifters, yielded design correlations for slumping, rolling/cascading and cataracting bed behaviours. The axial dispersion coefficient ranges from 10^{-7} to 10^{-4} m^2/s. The coefficients for kilns with lifters are about two orders of magnitude larger than those without lifters, in the range between 10^{-5} and 10^{-3} m^2/s (Sherritt et al., 1996).

2.2.2 Experimental

The axial dispersion coefficient from a flowing kiln can be experimentally determined from RTD. A considerable amount of mixing experimental studies (1965-2002) were carried out to measure axial dispersion coefficient (Table 2.3) in rotating kilns with or without lifters and end restrictions. Table 2.3 lists the key studies which are relevant to this topic and provided sufficient process details. The devices in all studies were operated at room temperature under steady state conditions without freeboard gas. A wide-range of dry free-flowing granular solid and powder was used, considering differences in particle size (0.015 mm – 11.2 mm), bulk density (730 kg/m^3 - 2500 kg/m^3) and angle of repose (27° to 45°), but in all cases the physical and chemical properties of solid were considered to be unchanged when the solid passed through the kilns.

The kiln size varied from the laboratory- to pilot-scales; the minimum kiln diameter studied was 0.08 m and the maximum 0.765 m, and the ratio of the kiln length to diameter was between 2 and 40. The devices were operated at total kiln volumetric filling fractions of 0.85 - 51 %, the rotational Froude number (8.22×10^{-5} – 8.46×10^{-1}). In most industrial applications, cascading motion is favourable because of its high intensity of mixing. The slope of the kiln axis was small, lying between horizontal and 4.3°.

All mixing experimental studies carried out the measurement of the RTD at the kiln discharge end using a tracer technique (Levenspiel, 1999). The technique is a stimulus/response technique method. It imposes an interference factor on the kiln whilst it is in stationery operation and observing how this interference is broken down inside it. While the kiln is operating in a steady-state, a fixed small amount of dyed tracers was introduced without changing the flow pattern. This enables the production of tracer concentrations were measured at the kiln's outlet by collecting the tracer/bulk mixture into cups. Samples were then collected until the entire tracer has been discharged from the kiln. The tracers were manually separated from bulk mixture and weighed to determine tracer concentrations. At end of the run the total hold-up in the kiln was determined.

The RTD may also be determined using a non-intrusive image measurement technique using a transparent rotating kiln (Sudah et al., 2002). This technique does not disturb the structure of the mixture and allows a quantitative and evaluation of local mixing degree in axial direction along the kiln. Image analysis allows determining proportions of different colours at the entire exposed surface of the mixing volume. Image analysis can be done off-line after picture taken within a relatively short term of sampling. Previous study showed that the image analysis technique is a powerful tool to characterise the mixing behaviour of the whole mixture (Dauman and Nirschl, 2008).

The previous studies (Table 2.3) considered the effects of kiln rotational speed, volumetric fill, feed rate, kiln axis slope, particle properties and dam height on the axial-dispersion coefficient or Peclet number. For rotating kilns without lifters, the RTD was found to consist of a narrow and approximately symmetric central peak. The Peclet number was found to be high, indicating the granular flow being close to plug flow behaviour of a pipe reactor. To obtain higher axial mixing coefficient or lower Peclet number corresponds to wide and asymmetric RTD, short kiln length ($L/D \approx$ 2-5), high kiln rotational speed (high Froude number) , low volumetric fill, inclined kiln position and lifters, should be considered.

It was also found that the dispersion coefficient was weakly independent on feed rate and end constriction. However, the coefficient was strongly dependent on the particle properties, i.e size, shape, angle of repose and density. Increasing the particle diameter increases the dispersion coefficient. Long particles give lower coefficients than spherical particles and those wet-sticky particles give lower coefficients than dry free-flowing granules (Rutgers, 1965). The dispersion number was strongly dependent on the type of tracer in terms of its angle of repose, density and size (Sai et al., 1990).

Values of axial-dispersion coefficients range from 7.02 x 10^{-7} to 2.61 x 10^{-5} m^2/s (corresponding to *Pe* between 71 and 3788) for kilns without lifters and 7.37 x 10^{-7} to 1.23 x 10^{-4} m^2/s (corresponding to *Pe* between 13 and 388) for kilns with lifters. Wes et al. (1976) found that the axial mixing coefficient is strongly affected by the quantity of solid moving with the lifter, the orientation and number of the lifters. Venkataraman et al. (1986) reported that the degree of mixing in the kiln fitted with forward-spiralling square lifters was considerably greater than that in the kiln with reverse-spiralling square lifters. The steady-state total hold-up in the kiln fitted with the forward-spiralling square lifters was less than that in the kiln fitted with reverse-spiralling square lifters. The solid transport in a kiln with the conventional bar lifters ($50 < Pe < 110$) behaved more towards plug flow when compared with that of the kiln fitted with these spiralling lifters ($30 < Pe < 60$), over the same range of feed rates.

2.3 Heat Transfer

There are some unique challenges associated with the heat transfer in rotary kilns. Typically, the kiln is inclined at a slight angle to the horizontal direction and the solid bed is at an angle to the kiln due to rotation. Two distinct regions are present in the cross-section of the kiln, i.e. the freeboard and the solid bed. The gases flow in the freeboard while the solid material occupies the bed. The bed moves, but not in as

well-defined a manner as a liquid or a gas. The bed is constantly tumbled and mixed by the kiln rotation and is continuously being exposed to the heat sources, i.e. under the bed, on top of the bed, flame (for direct-fired kilns) and also rotating kiln wall. Depending on applications, gases may evolve from the bed, which can be an additional source of energy. Materials processing may also be exothermic or endothermic depending on the involved chemical reactions (Martins et al., 2001; Ortiz et al., 2005; Patisson et al., 2000; Ramakrishna et al., 1999). Some processes may involve three-phase if the solid feed material melts and becomes liquid in the kilns, in addition to the combustion gases and possible gases evolving from the process.

2.3.1 Modelling

Over the last 40 years, there has been a continued interest in the modelling work on axial heat transfer typically considered under steady state conditions. Zonal models of heat transfer, where the kiln is divided into isoheat transfer slices, become standard in heat transfer modelling of rotary kilns. The heat transfer component of the one-dimensional models can be divided the slice into separated control volumes of freeboard and bed.

Sass (1967) proposed one of the first early representations of one-dimensional modelling of a directly heated rotary kiln without lifters. The model of Sass (1967) formed the basis for the various subsequent models in the literatures for: (1) directly heated rotary kilns without lifters (Barr et al., 1989; Brimacombe & Watkinson, 1978; Davis, 1996; Davis & Englund, 2003; Georgallis et al., 2005; Ghoshdastidar et al., 2002; Klose & Wiest , 1999; Kroger et al., 1979; Li et al., 2005; Marias, 2003; Mitchell et al., 2002; Mujumdar & Ranade, 2006; Mujumdar et al., 2006, 2007; Palmer & Howes, 1998; Sammouda et al., 1999; Watkinson & Brimacombe, 1978, 1982; Wild, 1994) and with lifters (Kamke et al., 1986; Riquelme et al., 1991); and (2) indirectly heated rotary kiln without lifters (Marias et al., 2005) and with lifters (Wes et al., 1976).

Those models are capable of predicting average local compositions within the bed and freeboard; and temperatures within the bed, kiln wall and freeboard as function of axial position. Axial transport of solid in the kiln was considered to simulate total volumetric filling fraction, solid residence time, variation in height of the bed, axial velocity and the heat transfer area of exposed bed. However, axial mixing was neglected for both rotary kilns.

The conditions in the freeboard and bed were each assumed to be well mixed hence uniform in the transverse plane, yielding ordinary differential equations relating axial gradients of temperature and composition to the net rates of heat transfer for each control volume. It is also assumed that no net energy accumulation can occur within the wall. The system of equations are therefore simultaneously for successive axial positions.

Heat transfer inside rotary kilns occurs via conduction, convection and radiation. The heat transfer modes can be divided into heat transfer outside, inside and across the kiln wall. Each mode may involve one or more heat transfer mechanisms. In general, radiative transfer is dominant at > 1000°C (Barr et al., 1989; Gorog et al., 1981, 1982). The relative importance of each mode depends on the solid, gas and kiln wall thermo-physical properties; kiln designs and kiln operating conditions.

The heat transfer outer, inner and across kiln wall includes mainly

1. the convection and radiation heat transfer from the flue gases to the kiln wall for an indirectly heated rotary kiln or from the kiln wall to the ambient for a directly heated rotary kiln,
2. the conduction and radiation heat transfer between the covered wall and the covered bed,
3. the convection and radiation heat transfer between the exposed wall and the freeboard gas,
4. the convection and radiation heat transfer between the freeboard gas and the exposed bed,

5. the radiation heat transfer between exposed wall to exposed bed,
6. the convection and radiation heat transfer between the freeboard gas to the falling particles for a rotary kiln with lifters, and
7. the conduction heat transfer from the outer kiln wall to the inner kiln wall for an indirectly heated rotary kiln and visa versa for a directly heated rotary kiln.

For direct heating operations without lifters at temperatures up to 873°C, Ding et al. (2001) indicated that heat transfer from the covered wall to the covered bed is the dominant mechanism in supplying heat to the bed. Heat transfer between the freeboard gas and the exposed bed accounts for only a small portion. The heat transfer rate between the freeboard gas and the exposed wall may be comparable to that between the covered wall and the covered bed indicating that both steps could be controlling. Li et al. (2005) reported that heat transfer from covered wall to covered bed and convection heat transfer from freeboard gas to exposed bed play a crucial role in the fast heating of solid at the kiln inlet (up to 700°K). Gorog et al. (1982) stated that in the high temperature regions of kiln (>1200°K), 60 to 80 % of the heat received by the solid results from their radiative interaction with the freeboard gas and exposed wall. With the low temperature regions of the kiln (< 1200°K), 70 % of heat received by the solid results from the combination of freeboard convection and the regenerative heating of the wall. Tscheng and Watkinson (1979) and Barr et al. (1989) indicated that the heat transfer coefficients between the freeboard gas and exposed bed are in the order of five to ten times the values between the gas and the exposed wall.

Except the convection heat transfer from the flue gases to the outer kiln wall, reliable correlations are available in the literature to determine heat transfer coefficients related to each mode at <1273°K:

1. the convection heat transfer from the outer kiln wall to the ambient (Churchill & Chu, 1975),
2. heat transfer between the covered wall and the covered bed accounting for conduction and advection using penetration theory (Ferron & Singh, 1991; Lehmberg et al., 1977; Li et al., 2005; Lybaert, 1987; Tscheng & Watkinson, 1979; Wes et al., 1976; Wachters & Kramers, 1964),

3. convection heat transfer between the freeboard gas and the exposed wall (Tscheng & Watkinson, 1979),
4. convection heat transfer between the freeboard gas and the exposed bed (Tscheng & Watkinson, 1979) and
5. convection heat transfer between the freeboard gas and the falling particles (Churchill, 1983; Hirosue & Shinohara, 1976a, 1976b; Hirosue, 1989; Hirosue & Mujumdar, 1993; Ranz & Marshall, 1952a, 1952b; Whitaker, 1972).

2.3.2 Experimental

Experimental studies can best be utilized for verification and enhancing the reliability of the derived models. The common basis for the previous experimental studies is the measurement of a set of axial gas, solid and kiln wall temperatures by outfitting the kiln heavily with thermocouples. However, few experimental studies (1976-2008) have been undertaken on axial heat transfer in rotary kilns with or without lifters and end restrictions, due to the difficulty of making measurements on a rotating vessel, particularly under industrial conditions.

Table 2.4 summarises the key studies which are relevant to this topic and provided sufficient process details. The devices in all studies in Table 2.4 were operated under steady state conditions. A wide-range of dry free-flowing granular solid and powder were used, considering differences in particle size (0.015 mm – 30 mm) and bulk density (769 kg/m^3 – 1680 kg/m^3). The kiln size varied between the laboratory- and industrial-scales; the minimum kiln diameter studied was 0.12 m and the maximum 2.84 m, and the ratio of the kiln length to diameter was between 1.6 and 25. The devices were operated at total kiln volumetric filling fractions of 5 – 25 %. A wide range of rotational Froude numbers of 2.84 x 10^{-5} – 2.84 x 10^{-2} was investigated, resulting in cascading motion in the transverse plane of the granular bed, as described by Mellmann (2001). The slope of the kiln axis was small, lying between horizontal and 8°. Most kilns were built up with end restrictions; however, few kilns studies considered lifters.

Table 2.1

Summary of experimental studies on axial bed depth measurements in rotating kilns with/without lifters and end restrictions

References	Kiln designs					Kiln operating conditions		Solid characteristic			Axial bed depth	
	Kiln axis slope θ, °	Lifters	End constriction	Kiln diameter D, m	L/D ratio, -	Feed rate m, kg/min	Kiln rotation speed n, rpm	Static angle of repose ϕ, °	Particle size $d.10^3$, m	Bulk density ρ, kg/m^3	Positions	Profile
Sullivan et al. (1927)	1-6	N/A	N/A	0.15	14.2	0.04 – 0.45	2.5	34.4	0.72	1700	13	Incline
Chaterjee et al. (1983a, 1983b)	1-3	N/A	Yes/No	0.2-0.6	3.3-16	0.25 – 1.25	0.3 - 0.7	35	6	1600	8	Incline/flat
Sai et al. (1990, 1992)	0.78-1.37	N/A	Yes/No	0.147	40	0.11 – 0.60	1 - 3	27.4	0.19	2500	6	Incline/flat
Lebas et al. (1995)	1	N/A	N/A	0.6	10	5.30 – 10.44	2 - 4	47,47	15	480, 750	31	Incline
Spurling (2000)	1-2	N/A	Yes/No	0.0515	19.42	0.006 – 0.2	5.82	32	0.46	1600	37	Incline

Table 2.2

Summary of experimental studies on total hold-up measurements in rotating kilns

References	Kiln designs					Kiln operating conditions		Solid characteristic			Dimensionless empirical correlation developed
	Kiln axis slope θ, °	Lifters	End constriction	Kiln diameter D, m	L/D ratio, -	Feed rate m, kg/min	Kiln rotation speed n, rpm	Static angle of repose ϕ, °	Particle size $d.10^3$, m	Bulk density ρ, kg/m^3	
Vahl and Kingma (1952)	0	N/A	N/A	0.11	5.91	0.16 – 1.94	9 - 41	33	0.6	1490	Yes
Kramers and Croockewit (1952)	0.5 – 3.2	N/A	N/A	0.197	9.04	0.14 – 2.36	2.40 – 14.28	40, 36	0.9, 1.0	560, 1480	No
Hogg et al. (1974)	0	Single Throughout	Yes	0.095	2.61	0.08 – 0.24	90	38	0.4	1460	No
Chaterjee et al. (1983a, 1983b)	1 – 3	N/A	Yes	0.2 – 0.6	3.3 – 16	0.25 – 1.25	0.3 – 0.7	35	6	1600	Yes
Afacan and Masliyah (1990)	0	Single Throughout	N/A	0.192	5.47	0.38 – 1.82	4.77 – 91.93	36	2.0	1640	No
Li et al. (2002a)	0.62 – 2.40	Single Throughout	Yes	0.30	6.00	0.19 – 1.04	2 - 8	48.5	2.5	225	No
Pan et al. (2006)	0	Single Throughout	N/A	0.374	3.21	0.42 – 1.40	3 – 9	30	3.0	695	No

Table 2.3

Summary of experimental studies on axial dispersion coefficient measurements in rotating kilns

References	Kiln designs					Kiln operating conditions		Solid characteristic			Measurement		
	Kiln axis slope θ, °	Lifters	End constriction	Kiln diameter D, cm	L/D ratio, -	Feed rate m, kg/min	Kiln rotation speed n, rpm	Static angle of repose ϕ, °	Particle size $d.10^3$, m	Bulk density ρ, kg/m^3	Positions from feed end, z/L,-	Technique	Tracer, g
Rutgers (1965)	0 - 4	Single Throughout	Yes	16 – 76.5	2 - 3	0.03-0.40	8 – 97	N/A	7x2.1x1.7, 5x2.8x2.1 mm	822	1.0	separate manually & weight	N/A
Abouzeid et al (1974)	0 - 3	Single Throughout	Yes	8	3	0.018-0.228	10 - 126	N/A	28x35, 35x48, 48x65 mesh	865	1.0	separate manually & weight	1
Wes et al (1976)	0	Single Throughout	Yes	60	15	4.75	2 - 6	N/A	0.015 – 0.1 mm	769	0.4 , 1.0	atomic absorption spectrophotometer	4500
Karra et al (1977)	0 - 3	Single Throughout	Yes	8	3	0.09 – 0.10	40	32	35x48 mesh	1300	1.0	separate manually & weight	1
Hehl et al (1978)	0	N/A	Yes	25	2.4	0.012-0.24	1-10	N/A	0.137 mm	865	1.0	heat transfer decomposition & weight loss	100
Abouzeid et al (1980)	0 - 3	Single Throughout	Yes	8-12.7	2-6	0.018-0.228	10-126	N/A	28x35, 35x48, 48x65 mesh	865	1.0	separate manually & weight	1
Mu and Perlmutter (1980)	0	N/A	N/A	10.1	4	300 cc/min	20	27	2x5 mm	N/A	1.0	separate manually & weight	200 particles
Venkatarman et al (1986)	0	Single Throughout	Yes	12.7	3	0.21 – 0.66	79	N/A	1.17x0.83 mm	2200	1.0	separate manually & weight	2
Sai et al (1990)	0.78 – 1.37	N/A	Yes	14.7	40	0.11– 0.60	1 - 3	27.4	0.19 mm	2500	1.0	separate manually & weight	570, 245
Hatzilyberis & Androutspoulos (1999a)	0.6 – 4.3	N/A	N/A	12	25	0.10 - 0.23	1.5 – 8.5	45	+8-11.2 mm	889	1.0	N/A	N/A
Hatzilyberis & Androutspoulos (1999b)	3	Single Throughout	N/A	12	25	0.03 - 0.07	4 - 6	34.7	2 mm	749	1.0	N/A	N/A
Sudah et al (2002)	1.8 – 2.5	N/A	N/A	15.25	21	0.02 - 0.09	2 - 5	38.6	3x1.5 mm	730	3 different positions, 1.0	digital photos	16.2

Table 2.4

Summary of experimental studies on axial heat transfer in rotary kilns

References	Kiln designs					Kiln operating conditions		Solid characteristic			Measurement		Heating mode
	Kiln axis slope θ, °	Lifters	End constriction	Kiln diameter D, cm	L/D ratio, -	Feed rate m, kg/min	Kiln rotation speed n, rpm	Static angle of repose ϕ, °	Particle size $d.10^3$, m	Bulk density ρ, kg/m^3	Max operating temperature, °C	Temperature measured	
Wes et al (1976)	0	Single Throughout	Yes	60	15	n/a	1.6-6.5	N/A	0.015-0.1	769	133	gas, solid, kiln wall	indirect
Brimacombe & Watkinson (1978)	2.4	N/A	Yes	40.6	13.5	0.3-2.3	0.25-2	31	0.58	1587	987	gas, solid, kiln wall	direct
Kroger et al (1979)	0	N/A	Yes	25	2.4	2.5 – 10.2 l/h	1-10	N/A	16	N/A	119	solid, kiln wall	direct
Watkinson & Brimacombe (1982)	0.625-2.53	N/A	Yes	40.6	13.5	0.6-1.4	0.75-3	38.5 - 39.9	0.75 – 3.5	1370-1670	1327	gas, solid, kiln wall	direct
Kamke et al (1986)	0	Single Throughout	N/A	N/A	N/A	4.7-4.9	2.8-5.5		wood		267	gas, kiln wall	direct
Barr et al (1989)	> 0	N/A	Yes	40.6	13.5	0.6-1.1	1-1.5	N/A	0.088 - 0.841	775-1680	1427	gas, solid, kiln wall	direct
Klose et al (1999)	> 0	N/A	N/A	13	8.8	N/A	N/A	N/A	< 10	N/A	800	gas, solid	indirect
Sammouda (1999)	5 - 8	N/A	Yes	64	1.9	6.8-10	N/A		sand		977	solid, kiln wall	direct
Patisson (2000)	> 0	N/A	N/A	284	21.1	N/A	1	N/A	4-20	N/A	1090	gas, solid, kiln wall	direct
Marias et al (2005)	> 0	N/A	N/A	N/A	N/A	N/A	N/A		aluminium		570	gas, solid, kiln wall	indirect
Androutsopoulos et al (2003)	5.4	Single Throughout	Yes	40	15	0.3-1.7	1.5–5.5	N/A	30	N/A	900	gas, solid, kiln wall	indirect
Ortiz (2005)	2 - 6	N/A	N/A	30	12.3	0.3	1-3	N/A	2	N/A	1327	gas, solid	direct
Hatzilyberis & Androutsopoulos (2006)	5.4	Single Throughout	Yes	40, 12	15, 25	0.17, 1.67	1.5-5.5	N/A	<15	N/A	900	gas, solid, kiln wall	indirect
Zhang et al (2008)	0	N/A	Yes	25.4	1.6	0.33	1		copper scrap		>1400	kiln wall	direct

2.4 Summary

Through a thorough review of the literature, it is clear that little work has been done so far on the influences of the installed segmented lifters on solid transport, mixing and heat transfer. Much of the past research work focused on experimental and modelling studies in directly heated rotary kilns without lifters. Less attention was paid on identifying the controlling steps of heat transfer. Solid transport and mixing are accountable for the heat transfer rate inside the kiln tube, i.e. between freeboard gas and exposed bed, covered wall and covered bed and; freeboard gas and falling particles. These limiting rates directly affect the yield and efficiency of the process and are quite commonly a bottleneck.

Most of the transport and mixing experiments were based on rotating kilns with single throughout lifters parallel to the axis of the kilns using a specific granular solid. None of the transport experiments studied the bed depths determined in rotating kilns with lifters. The effects of segmented lifters on solid transport and mixing have not yet been researched and not well understood while such understanding of this is essential to optimising lifter designs and configurations for enhanced axial solid transport and mixing.

Unlike a non-invasive experimental technique, most axial dispersion coefficients were quantified by separating the tracers manually and weighting at the kiln discharge end. This procedure is tedious when the sample size is big. Moreover, due to transport experiments were carried out after mixing; the amount of tracers used in all mixing experiments was kept constant at different volumetric fill.

Through literature review, it is clear that developing transport and mixing models are essential to the development of a model for kiln design and scaling considering applications, kiln designs and operating conditions. Dimensionless correlations are very

useful for industry scale-up purpose but such correlations must be validated by experimental investigations. Previous mechanistic and semi-empirical transport models are also likely specific to the solid, lifter and end constriction types used. However, the required depth and quality of experimental data for model development is often difficult to obtain. DEM simulation is an emerging simulation tool but no DEM simulation has been done on horizontal rotating kilns with segmented lifters. Therefore, there is a strong need to develop transport, mixing and heat transfer models for an indirectly heat rotary kiln with segmented lifters. This requires a systematic investigated research program.

Based on the literature review and key research gaps identified, the specific objectives of the present research are as follows:

- To study the effect of segmented lifter designs, lifter configurations and end constriction on solid transport and mixing experimentally in horizontal kilns, aiming to investigate the potential of the use of segmented lifter to enhance axial solid transport and mixing under various solid, kilns designs and operating conditions.
- To perform a preliminary DEM simulation on solid transport, aiming with attempts to provide further insight into the role of lifters in axial displacement and to develop a solid transport model, considering any measurable key engineering parameters at industry level.
- To develop dimensionless empirical transport and mixing correlations and criteria considering all three (over-, design-, and underloading) regimes.
- To carry out experimental study using a hot kiln to measure the temperature profiles in the solid bed, freeboard gas, inner kiln wall and flue gas, and use the obtained data for the validation of heat transfer model subsequently developed.
- To develop an integrated steady state axial heat transfer model in a hot kiln with segmented lifters incorporating the developed solid transport and mixing correlations, suitable heat transfer modes and reaction rate model.

Chapter 3
Methodology

This chapter details the research methodology employed in this thesis in order to achieve the objectives outlined in Chapter 2. As discussed in Chapter 2, there are several modes of heat transfer involved in the indirectly heated horizontal rotary kiln. Solid transport and mixing are expected to be the key factors influencing the heat transfer inside the kiln. Therefore, a systematic research methodology has been deployed, as illustrated in Figure 3.1, considers both experimental and modelling studies.

The experimental investigations include mainly two parts, pilot-scale cold kilns and hot kiln experiments. Various carefully-selected solid materials were used in our experimental program covering a wide-range of static angle of repose, size and bulk density. Dimensional analysis was also performed and a systematic experimental program was then carried out to quantitatively investigate solid transport and mixing, considering various kiln designs, kiln operating conditions and solid physical properties. The key variables measured include total hold-up, bed depth and tracer concentration. The cold kilns were designed with several removable rotating windows for the image sampling method and axial bed depth profile measurement. The hot kiln has been retrofitted to incorporate a temperature logging system, enabling the measurement of the temperature profiles of flue gas, inner kiln wall, bed and freeboard gas.

The mathematical modelling includes three aspects, a theoretical transport model, a set of dimensionless empirical correlations and a steady state axial heat transfer model. A preliminary DEM simulation on solid transport was also performed to provide further insight the role of segmented lifters. A theoretical transport model has also been

developed to predict the average bed depth. Dimensionless transport and mixing correlations have also been developed based on the extensive experimental data.

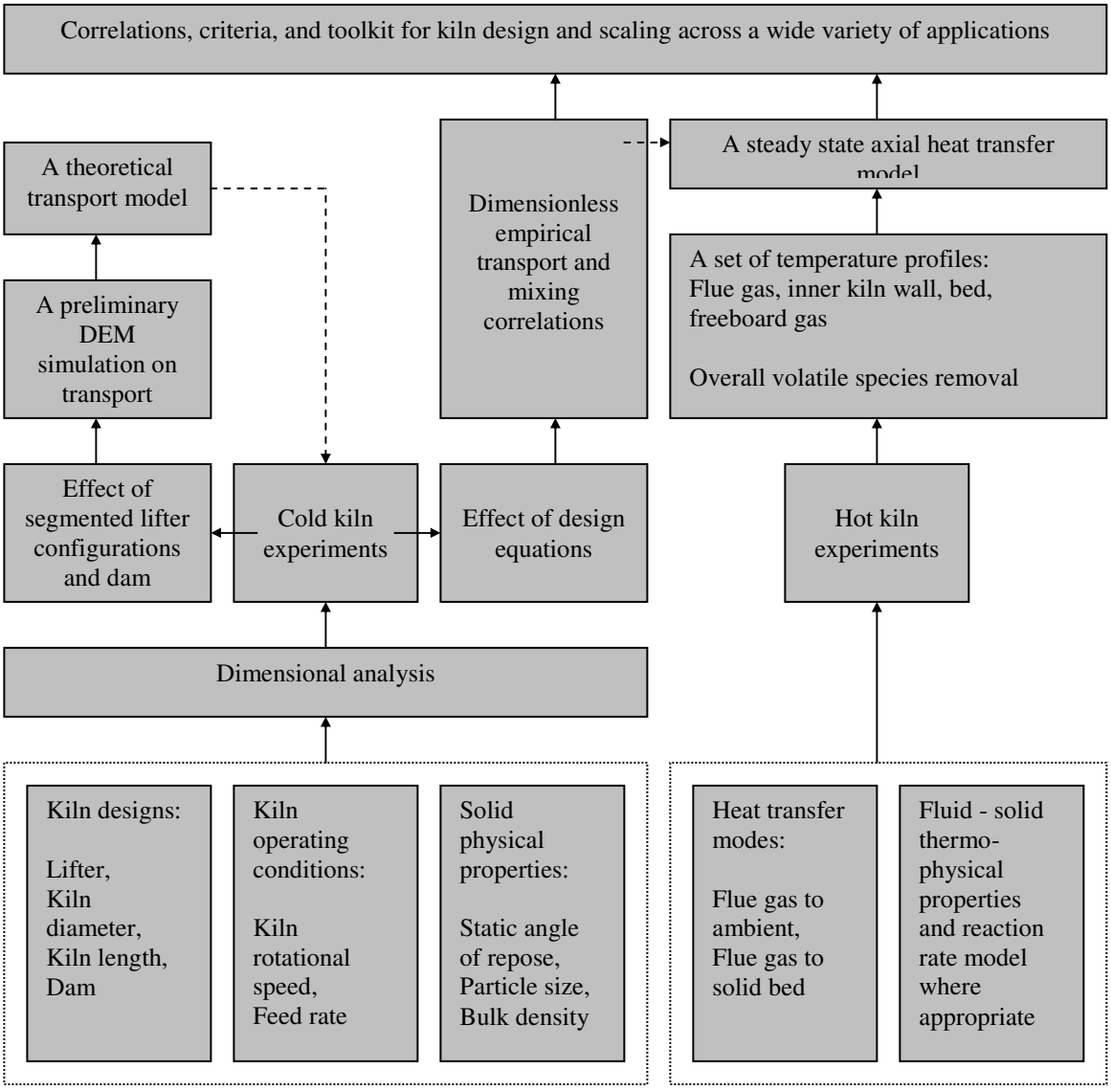

Figure 3.1. Research methodology

Attempts have also been made to test the developed correlations with previous selected transport and mixing experimental studies. As the ANSAC kiln typically operates at 873-1073°K, the heat transfer modes are mainly the convection and conduction heat

transfers. The input data necessary for the model were obtained by own experiments or from the literature. The model predictions were also compared with experimental data for validation.

3.1 Dimensional analysis

Dimensional analysis can provide important guidance in experimental design, similarity laws and data correlation. Compared to similitude based on governing differential equations in batch mode, which resulted in 19 controlling dimensionless groups (Ding et al., 2001), dimensional analysis is a simple, straightforward and powerful approach to developed useful correlations for applications. The use of dimensional analysis requires only knowledge of the variables that influence the phenomena of interest. The previous experimental studies (Table 2.1, 2.2, 2.3) are very useful in compiling a set of measurable key engineering parameters involved in the solid transport and mixing. The objective is to determine an appropriate reduced set of dimensionless forms of these dimensional variables. Such dimensionless terms can then be used in place of the original individual variables and parameters to completely define the system behaviour using conservation law of dimensions.

3.2 Granular solids

A wide range of dry monosize granular solid were carefully selected and tested. The set of measurements was repeated five times and the characteristics of these granular solid are listed in Table 3.1, 3.2 and 3.3. The static angle of repose, which is sensitive to shape and roughness, was measured by a vertical quasi-two-dimensional Hele-Shaw cell (SEED, n.d.).

Table 3.1

Granular solids used in the experimental studies in the cold kilns

Materials	ρ, kg/m^3	ϕ, degree	$d.10^3$, m
granite	1438	45	7.0
zeolite	1164	38	1.5
sand	1438	32	0.5
rice	822	30	7.0
urea	685	35	2.0
urea	685	35	3.0
urea	685	35	4.0
coriander seed	274	35	3.5
bean bag	5	27	6.0
glass bead	1438	25	2.0

Table 3.2

Tracers used for mixing experimental studies in the cold kilns

Materials	ρ, kg/m^3	ϕ, degree	$d.10^3$, m
sand	1507	32	0.5
rice	801	30	7.0
urea	719	35	3.0
coriander seed	247	35	3.5
glass bead	1363	25	2.0

Tracers were prepared from selected granular solid by colouring using a water-based food dye, in order to minimize the effect on their surface properties. The colour chosen was green, due to its contrast with original granular solid, kiln wall and lifters used, which can be easily distinguished by the image analysis program. As shown in Table 3.2, the angle of repose did not change, indicating that the water based dye did not significantly affect the surface properties of the particles. The bulk densities of the coloured solid also only have slight change. Therefore, the solid would not segregate due to density differences as previously described (Alonso et al., 1991; Uhl and Gray, 1967).

A low-rank coal sample was used in the experiments in a hot kiln. The characteristics of the low-rank coal particles are listed in Table 3.3.

Table 3.3
A low-rank coal sample used for experimental studies in a hot kiln

Material	pre-dried low-rank coal
ρ, kg/m^3	600
ϕ, degree	45
$d.10^3$, m	30
Proximate analysis	
Fixed carbon, %	39.95
Ash, %	2.55
Volatile matter, %	42.50
Moisture, %	15.00

3.3 Rotary kilns

3.3.1 Cold kilns

Experiments reported in this study were performed in a set of specially-designed pilot-scale rotating kilns. A schematic diagram of the experimental system is shown in Figure 3.2. The experimental system has a 3 mm thick mild steel kiln with three removable rotating windows each being 920 x 250 mm, hoppers, a feeding plate, an adjustable motor driving the kiln (Telemecanique, Altivar 08, 15.0–50.0 Hz) and screw feeders

(Telemecanique, Altivar 31, 0–50.0 Hz). The last two devices were calibrated versus kiln rotational speed and feed rate for each solid.

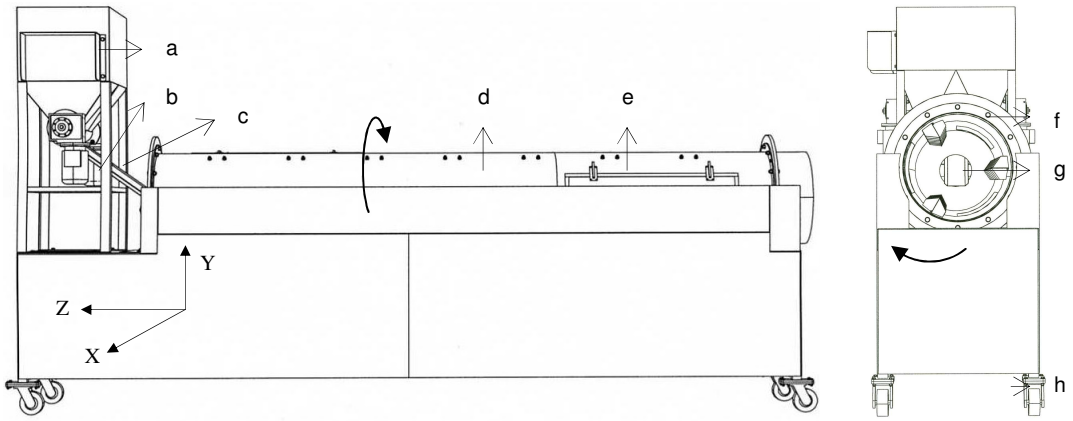

Figure 3.2. A schematic diagram of the cold-kiln experimental system: (a) hoppers, (b) feeding plate, (c) fix end constriction (d) rotary kiln, (e) removable windows (a total of 3, arranged in series), (f) screw feeders, (g) removable lifters and (h) house jack

The rotating kiln is made up of a supporting frame equipped with a house jack mechanism provided at the kiln feed and discharge ends which capable of adjusting the axis kiln slope. The system can be checked, measured and adjusted using a SmartTool™ digital spirit level, 1200 mm level with an accuracy of 0.1°. The kiln movement is supported on four metal rollers.

This study employs three different kilns with diameters *D* and lengths *L* (*D x L*: 0.618 x 3.0, 0.510 x 3.6 and 0.400 x 4.0 m) which give *L/D* ratios of 5, 7 and 10. Fixed feed end constrictions of height 0.20, 0.15 and 0.10 m from the kiln wall were used. The feed end constrictions are to prevent back-spillage of the feed, through which a feeding plate could be inserted into the rotating kiln.

Outflow of solid at the kiln discharge end was directed into a 20 L collection plastic bucket. The bucket stands on top of a Mettler TE30 digital platform balance which has a maximum load of 30 kg and an accuracy of 0.01 kg.

3.3.2 Lifters

There are three rows of removable segmented lifter sets with being 120° evenly distributed on the kiln inner wall and helix, as shown in Figure 3.3. The numbers of lifters for each row are 6, 7 and 8 for kilns with *L/D* ratios of 5, 7 and 10. Two removable helixes at different heights with h_l/D ratio of 0.16 may also be fitted at the outlet of the kiln. The segmented lifter consists of three parts. Two side parts of the lifters are of opposite direction and axially oriented such that the flow towards to the kiln discharge end, and can be termed as 'folded lifter sections'. Six sets of lifters at different heights h_l were used with h_l/D ratios of 0.16 and 0.08. The height b_1 of lifters are adjusted accordingly. The width b_2, b_3 and folded angle α are 0.08 m, 0.16 m and 135°.

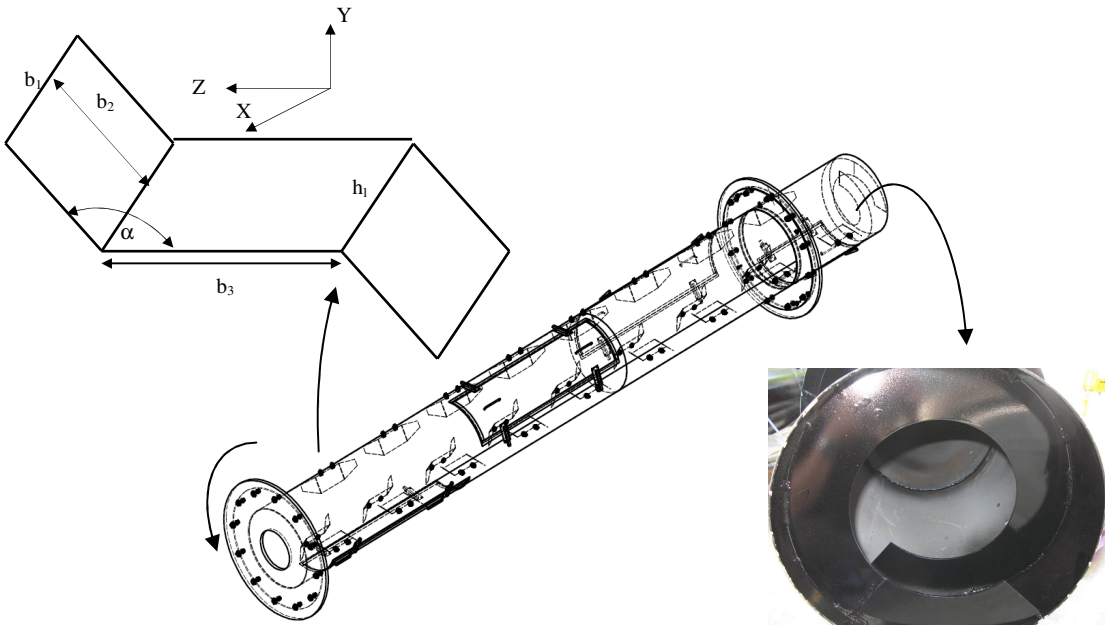

Figure 3.3. Design and configurations of removable segmented lifters and helix in a horizontal rotating kiln with *L/D* ratio of 10. (do not scale)

A number of different lifter designs were specially considered as shown in Figure 3.4. These designs were chosen in order to investigate the effect of the segmented lifter design and configurations, namely lifter configurations, folded lifter section, lifter slope and number of lifters per row.

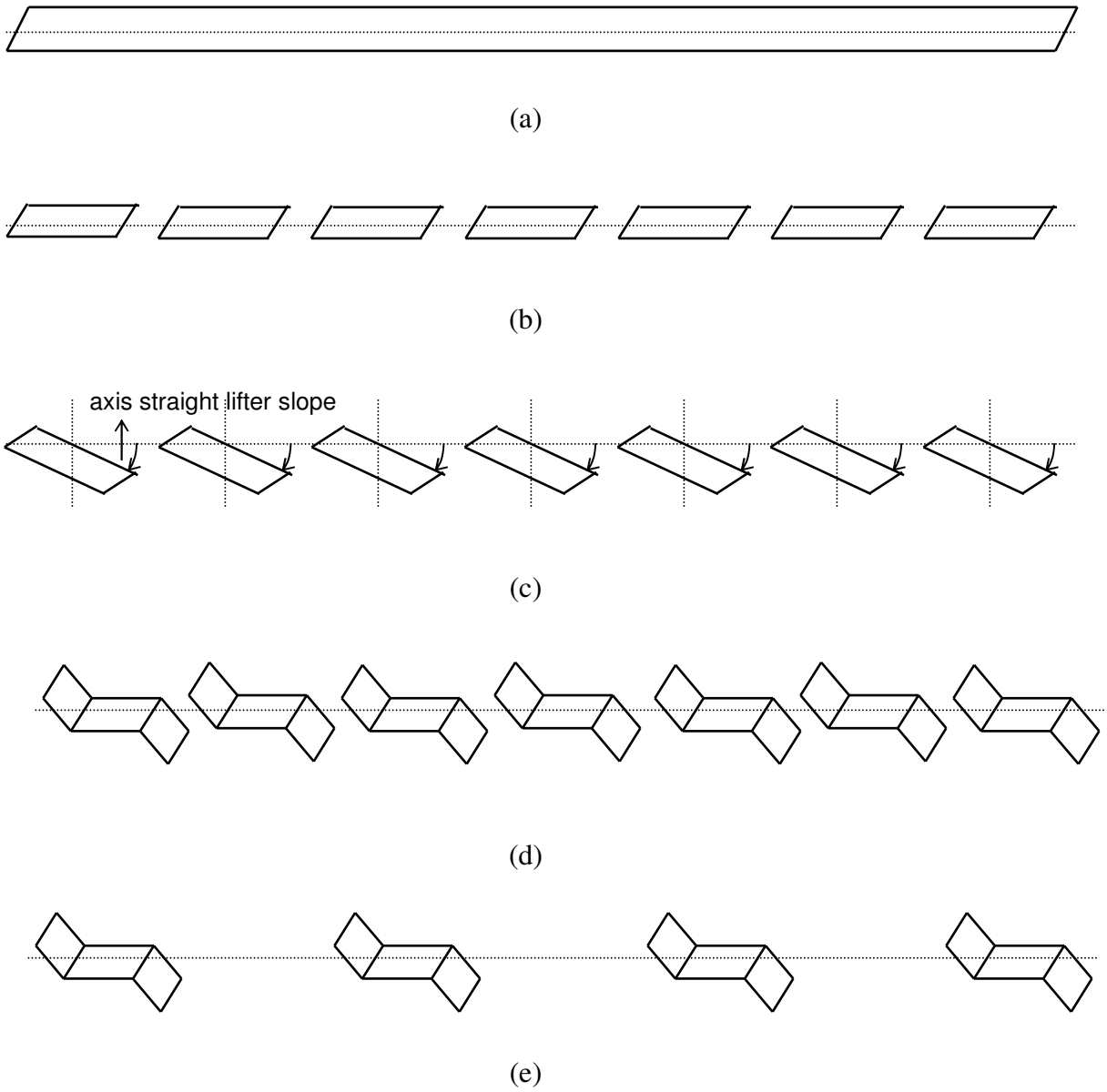

Figure 3.4. Designs and configurations of lifters per row with h_l/D ratio of 0.16 in a horizontal rotating kiln with L/D ratio of 7: (a) single throughout lifters 80 x 2840 mm, (b) horizontal straight lifters 80 x 270 mm, (c) inclined straight lifters 80 x 270 mm, (d) 7 lifters and (e) 4 (out of 7) lifters. (do not scale)

3.3.3 A hot kiln

The hot kiln used in this study is briefly described below. A schematic diagram is shown in Figure 3.5. The system was designed for continuous operation. The pilot unit includes an indirect heat rotary kiln, char and off-gas handling sections.

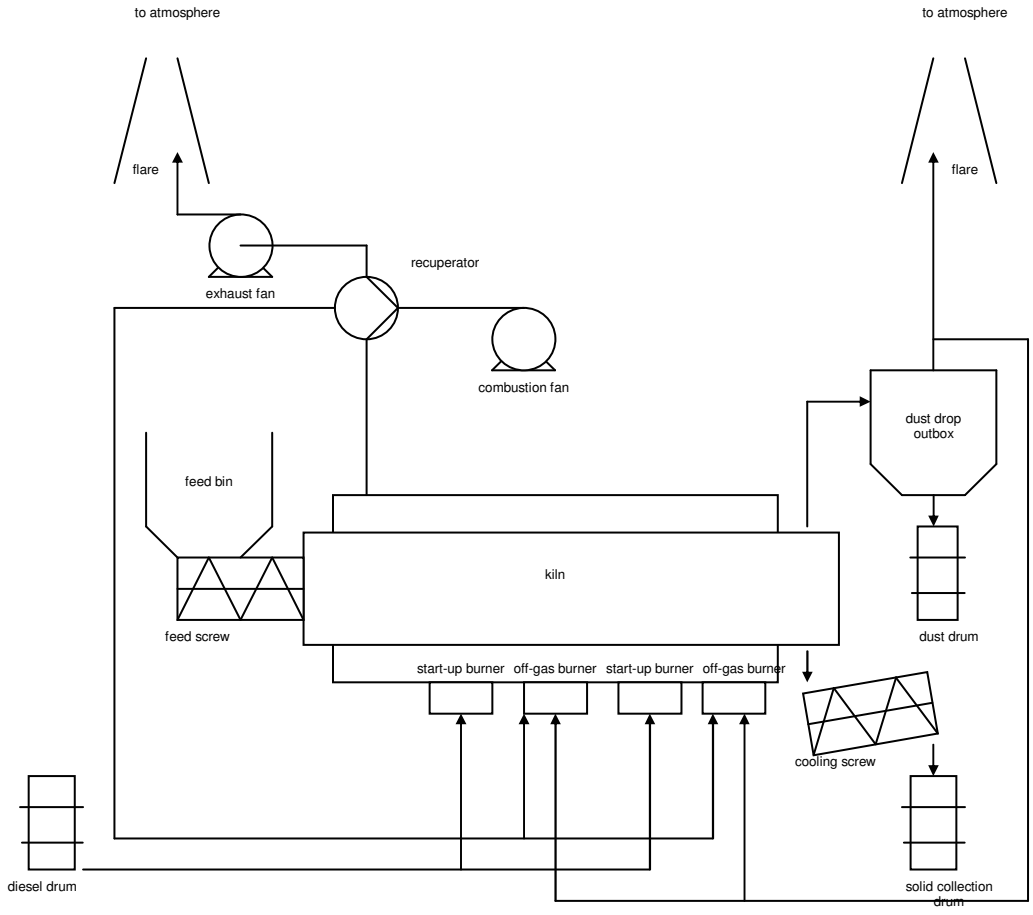

Figure 3.5. Pilot plant basic flow sheet (do not scale)

The main part of the 3.98 m long x 0.51 m outer diameter rotary kiln has a 6 mm thick tube with an adjustable motor driving the kiln and a screw feeder at the base of the

hopper. The kiln case is lined with a 75 mm thick layer of insulating ceramic fiber. The kiln has 21 segmented lifters (7 lifters per row, lifter height of 80 mm, spacing of 488 mm between all lifters), fix feed and discharge end (helix) constrictions. The heat tube is a rotating tube driven from the discharge end by a gearbox and motor.

Material travels through the heat tube and was heated to a monitored and controlled temperature of 800°C at the kiln inlet section and excess oxygen level at the exhaust section by manipulating the amount of recycled off-gas and preheated air. The temperature measurement is located on the outside skin surface of the heat tube. The temperature of the material reaches approximately 873°K.

The solid product is collected in a jacketed cooling screw conveyor. This removes a considerable amount of the heat in the material before it drops into a sealed 150 L collection kiln which then stood on top of a digital platform balance. A slide-gate valve mounted between the kiln and cooler was used to isolate the kiln when it requires replacement. Operators move the kiln using a forklift and seal it, whilst replacing it with an empty kiln.

The off-gas discharges out of the top of a disengagement chamber at the discharge end of the kiln. The gas then proceeds through a dust drop out box. By allowing the velocity of the gas to drop to very low speeds, dust particles settle in the chamber and into a kiln below. If combustible, the off-gas from the dust drop out box may be recycled for heat recovery.

Air to kiln burner is drawn in through a forced-draught fan. Combustion air is then preheated by running counter-current through the shell-side of a shell and tube recuperator mounted on the kiln combustion exhaust.

For characterization the various axial heat flows within the kiln and model validation purposes, the pilot unit were also designed to measure 6 designated locations at a kiln

cross-section, as shown in Figure 3.6. The 3 mm diameter type-K shielded thermocouples are directly mounted at 30 (6 x 5) designated locations and clustered into three data takers. The five axial distances from the entrance of the kiln are 670 mm, 1530 mm, 2020 mm, 2570 mm and 3100 mm respectively. The first two designated locations (1 and 2) are fixed to the kiln; the others (3, 4, 5 and 6) are attached to a thermocouple holder and thus rotated with the kiln. The designated transverse location no 2 is 5 mm from the outer wall. A stand alone and internal power data takers, DT80's, were used featuring USB memory stick support for data acquisition and logging.

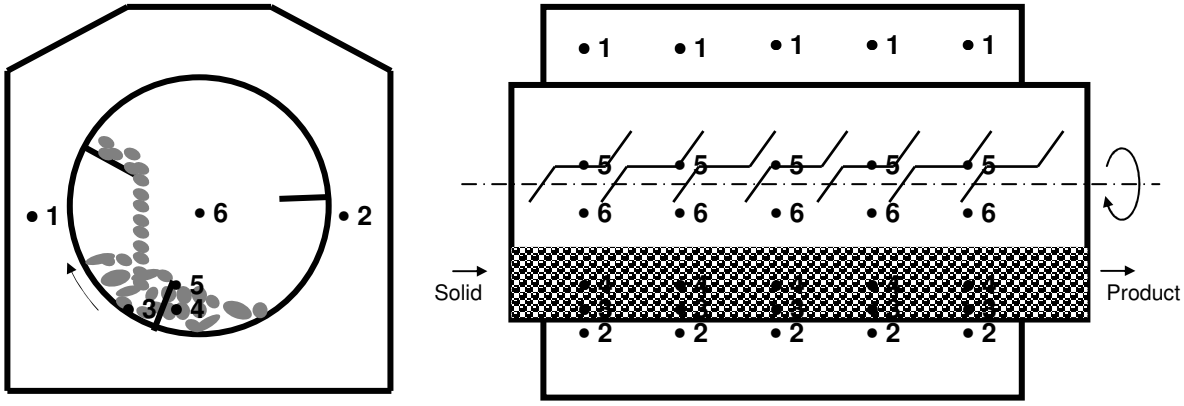

(a) (b)

Figure 3.6. A pilot hot kiln showing the designated (a) transverse and (b) axial locations of the thermocouples: (1) flue gas, (2) outer wall, (3) inner wall, (4) bed, (5) lifter and (6) freeboard gas. (do not scale)

3.4 Image processing

The degree of axial dispersion along the kiln length was tracked by opening the windows and taking digital photos of the surface tracers/bulk mixture each being 3648 x

2736 pixels (3648 pixels along the axis of rotation, 2736 pixels along cross-section). Each image in RGB-colour format was pre-processed using Adobe Photoshop CS2 as shown in Figure 3.7a. The visible part of the kiln wall and lifters were eliminated and filled with white colour as shown in Figure 3.7b. Tracers and tracers/bulk mixture were selected and coloured black as shown in Figures 3.7c and 3.7d. The last two separated digital images were converted to 8-bit colour format using ImageJ 1.39. All images were saved as sequential files. By using threshold method (Russ, 2002), the total area of tracers/bulk mixture and tracers in pixels were determined using UTHSCSA ImageTool 3.0. From the counted pixels, the surface concentration of tracers for each image can then be obtained.

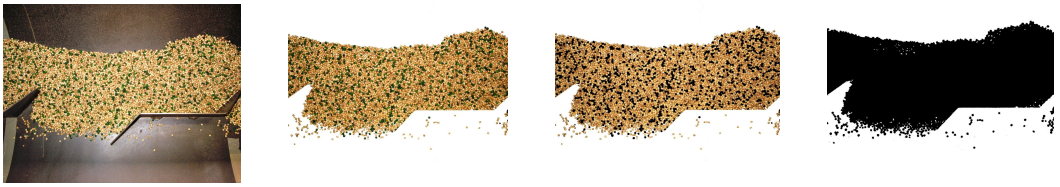

(a) (b) (c) (d)

Figure 3.7. Image processing steps to get the threshold of the surface tracer fractions: (a) original image in RGB colour, (b) tracers/bulk mixtures without visible kiln wall and lifters, (c) surface area of black tracers, (d) surface area of black tracers/bulk mixtures

3.5 Experimental methods

3.5.1 Solid transport

Experiments were performed to measure axial bed depth profile h in m and total hold-up H in kg for steady state flow of granular solid. The system was operated for a given

solid, kiln designs and operating conditions at room-temperature and without freeboard gas. The minimum Re_ω value was limited by total hold-up of ~ 80 kg and total kiln volumetric filling fraction of ~20%. It was found the kiln rotational speed varies between 1.16 and 3.88 rpm which corresponds to 15.0 to 50.0 Hz, giving Fr values from 3.01×10^{-4} to 5.21×10^{-3}. An independent set of experiments verified that the solid feed rate at a given controller setting was constant and reproducible for each solid.

During the period prior to steady state being reached, the solid were recycled from the discharge back to the feed hopper. This was done to ensure that the level of solid in the feed hopper remained constant. After the system was at steady state when the discharge rate is equal to the feed rate and no longer fluctuated with time, the kiln rotation and screw feeder were then stopped simultaneously.

The bed depth at different axial kiln lengths was measured by opening the kiln windows using a rod and pointer configurations similar to those in previous studies (Sai et al., 1990, 1992; Chatterjee et al., 1983a, 1983b). Measurements were made in between lifters at five distances of 640, 1060, 1905, 2345 and 2845 mm (L/D = 5), six distances of 540, 1008, 1512, 1980, 2628 and 3060 mm (L/D = 7) and eight distances of 730, 1090, 1420, 1860, 2180, 2610, 3040, 3450 mm (L/D = 10) from the kiln feed end. The bed depth within 540 mm from the kiln feed end was not considered due to feeding plate. The axial solid velocity profile along the kiln was determined by dividing the volumetric flow rate of solid by the cross-sectional area of the bed.

In order to measure the total hold-up, the solid in the kiln were discharged mechanically and weighed. The mean residence time and average axial solid velocity can simply be determined by $\tau = H / m$ and $u = L / \tau$. It was verified that the experimental measurements were reproducible by comparison of three independent sets of measurements of the same steady state axial bed depth profile and total hold-up.

3.5.2 Solid mixing

Experiments were performed to determine the degree of axial dispersion for steady state flow of granular solid. The system was operated for a given solid, kiln designs and operating conditions at room-temperature and without freeboard gas. Once steady state was achieved, the kiln rotation and feeder were simultaneously turned off and the tracers were injected from the feeding plate. Tracer initial concentration, mass of pulse injection divided by total hold-up, was kept the same for all experiments. The tracer was carefully injected at the same time as a coherent blob to minimize initial tracer dispersion. Due to feeding plate position, it was found that the tracer was already on the first half window.

Upon injection, the kiln rotation and feeder were restarted, with images being captured from each half window until no tracer on the surface bulk mixture. Effects like shadow or reflection must be prevented by light intensity, optimum positioning of the camera and windows. The position of the camera was adjusted so as to locate the camera perpendicular to the bulk mixture. Each individual digital image is a copy of a certain mixing state in the bulk mixture of a certain time. The photos were taken each time when the rotating windows were on the top kiln position. As a result, 150 – 200 images were extracted for each experiment, depending on the solid, kiln designs and operating conditions.

By processing all the images using the method described in Section 3.4 and obtaining an axial surface tracer concentration for each image, the Peclet number at the end for each half window was calculated using Equation (2.2). As shown in Figure 3.8, it was verified that Peclet number profile based on each half window may reflect the overall behaviour of the system, under the current experimental conditions.

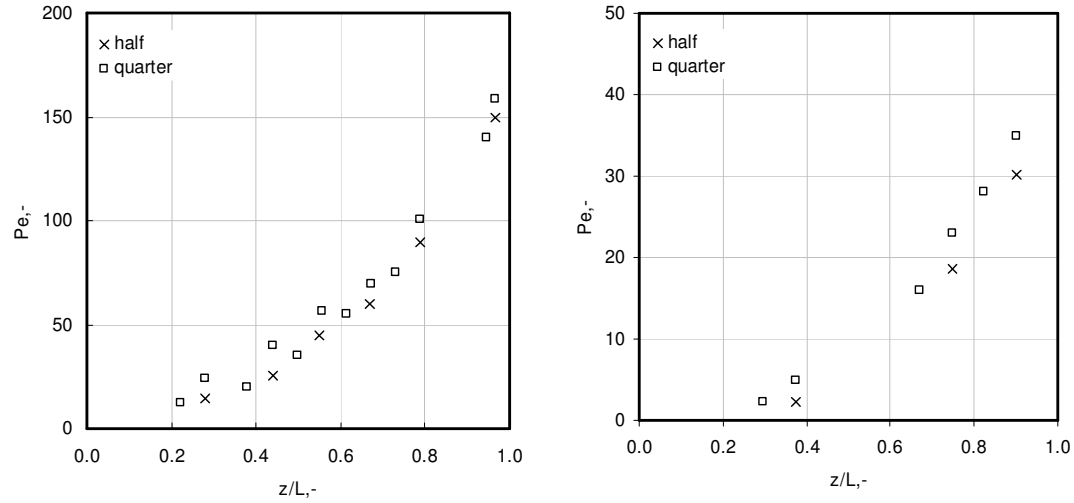

(a) (b)

Figure 3.8. Comparison of *Pe* profiles based on half and quarter opening windows in horizontal rotating kilns with segmented lifters (*hl/D* = 0.08): (a) *L/D* = 10, Re_ω= 1353, (b) *L/D* = 5, Re_ω= 2818.

3.5.3 Heat transfer

Experiments were carried out to measure a set of axial temperature profiles under steady state conditions through an indirectly heated rotary kiln. The low-rank coal sample was fed into the hopper and flows to the discharge end. Each heat transfer run was operated for a given feed rate at monitored and controlled heat tube temperature of 1073°K and excess oxygen level under nearly atmospheric pressure. Apart from the axial temperature measurements at 20-s intervals, solid samples at the discharge end were taken from the collection kiln. The discharge rate was determined over the time once the collection kiln was full.

The kiln was started with diesel fuels The empty kiln was preheated with rotation for two to three hours till the heat tube has reached greater than a setting typically 823°K prior to commencing the feed.

All conditions were then maintained constant until all monitored variables stabilized. All experimental results reported are based on the measured data during the steady-state operations.

The obtained temperature profiles were used to determine the heat flux profiles, relative distribution of various heat transfer modes along the kiln, the overall heat transfer coefficients and heat transfer efficiency, considering all the heat transfer processes from the flue gas to the bed. The importance of each of the heat transfer modes to the overall heat transfer was then evaluated to determine the controlling steps of heat transfer.

3.6 Modelling

A part from experimental work, modelling work was also carried out to simulate solid transport, mixing and heat transfer. To accomplish the mathematical solutions of the models, the Polymath Version 5.1 was used. A preliminary DEM simulation, an emerging simulation tool at particle level, using EDEM Version 1.3 was also performed in a single 3.16 GHz processor mode of a E8500 – processor Intel(R) Core(TM) 2 Duo CPU running 3.25 GB of RAM.

3.7 Summary

The chosen methodology to investigate the heat transfer mechanisms in an indirectly heated rotary kiln with segmented lifters are described in this chapter. Systematic investigation of the solid transport and mixing will provide crucial information for developing the predictive tool of kiln design and scaling.

The utilisation of different techniques for cold and hot experiments enables the isolation of the comprehensive analysis for both solid transport and mixing from heat transfer. A combination of these techniques used in an innovative approach of the problem will provide a better understanding of the overall heat transfer mechanisms.

Chapter 4
Solid Transport

In this chapter, dimensional analysis was performed and a systematic experimental program was then carried out using the cold kilns under steady state condition to quantitatively investigate the effect of segmented lifter configurations, helix and design equations on solid transport. The study considers various kiln designs, kiln operating conditions and solid physical properties. The key solid transport variables to be measured were total hold-up and bed depth profile. The modelling and simulation work include three parts: (1) a preliminary DEM simulation, (2) a theoretical transport model and (3) dimensionless empirical correlations.

The solid, kiln design and operating condition parameters can affect the bulk solid transport variables, namely total hold-up H in kg, mean residence time τ in s and axial solid velocity u in m/s. These key solid transport variables are generally a function of kiln design (kiln length L in m and kiln diameter D in m), kiln operating conditions (feed rate m in kg/s, kiln rotational speed ω in rad/s), solid characteristics (mean particle size d in m, particle bulk density ρ in kg/m^3, particle static angle of repose ϕ in radian), the acceleration of gravity g in m/s^2 and lifter geometries (lifter height h_l in m)

Based on Buckingham's Π theorem (Munson et al., 2006), a dimensional analysis has been carried out. The following applicable correlations are developed among a set of dimensionless numbers:

$$C_H = \frac{H}{\rho D^2 L} = \Phi_1\left(\phi, \frac{d}{D}, \frac{L}{D}, \frac{h_l}{D}, \frac{\omega^2 D}{g}, \frac{\rho\omega D^2}{m/D}\right),$$

$$C_\tau = \frac{\tau m}{\rho D^2 L} = \Phi_2\left(\phi, \frac{d}{D}, \frac{L}{D}, \frac{h_l}{D}, \frac{\omega^2 D}{g}, \frac{\rho\omega D^2}{m/D}\right),$$

$$C_u = \frac{u\rho D^2}{m} = \Phi_3\left(\phi, \frac{d}{D}, \frac{L}{D}, \frac{h_l}{D}, \frac{\omega^2 D}{g}, \frac{\rho\omega D^2}{m/D}\right).$$

The first three prediction equations are $H/\rho D^2 L$, $\tau m/\rho D^2 L$ and $u\rho D^2/m$, known as the solid transport coefficients: C_H, C_τ, and C_u. C_H is a ratio between volumetric hold-up and kiln volume. In practical applications, C_H is generally replaced by total kiln volumetric filling fraction f, with a simple conversion of $f = C_H \times (4/\pi)$.

The six design equations are ϕ, d/D, L/D, h_l/D, $\omega^2 D/g$ and $\rho\omega D^2/(m/D)$. The first and second groups denote the solid characteristics. The third and fourth groups denote the geometric ratio of the system. The fifth and sixth groups denote the dynamic ratio of the system. The fifth group is Froude number Fr, $\omega^2 D/g$ *or* $\omega^2 R/g$, which is the ratio between inertial and gravitational forces. The sixth group corresponds to the rotational Reynolds number Re_ω, i.e. the ratio between inertial forces and the resistant forces which the solid have to overcome.

The axial profile of velocity along the kiln u_{local} in m/s is determined by dividing the volumetric flow rate of solid Q in m^3/s by the cross-sectional area of the bed A_{bed} in m^2. In a dimensionless form, u_{local} is replaced by D^2/A_{bed}, known as the local solid transport coefficient $C_{u,local}$ in which A_{bed} is a function of bed depth.

4.1 Effect of segmented lifter designs, lifter configurations and helix on prediction equations and axial bed depth profile

In this section, a systematic experimental program was carried out using the cold kilns to quantitatively investigate the presence (inclined kiln without lifters) and effect of segmented lifter designs (folded lifter section and lifter slope), lifter configurations (single throughout lifters, number of lifter per row) and helix on solid transport. All experimental result plots are limited for glass bead and/or sand which are two extreme cases.

4.1.1 Inclined kiln without lifters

All experimental studies dealt with solid transport through inclined rotating kilns without lifters as shown in Table 2.1. However, design variables of rotating kilns and its value as well as matrix combinations greatly vary between authors. In the present study, the effect of the axis kiln slope on solid transport in a rotating kiln (L/D = 7) without lifters was investigated and fairly compared with segmented lifters.

Figure 4.1 shows the impact of axis kiln slope without or with segmented lifters on solid transport of sand under various Re_ω. The f in a horizontal kiln with segmented lifters is lower than the ones without lifters at the same Re_ω (Figure 4.1a). The solid movement in a kiln with segmented lifters is dominantly driven by physical push towards kiln discharge end. As axis kiln slope increases from 0° to 0.5°, f decreases. This is understandable because higher Re_ω translates into greater inertial forces (mainly due to kiln rotational speeds) and leads to faster solid transport therefore lower f.

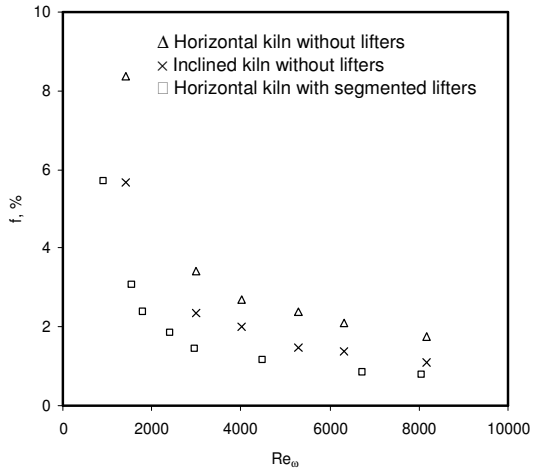
Δ Horizontal kiln without lifters
× Inclined kiln without lifters
□ Horizontal kiln with segmented lifters
f, %
Re$_\omega$
0
2
4
6
8
10
0
2000
4000
6000
8000
10000

(a)

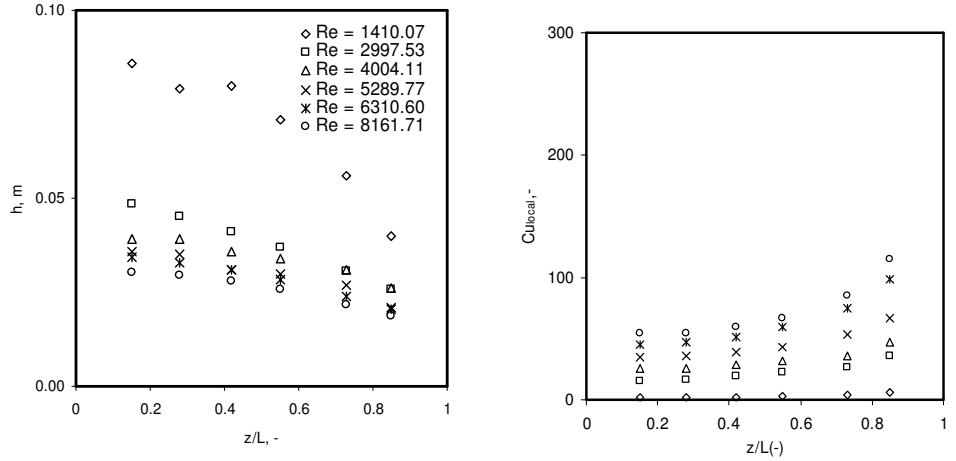
◇ Re = 1410.07
□ Re = 2997.53
△ Re = 4004.11
× Re = 5289.77
✳ Re = 6310.60
○ Re = 8161.71
h, m
z/L, -
Cu$_{local}$, -
z/L(-)
0.00
0.05
0.10
0
0.2
0.4
0.6
0.8
1
0
100
200
300

(b)

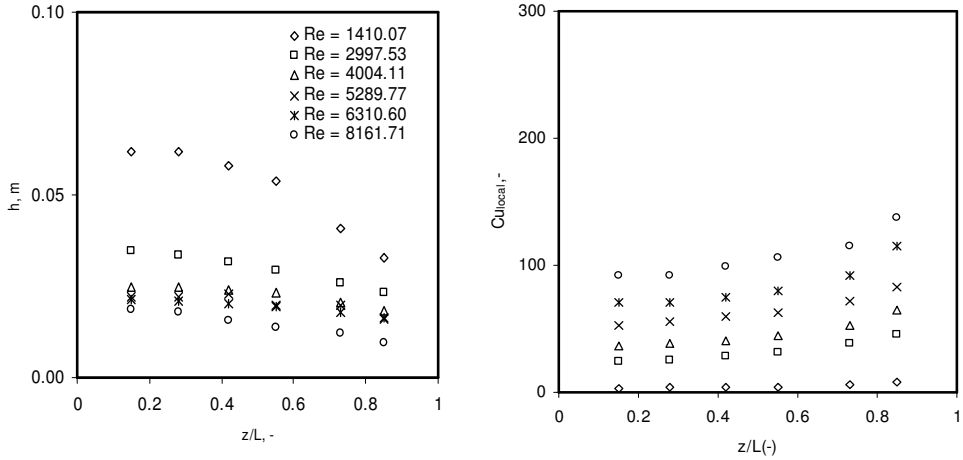
◇ Re = 1410.07
□ Re = 2997.53
△ Re = 4004.11
× Re = 5289.77
✳ Re = 6310.60
○ Re = 8161.71
h, m
z/L, -
Cu$_{local}$, -
z/L(-)
0.00
0.05
0.10
0
0.2
0.4
0.6
0.8
1
0
100
200
300

(c)

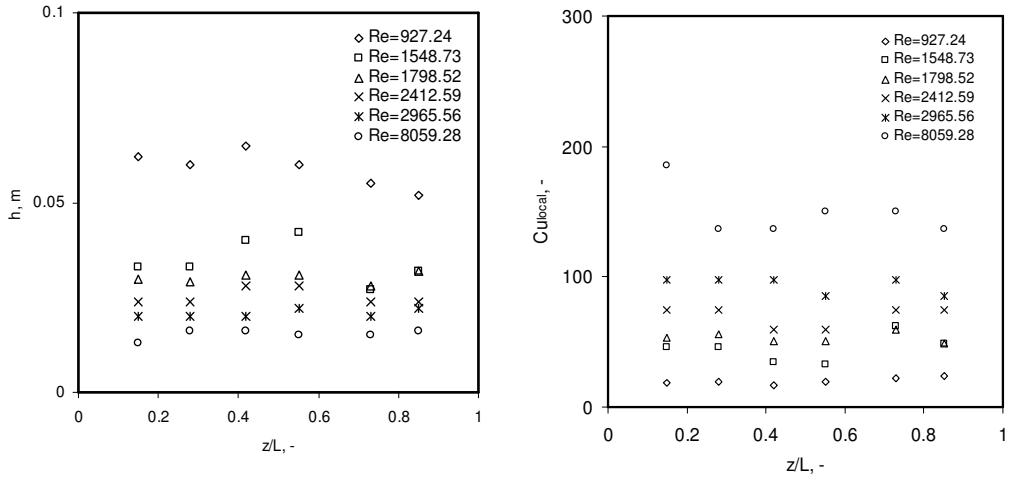

(d)

Figure 4.1. The f, h and C_{ulocal} of sand in a rotary kiln (L/D = 7) without and with segmented lifters (h_l/D = 0.16): (a) f vs Re_ω at different axis kiln slopes without and with segmented lifters; h and C_{ulocal} vs z/L under various Re_ω in: (b) a horizontal kiln without lifters, (c) an inclined kiln without lifters, (d) a horizontal kiln with segmented lifters

The bed depth profile increases with f. For kilns without lifters with inclined bed depth profiles (Figures 4.1b and 4.1c), solid are transported faster in inclined kilns compared to horizontal kilns. It is possible that the increasing axis kiln slope causes the increment of the gravitational forces component in the axial direction of individual particle during cascading. Governed by conservation theory, $d(\rho.u_{local}.A_{bed})/dz = 0$, lower bed depth corresponds to larger axial local velocity and smaller f, which finally causes a decrease in residence time.

In case of a rolling mode in transversal bed motion, the axial transport of solid in kilns without lifters mainly occurs in the thin active layer of bed surface follows the steepest line of descent (Saeman, 1951). Within the passive layer (sub-surface), the bed is close packed and the particles rotate with the kiln at fixed radius and axial position; this is plug flow and particle interaction is limited. As Re_ω increases, particles entering the active layer per unit time increase, which further results in the increase of the particle's axial displacement and the decrease of f.

The results indicate that the presence of segmented lifters are more effective in enhancing solid transport toward to kiln discharge end by disturbing the passive layer with flat bed depth profiles and higher Cu_{local} (Figure 4.1d) considering underloading regimes at $f <$ ~10%.

4.1.2 Lifter configurations

The lifters configurations, designated by the horizontal rotating kiln with segmented lifters and single throughout lifters, inevitably affect the axial transport of solid. Compared to segmented lifters, there are only three single throughout lifters in total with width of 2.84 m at the same h_l/D ratio of 0.16 as shown in Figure 3.4a. Figure 4.2 presents the variation of f and h of glass bead under various Re_ω in underloading regimes. The f of a kiln with single throughout lifters throughout the kiln is remarkably higher than segmented ones with non-uniform h.

Unlike segmented lifters, single throughout lifters have more contact surface area with solid bed but only to scoop, lift and spill the granular solid at the same axial kiln positions. In addition, the influence of single throughout lifters on axial solid transport can be explained by their similarity to the horizontal kiln without lifters whose influence has been already tested to be significant (Figure 4.1a). These mechanisms cause f of a horizontal kiln with single throughout lifters is higher than the one without lifter.

In underloading regimes at $f <$ ~10 %, the single throughout lifters have the capability to scoop, lift and spill all solid bed. That is, the entire throughput can be transported by cascade motion which utilizes the entire cross-section of the kiln. However, there is little solid bed left on the bottom of the kiln which is an undesired operating condition for indirectly heated rotary kilns.

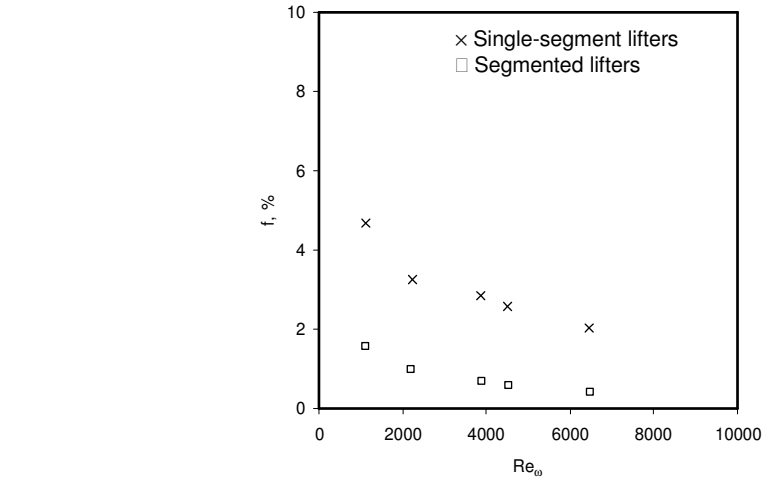

(a)

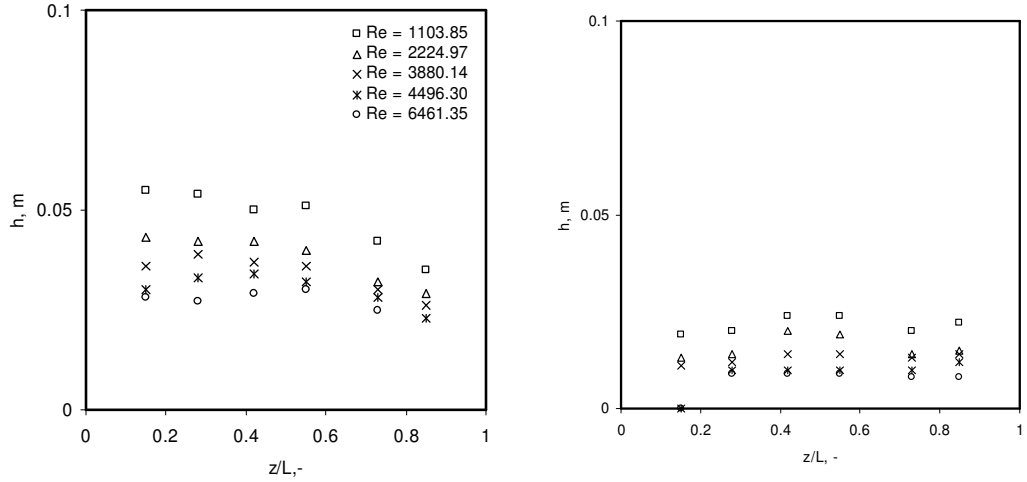

(b) (c)

Figure 4.2. The *f* and *h* of glass bead in a horizontal rotating kiln (*L/D* = 7): (a) *f* vs Re_ω at different lifter configurations; *h* vs *z/L* at various Re_ω with: (b) single throughout lifters and (c) segmented lifters

Therefore, in comparison to horizontal kilns without lifters or with segmented lifters, it may be concluded that the presence of single throughout lifters significantly increases *f*

of granular solid, which was observed in previous experimental studies (Afacan and Masliyah, 1990; Hogg et al., 1974; Pan et al., 2006; Li et al., 2002a), leading to non-uniform bed depth.

4.1.3 Folded lifter section

The impact of the segmented lifters without folded lifter sections, namely segmented straight lifters, on axial granular solid transport in horizontal rotating kilns is shown in Figure 4.3. In addition to width b_3 of segmented lifter (Figure. 3.3), the segmented straight lifters were extended by 0.055 m for each side to compensate the absence of the folded lifter sections. At the same h_l/D ratio of 0.16, the segmented straight lifters lead to a higher f (Figure 4.3a) and non-uniform bed depth profiles (Figure 4.3b). With less contact surface area, the influence of segmented straight lifters on axial granular solid transport can be explained by their similarity to the single throughout lifters whose influence has been already tested to be notable (Figure 4.2a).

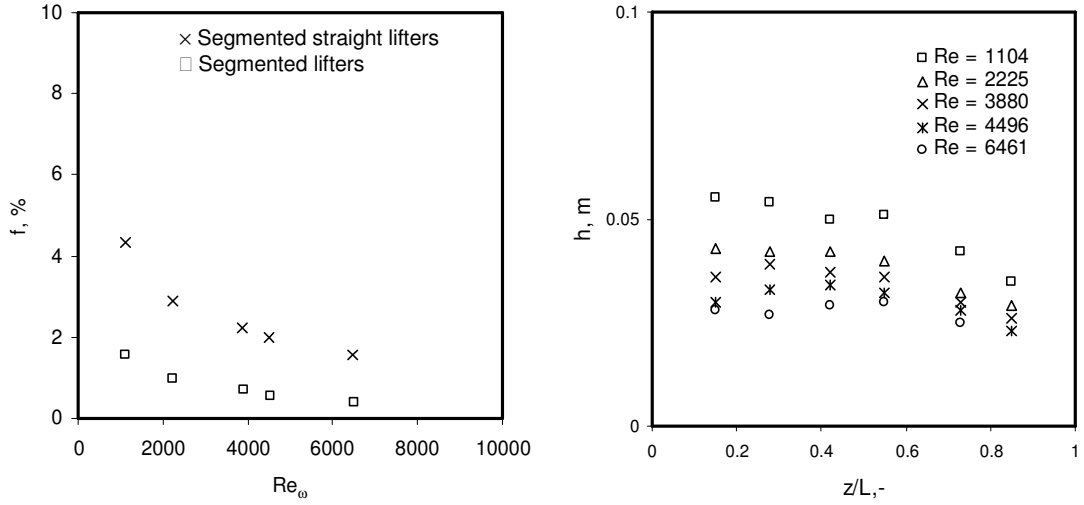

(a) (b)

Figure 4.3. The f and h of glass bead in a horizontal rotating kiln (L/D = 7): (a) f vs Re_ω at different segmented lifters, (b) h vs z/L at various Re_ω with segmented straight lifters

Compared to segmented lifters, small proportions of the solid was pushed along the bed arc length and spilled in the negative (toward to kiln discharge end) and positive (toward to kiln feed end) axial kiln directions with segmented straight lifters. That is, the net axial transport is close to zero. The results indicate that the usage of folded lifter sections is an effective method to largely push and spill in the negative axial kiln directions, leading to uniform bed depth profiles (Figure 4.2c).

4.1.4 Axis straight lifter slope

Conventional rotary kilns (Afacan and Masliyah, 1990; Hogg et al., 1974; Li et al., 2002a; Pan et al., 2006), typically utilise single throughout which are parallel to the axis of the kiln. Thus, for enhancing the axial solid transport, the kilns must be inclined. The only study in the past was done by Pan et al. (2006). Pan et al. (2006) obtained experimental results on total hold-up measurements in a horizontal kiln with inclined lifters which are similar to the conventional inclined kilns without lifters. The experimental range of lifter slopes varied from 3.2° to 7.2° using a relatively short kiln (*L/D* ratio of 2.61) with 12 rows of lifters. This study also carried out a set of experiments on the effect of present axis segmented straight lifter slopes (Figure 3.4c) on the axial bed depth and total hold-up.

The axis straight lifter slopes have significant influences of the axial transport behaviour of solid. Figure 4.4a illustrates the impact of lifter slopes on f of sand and glass bead with various Re_{ω}. It is obvious that the f decreases with an increase of lifter slope from 12° to 22°. This finding is consistent with those acquired by Pan et al. (2006). Besides, as lifter slope increases, the straight lifters are capable to enhance axial solid transport even more than with segmented lifters. Not surprisingly, this is due to higher pushing forward surface area per straight lifter of 2.16×10^{-2} m^2 compared to folded lifter sections of 8.80×10^{-3} m^2. Moreover, the straight lifters slope can be tuned to have same

f values in a kiln with or without segmented lifters within the range of cases considered in this study.

However, the present experimental results show that the *f* values differences are smaller at a higher lifter slope, especially from 15° to 22°. This suggests that at a higher lifter slope, instead of push towards the kiln discharge end, the lifters start to hinder particles entering and exiting the lifters. Therefore, it will cause an increase of *f*.

Unlike with segmented lifters in underloading regimes at $f <\sim 10$ %, the bed depth is uniform only at critical lifter slope. The value of the critical lifter slope is dependent on the granular solid characteristics. The comparisons of bed depth along the kiln under various Re_ω at different lifter types for sand and glass bead are shown in Figures 4.4b and 4.4c. The critical lifter slopes for both solid are slightly different. The critical lifter slope is smaller for granular solid with lower ϕ and higher *d*, e.g. ~ 12° for glass beads and ~ 15° for sand, respectively. In an extreme case with a lifter slope of 90°, a segmented straight lifter can be regarded as an end restriction dam or one circular rib. Literatures have shown that the influence on solid transport is significant (Chaterjee et al., 1983a, 1983b; Li et al., 2002a; Sai et al., 1990, 1992; Spurling, 2000). Hence, for a higher axial pushing effect toward to kiln discharge end, that is not worthwhile to decrease folded angle α of 135° (Figure 3.3).

4.1.5 Number of lifters per row

Figure 4.5 demonstrates the dependence of *f* and *h* on the Re_ω considering segmented lifters with two different lifter numbers per row, i.e. four and seven, in a horizontal rotating kiln. This was achieved by simply taking off the second, fourth and sixth lifters in each row as shown in Figure 3.4d and Figure 3.4e.

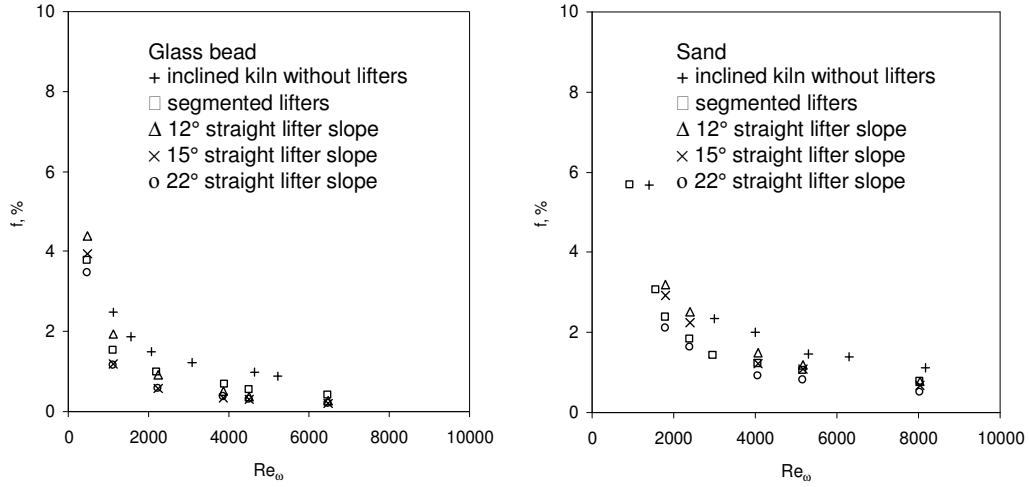
Glass bead
+ inclined kiln without lifters
□ segmented lifters
Δ 12° straight lifter slope
× 15° straight lifter slope
o 22° straight lifter slope
f, %
Re$_\omega$
Sand
+ inclined kiln without lifters
□ segmented lifters
Δ 12° straight lifter slope
× 15° straight lifter slope
o 22° straight lifter slope
f, %
Re$_\omega$

(a)

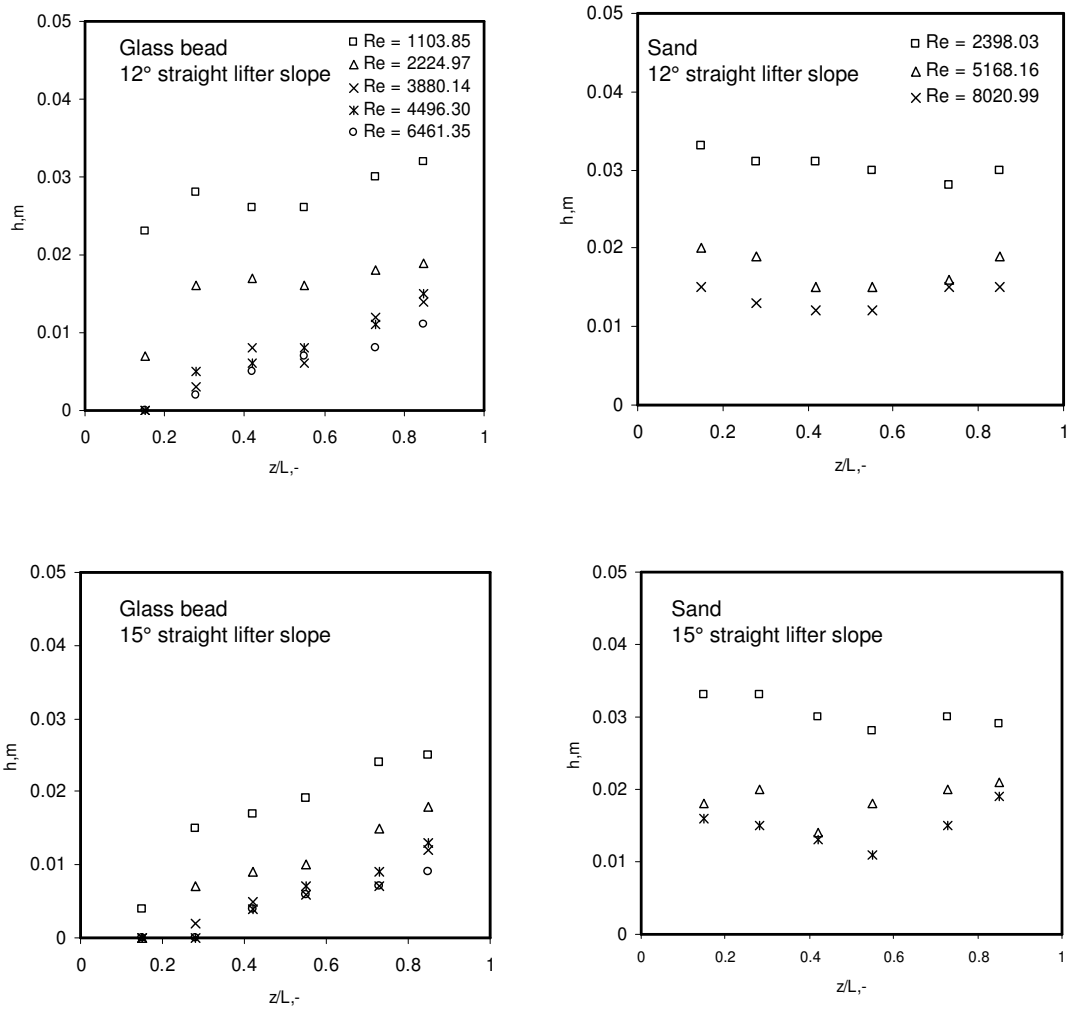
Glass bead
12° straight lifter slope
□ Re = 1103.85
Δ Re = 2224.97
× Re = 3880.14
* Re = 4496.30
o Re = 6461.35
h,m
z/L,-
Sand
12° straight lifter slope
□ Re = 2398.03
Δ Re = 5168.16
× Re = 8020.99
h,m
z/L,-
Glass bead
15° straight lifter slope
h,m
z/L,-
Sand
15° straight lifter slope
h,m
z/L,-

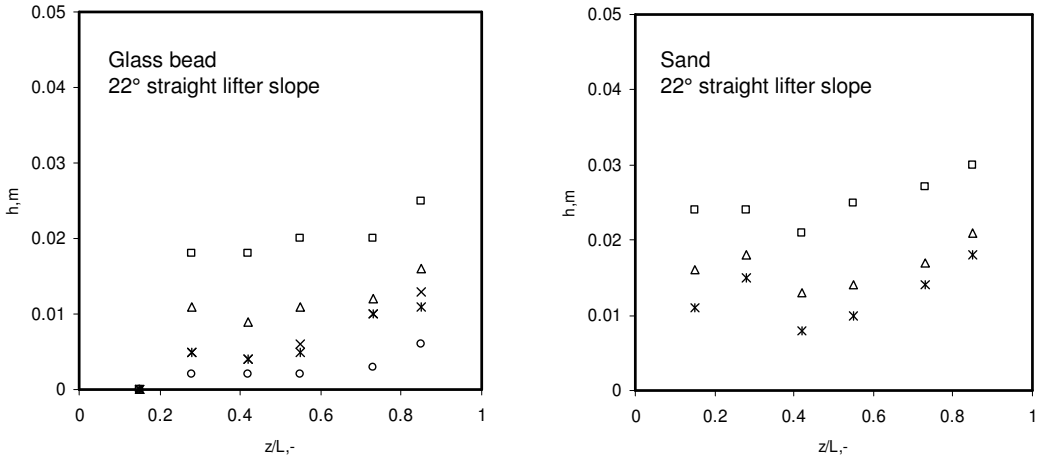

(b) (c)

Figure 4.4. The *f* and *h* of sand and glass bead in a horizontal rotating kiln (*L/D* = 7): (a) *f* vs Re_ω at different lifter types; *h* vs *z/L* at various Re_ω and lifter slopes: (b) glass bead and (c) sand.

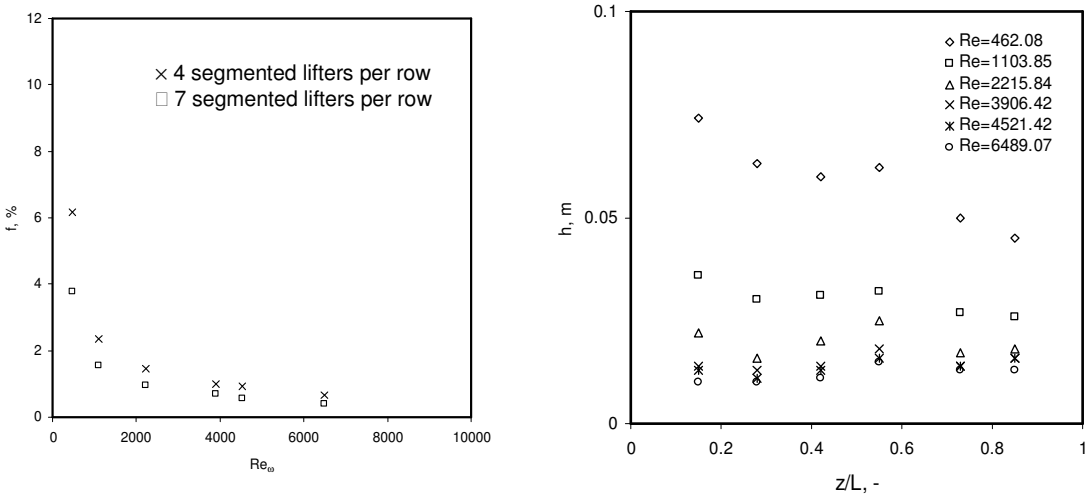

(a) (b)

Figure 4.5. The *f* and *h* of glass bead in a horizontal rotating kiln (*L/D* = 7): (a) Re_ω vs *f* at different segmented lifter numbers per row and (b) *h* vs *z/L* at various Re_ω with four segmented lifters per row

As the number of lifters per row decreases, the *f* increases as shown in Figure 4.5a. It is expected that granular solid near lifters will immediately receive a greater forward force relatively to those further away from lifters. The granular solid further away from lifters are only affected by the resulting forces from granular solid coming from the behind due to the inclined bed (Figure 4.5b). Consequently, at certain axial kiln sections with no lifters, the granular solid start to build-up with lower solid axial velocity as previous findings in a horizontal kiln without lifters. That is, the bed depth profiles resulted in four lifters per row case is non-uniform along the kiln. Comparisons both configurations indicate that minimum number of lifters per row are needed to consistently push granular solid toward to kiln discharge end.

4.1.6 Helix

Installation of a helix at the kiln discharge end acts as an additional flow resistance, leading to an increased *f* (Figure 4.6) and a gradually-increased solid bed depth along the kiln length (Figure 4.7) as Re_ω decreases. The increased bed depth profile decreases axial solid velocity and causes considerable increase of mean residence time. Similar observations were also reported by previous investigators in inclined kilns without lifters (Li et al., 2002a; Sai et al., 1990, 1992).

The impact of installed helix is more pronounced for glass bead than sand. At the same Re_ω, glass bead has smaller mean residence time and higher axial velocity than sand at the same. This is due to glass bead has better flowability than sand. Consequently, the glass beads start to build-up at near kiln discharge end where helix is located.

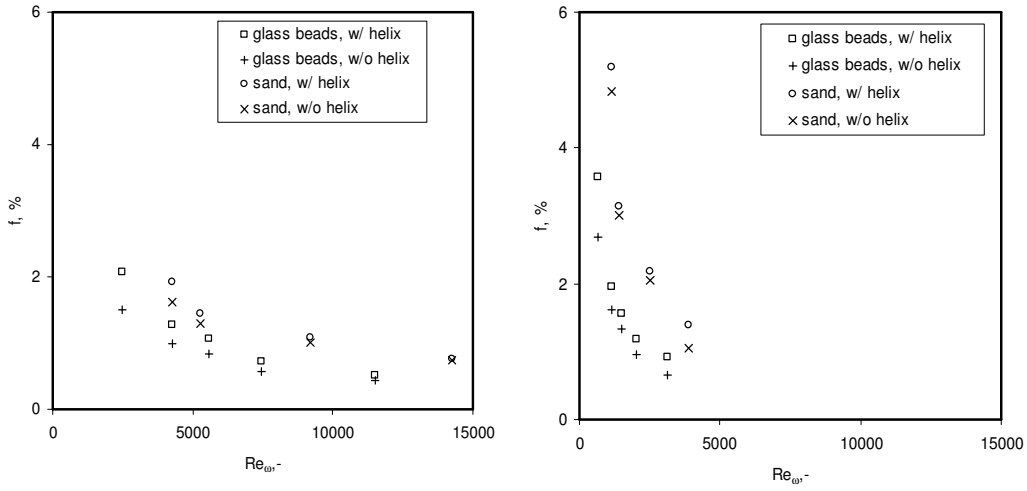

(a) (b)

Figure 4.6. The *f* of glass bead and sand in horizontal rotating kilns with segmented lifters (h_l/D = 0.16) and with or without helix at different Re_ω in horizontal rotating kilns with: (a) *L/D* = 5 and (b) *L/D* = 10.

However, the effect of helix is insignificant at high Re_ω (>~9000) as shown in Figure 4.6a, indicating that under those conditions, the solid flow with less resistance through the helix exit channel. The results show that helix can be an effective device to adjust *f* and solid residence time. Its installation can increase *f* and residence time, particularly near kiln discharge end where helix causes the bed depth profiles be flattened or increased gradually. Together with adjusting Re_ω, therefore the usage of helix is an effective method to maintain flat bed depth profiles of typical industrial solid with poor flowability (i.e. sand in Figure 4.7) at low Re_ω in horizontal rotating kilns with segmented lifters.

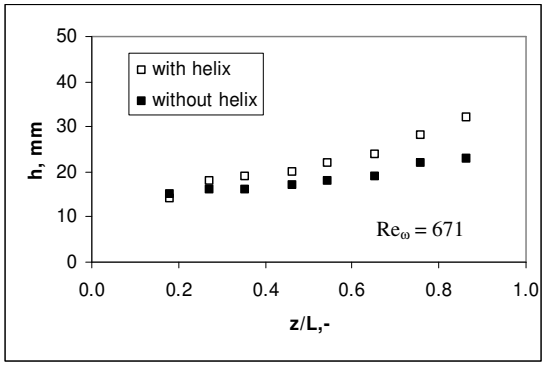
with helix
without helix
h, mm
z/L,-
Re$_\omega$ = 671

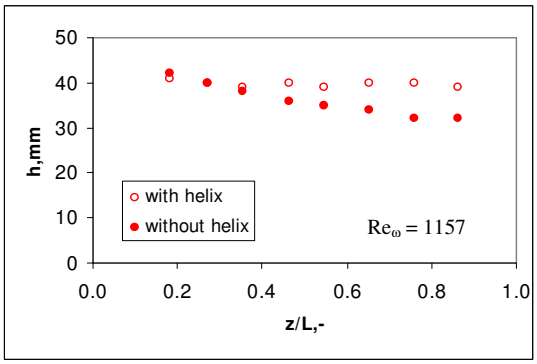
with helix
without helix
h,mm
z/L,-
Re$_\omega$ = 1157

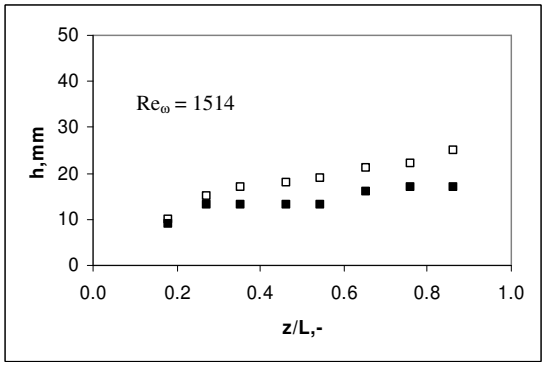
h,mm
z/L,-
Re$_\omega$ = 1514

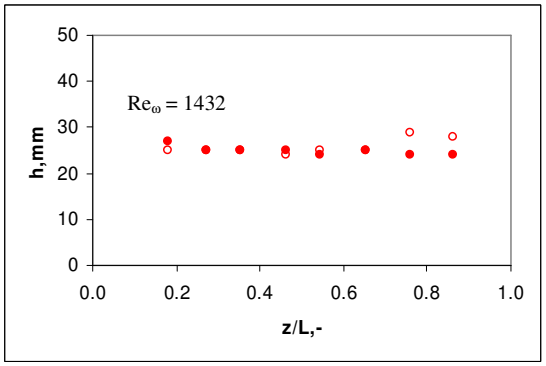
h,mm
z/L,-
Re$_\omega$ = 1432

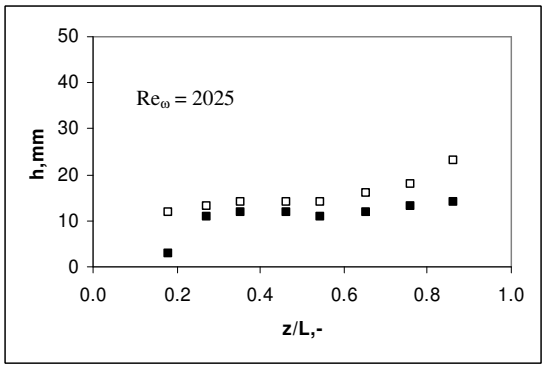
h,mm
z/L,-
Re$_\omega$ = 2025

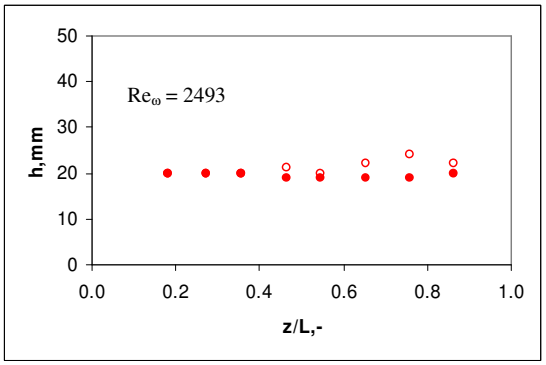
h,mm
z/L,-
Re$_\omega$ = 2493

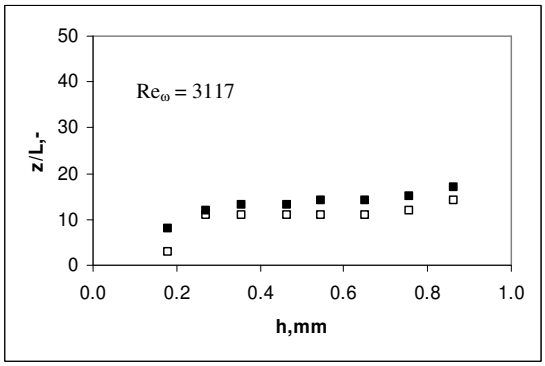
z/L,-
h,mm
Re$_\omega$ = 3117

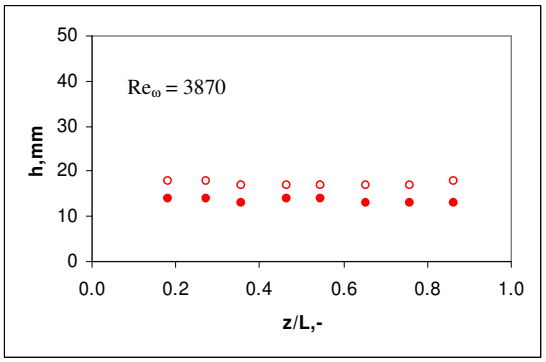
h,mm
z/L,-
Re$_\omega$ = 3870

(a) (b)

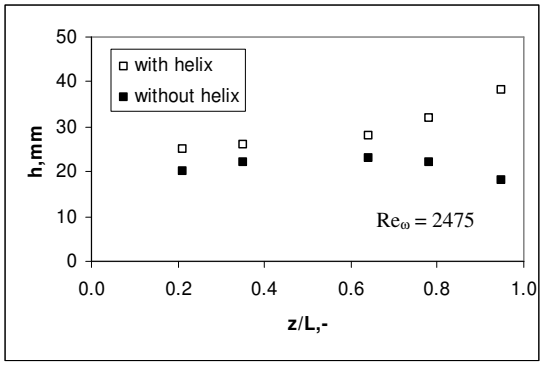
with helix
without helix
Reω = 2475
h,mm
z/L,-

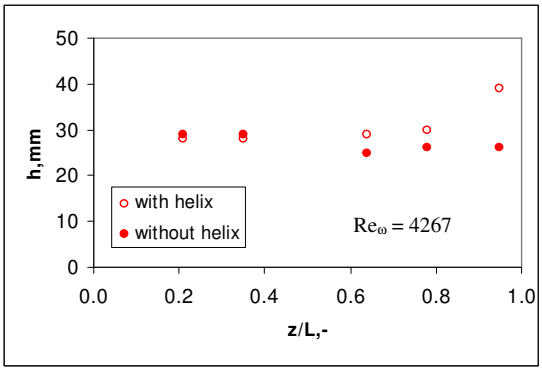
with helix
without helix
Reω = 4267
h,mm
z/L,-

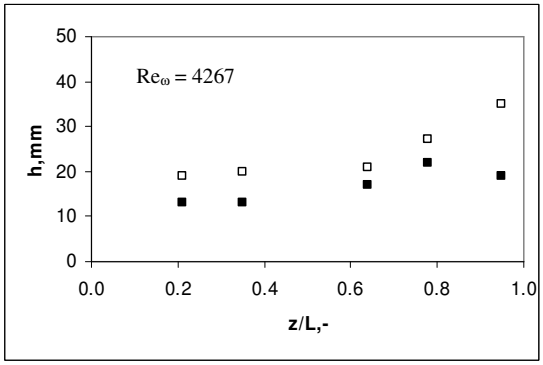
Reω = 4267
h,mm
z/L,-

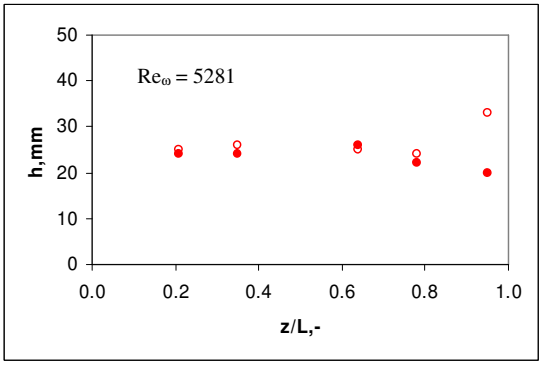
Reω = 5281
h,mm
z/L,-

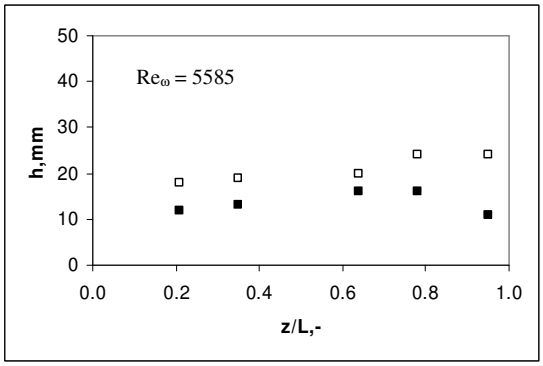
Reω = 5585
h,mm
z/L,-

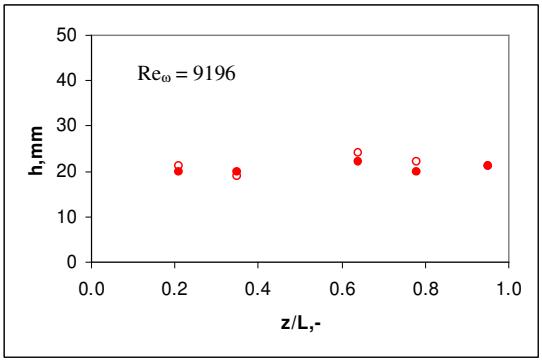
Reω = 9196
h,mm
z/L,-

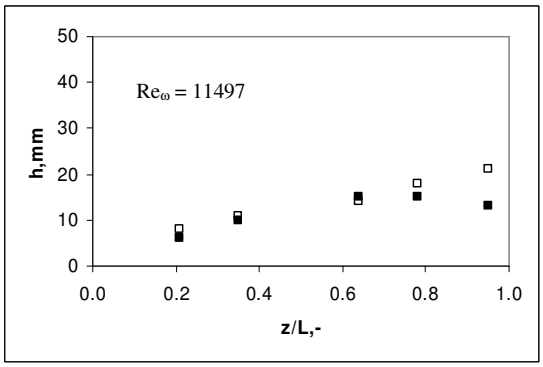
Reω = 11497
h,mm
z/L,-

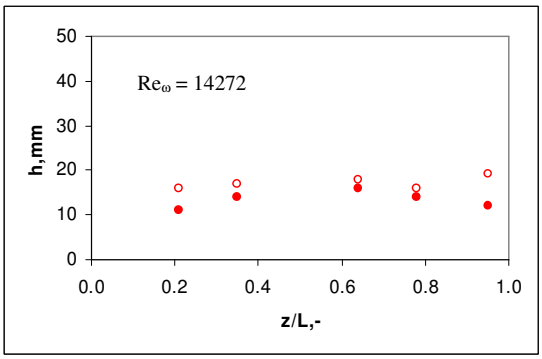
Reω = 14272
h,mm
z/L,-

(c) (d)

Figure 4.7. The axial bed depth profiles in horizontal rotating kilns with segmented lifters and with or without helix at different Re_ω of (a) glass bead and (b) sand in a kiln with L/D = 10; (c) glass bead and (d) sand in a kiln with L/D = 5.

4.2 Effect of design equations on prediction equations in horizontal rotating kilns with segmented lifters

In this section, a systematic experimental program was carried out using the cold kilns to quantitatively investigate the effect of design equations, i.e. dynamic ratio of the system, solid characteristics, geometric ratio of the system, on solid transport prediction equations, i.e. f, C_u.

4.2.1 Dynamic ratios

Figure 4.8 illustrates the dependence of f and C_u in underloading regime (f < 10 %) at different Re_ω. Figure 4.8 clearly shows that f decreases with increasing Re_ω, and there are rapid increase in f for glass bead and sand at Re_ω < ~1500 and ~3000. This is expected because a higher Re_ω leading to faster solid transport therefore lower solid inventory. Higher Re_ω translates into greater inertial forces (mainly due to high kiln rotational speeds) so that lifters have more energy to scoop and lift solid into the upper part of the kiln until its angle of repose and spill the solid under the influence of gravity.

As a result of the folded lifter sections, when the solid are scooped, the solid physically push toward kiln discharge end along the bed arc length, leading to axial solid displacement. The solid then fall from the lifters at the same time and enters into contact

with the bed again and may bounce, slide and roll before being recaptured by the subsequent lifter. The cycle of "scooped-pushed-lifted-spilled" process then repeats itself. Therefore, the segmented lifters employed can largely enhance solid transport by pushing forward and disturbing the passive layer as Re_ω increases.

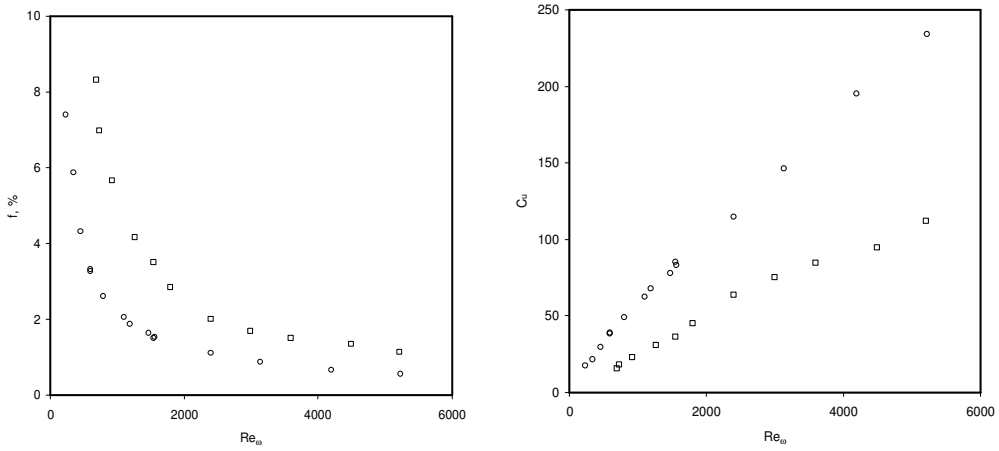

Figure 4.8. The f and C_u in dependence on the Re_ω at underloading regime in a horizontal rotating kiln (L/D = 7) with segmented lifters (h/D = 0.16)
(o = glass beads, = sand).

Figure 4.8 also indicates that f follows an inverse power law with Re_ω (details can be found in Section 4.3.3). Likewise, as shown in Figure 4.8, C_u is also significantly affected by Re_ω .The average axial velocity coefficient increases linearly with Re_ω. In brief, as solid transport is enhanced throughout the kiln at higher Re_ω, the f is lower, leading to expected increase in C_u as there is lower resistance to the transport of solid.

4.2.2 Solid characteristics

Data in Figure 4.9 shows an increase in d/D results in slight decreases in f. This may be due to possibly the increased degree of interlocking of the relatively small solid

(Kramers and Croockewit, 1952). A slightly higher transport resistance of small solid is expected when the solid move towards kiln discharge end in comparison to that of big solid. Nevertheless, f only slightly increased with d/D, indicating that the horizontal kiln with segmented lifters is fairly flexible to handle solid of heterogeneous sizes. However, solid of a higher ϕ has poor flowability and leads to increases in f, as well as decreases in C_u as shown in Figure 4.10. It is understand that sand has the highest f and the lowest C_u compared to other solid. The results indicate that a higher Re_ω is required in order to achieve the same f for granular solid of a higher ϕ, in other words, more energy input is required to drive the kilns.

4.2.3 Geometric ratios

Figure 4.11 illustrates the dependence of f on the Re_ω considering segmented lifters with two different h_l/D ratios of 0.08 and 0.16. The data in Figure 4.11 indicates that the lifter height h_l significantly affect the axial transport of solid. Figure 4.11 clearly shows f decreases with increasing Re_ω. At the same Re_ω, f is higher for smaller lifters. In other words, for smaller lifters, a higher Re_ω, i.e. more energy is needed to achieve the same f.

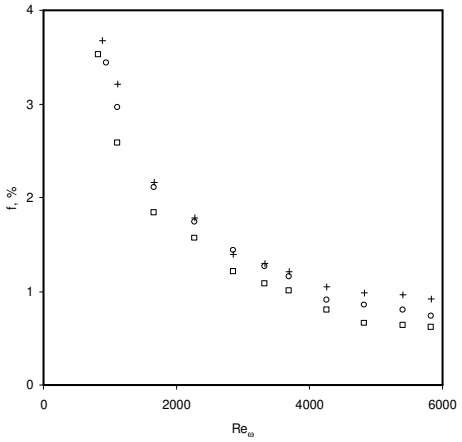

Figure 4.9 The f in dependence on the Re_ω at underloading regime in a horizontal rotating kiln (L/D = 7) with segmented lifters (h_l/D = 0.16)
(urea: + = 2 mm, o = 3 mm, = 4 mm).

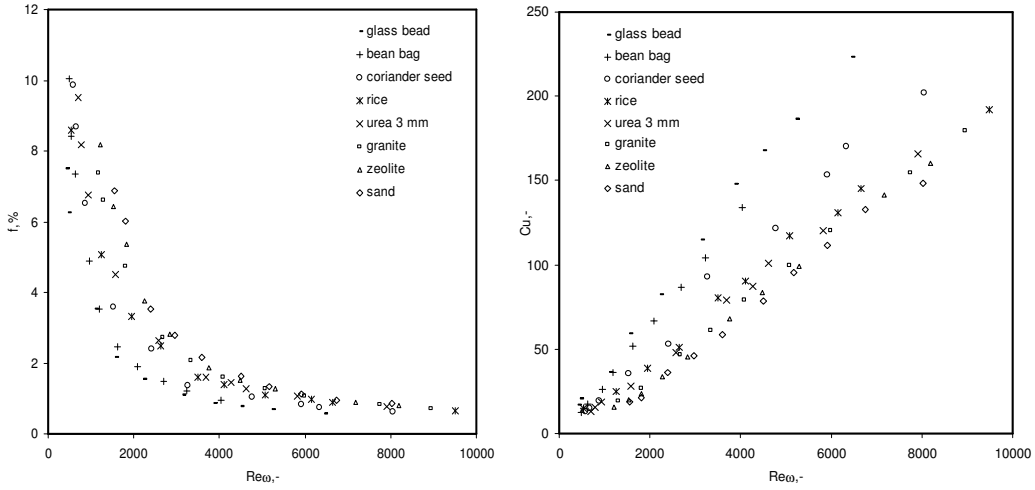

Figure 4.10.The f and C_u in dependence on the Re_ω at various solid in a horizontal rotating kiln (L/D = 7) with segmented lifters (h_l/D = 0.08)

It is interesting to note that at f >3.6 %, the increasing in f with decreasing Re_ω is steeper for h_l/D ratio of 0.08 compared to h_l/D ratio of 0.16. This may be attributed the shift of operation regimes from underloading at f < 3.6 % to design loading and overloading. In addition to axial transport via the folded lifter sections, as observed in Section 4.1.3, there is also additional kilning flow (i.e. flow above the lifters) moves axially via the solid rolling. The solid may sometimes bypasses one or more full lifters before be securely lodged in subsequent lifters.

It is therefore not surprising that the lifters have a greater impact on the solid in underloaded kilns compared to overloaded kilns. When a section of particles is scooped up and pushed forward along the bed arc length by a lifter in underloaded kilns, there are no obstacles from the upper part of the lifter to resist particle transport towards kiln discharge end. This results in the solid travelling at longer distances per push than in overloaded kilns. In overloaded kilns, more interference from the bed is also expected when a particle is pushed forward, especially from bed in the upper part of lifter.

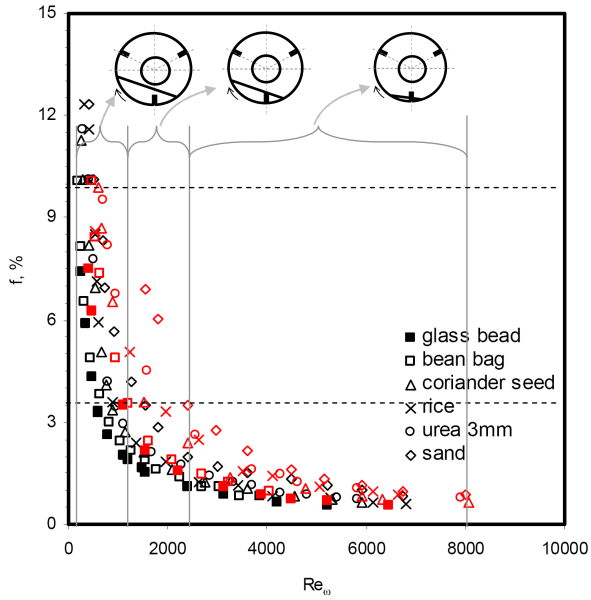

Figure 4.11. The f in dependence on the Re_ω at various solid in a horizontal rotating kiln (L/D = 7) with segmented lifters (black: h_l/D = 0.16, red: h_l/D = 0.08).

Figure 4.12 shows the dependence of f on the Re_ω considering segmented lifters with three different L/D ratios at an h_l/D ratio of 0.16. In general, Figure 4.12 clearly shows the same trends for all kilns that f decreases with increasing Re_ω. At the same Re_ω, f is similar for all kilns. The results indicate that the axial transport of solid is mainly driven by lifters. The effect of L/D on f is not significant.

4.3 Modelling

4.3.1 A preliminary DEM simulation

The DEM simulation was performed using a PC which has single 3.16 GHz dual Core CPU and 3.25 GB of RAM. A 3-D DEM simulation was carried out in a licensed EDEM 1.3 software package. The values of the model parameters are summarized in Table 4.1.

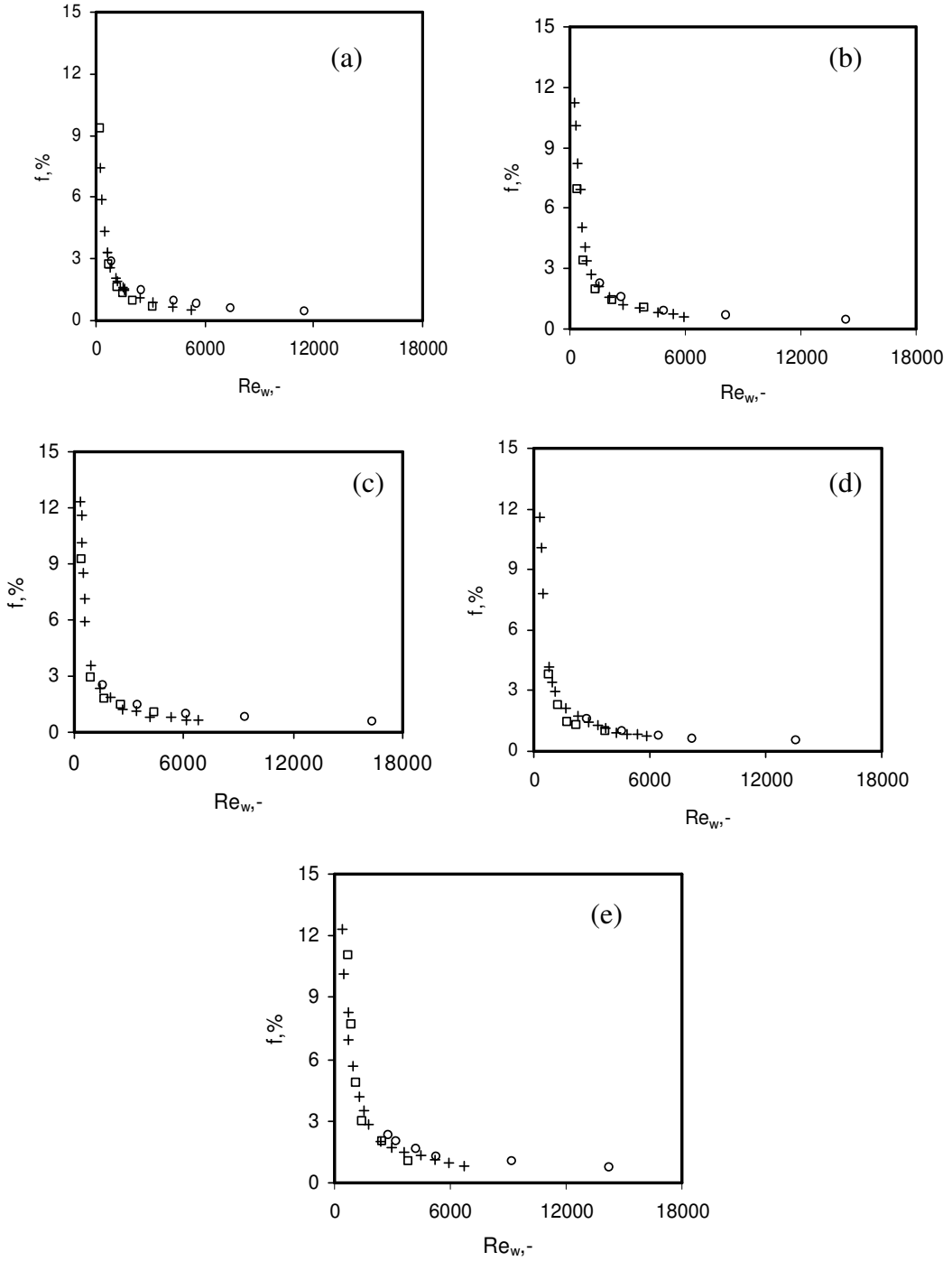

Figure 4.12. The f in dependence on the Re_ω at various kilns designs (L/D: o = 5, + = 7, = 10) with segmented lifters (h_l/D = 0.16): (a) glass bead, (b) coriander seed, (c) rice, (d) urea 3 mm, (e) sand

The model solves Newton's equations of motion, $m_i \frac{d\vec{u}_i}{dt} = \vec{F}_{total,i} + \vec{g}$, for each spherical particle in the system where m_i represents the mass of particles i, $\vec{u}_i$ its velocity, $\vec{F}_{total,i}$ is the total force acting on this particle and $\vec{g}$ is the gravitational acceleration. Vectors are defined in the traditional Cartesian coordinates with fixed space reference for position. The Hertz Mindlin contact model (Mindlin, R.D., 1949) is used for calculating the contact (normal, damping, tangential, tangential damping) forces among particles due to its accurate and efficient force calculation.

Table 4.1
Input Parameters used for the preliminary DEM simulation

Parameters	Values	Parameters	Values
Poisson's ratio p,-	0.2	Particle diameter , m	4E-3
Poisson's ratio w,-	0.29	Particle density, kg/m^3	2200
Shear Modulus p, Pa	2.6E+10	Kiln diameter, m	0.51
Shear Modulus w, Pa	8.0E+10	Kiln length, m	3.60
Coefficient of restitution pp, -	0.6	Kiln density, kg/m^3	7861
Coefficient of restitution pw, -	0.7	Kiln rotational speed, rpm	3.88
Coefficient of static friction pp, -	0.1	Particle creation rate, particles/s	230
Coefficient of static friction pw, -	0.3	Time step, s	1E-5
Gravitational acceleration, m/s^2	(0, -9.8, 0)	Initial particle velocity, m/s	(0, -0.58, -0.81)

The particle, kiln and lifter properties (density, Poisson's ratio, shear modulus, coefficient of restitution and static friction) are based on standard values for glass and steel, except for particle diameter. The values for kiln rotational speed, particle creation rate and initial particle velocity were taken from our experiments. Kiln and lifter geometries with curvature mesh was imported and merged from a Pro/ENGINEER software package. The model also considers the kiln rotation and lifter geometries, feeding plate and virtual dynamic surface particle factory. To enable the detection of contacts in active cells, the domain was divided into grid cells with a size twice as the particle diameter.

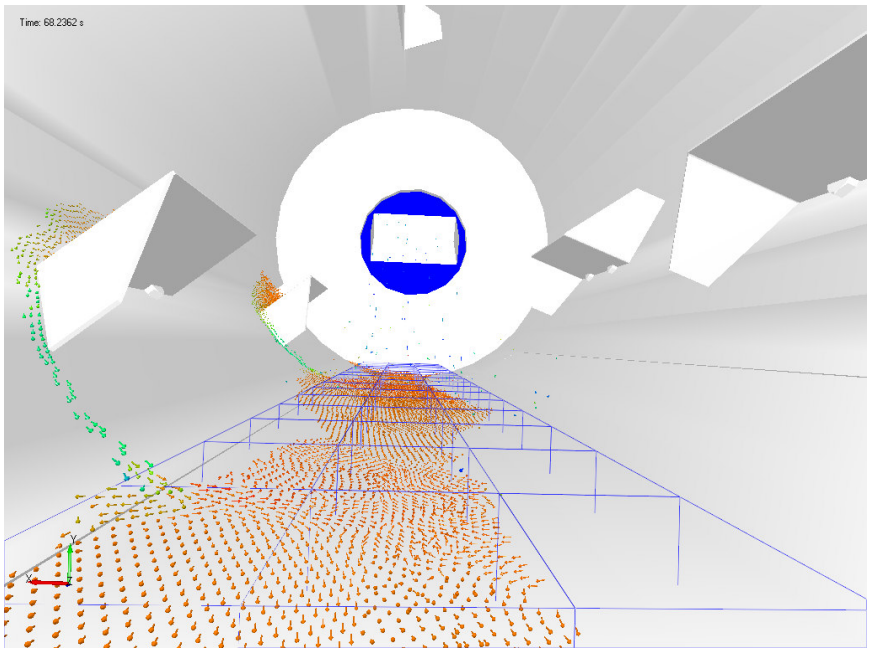

Figure 4.13. Orientation snapshot of a horizontal rotating kiln used for the simulation with particles as vectors, installed segmented lifters (h_l/D = 0.16), feeding plate, virtual dynamic surface particle factory and binning zones

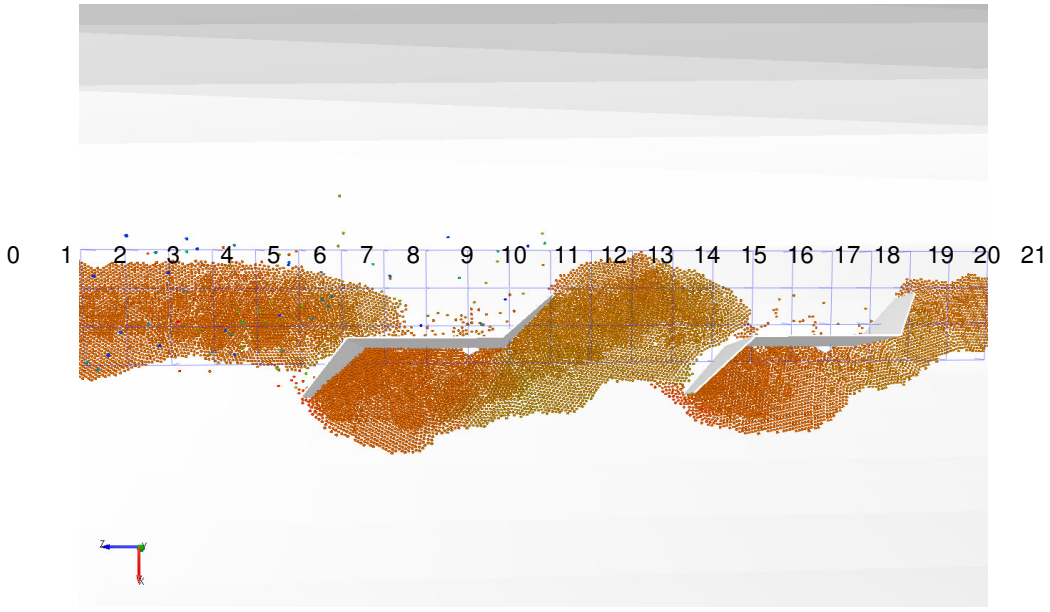

Figure 4.14. Binning zones with 22 zones along the z-direction from 50 to 1100 mm, 1 zone on the y-direction from -225 to 252 mm and 3 zones across the x-direction from -50 to 80 mm

To save computation time, the total domain length was shortened and particle diameter was increased. A domain length was selected that extended 1.2 m down the length of the kiln from the feed end dam, without having to physically shorten the kiln geometry, as EDEM permanently removes any particles which pass outside the domain area. This selected domain length contains an adequate number of lifters to assess their affect on particle velocity profile. By increasing particle diameter from 2 to 4 mm, the required particles creation rate per second reduced significantly from 1800 to 230 for a feed rate of 0.72 kg/min, allowing the simulation to be conducted at a sufficient pass without being too far from the experimental conditions. Rather than based on a single tracer particle, results from the simulation were post-processed on multiple-particle velocities in the z-direction along the kiln within the shortened domain length.

A 3-D internal view of the filled geometries of kiln and segmented lifters is shown in Figure 4.13. Particles are displayed as vectors. This image shows that the kiln length is aligned along the z-direction. This mainly has implications for the axial velocity profiles, as any particles moving toward the kiln discharge end have negative z velocity values.

Plots were only generated for a specific axial section which not intends to be compared quantitatively with the results obtained experimentally. The steady-state condition has not been reached in this study. But the results obtained have already demonstrated the applicability of DEM simulation for solid flow in a horizontal rotating with segmented lifters. In Figure 4.14, the binning zones were created to encompass the bed area from feeding plate to end domain consists of segment–lifter–segment-lifter-segment. The values across the x-direction were averaged.

Axial velocity profiles were taken at several time increments as the lifters move through the solid bed. Of key interest is the segment and folded lifter sections areas as this should be push effect towards to –z-direction. The effect of falling particles into the bed was eliminated from binning zones. Figure 4.15 shows the axial velocity profiles by binning zones along the kiln from 75 to 78 seconds, while Figures 4.16a to 4.16d are the

corresponding typical top view snapshots inside the kiln. The snapshots at 75 seconds represent bed with no lifter interference, 76 seconds show the effect of lifters as they enter the bed and 77 seconds show the lifters in the middle of the bed. Finally, snapshot at 78 seconds shows the bed just as the lifters have passed through it.

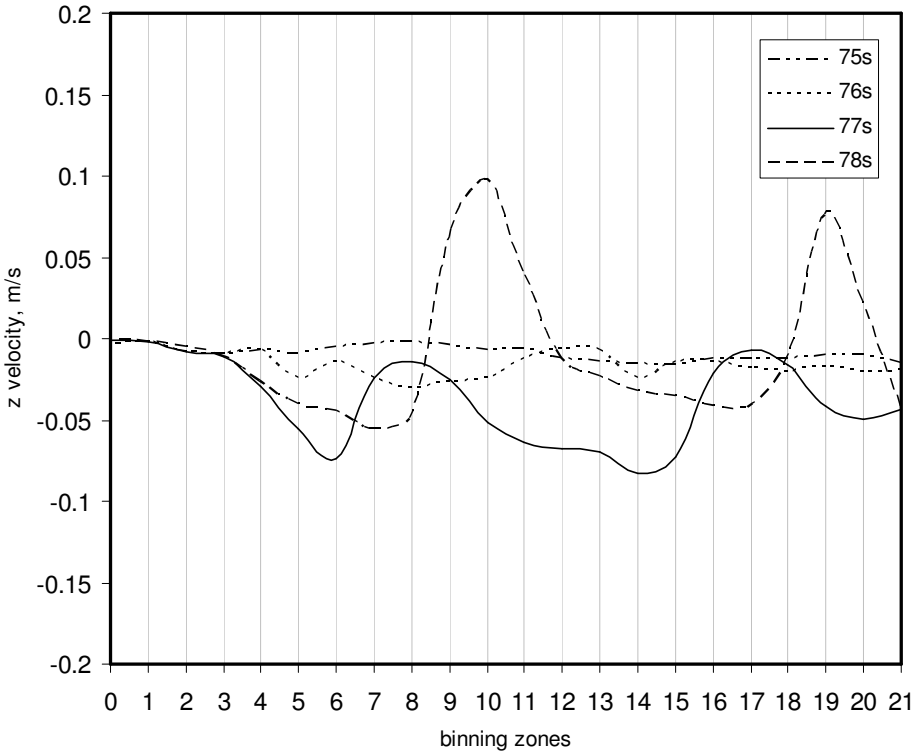

Figure 4.15. Axial velocity profiles from 75s to 78s.

At 75 seconds, with no effect from lifters it can be seen that the velocity profile is relatively flat. As the lifters enter the bed at 76 seconds, the –z velocity profile slightly increases in zones 5 and 14 with relatively flat in zones 6 to 10 and 15 to 19. That is, the incoming particles flow behind the folded lifter section after the particles just being scooped. At 77 seconds we see a further –z velocity profile increases between zones 5-6 and 10-15. The velocities also significantly decrease at the mid point of the lifters as at

76 seconds. This can be explained by the examination of the bed image at 77 seconds, which clearly shows a void created as the lifter move along the bed arc length. This image also demonstrates that a large amount of particles are scooped up by the lifters and then which fall back to further mix with the incoming bed from both sides (-z and +z directions). The velocity profile at 78 seconds shows the bed flowing into the voids which were created at 77 seconds. There are two peaks in +z velocity which are due to back flow into the voids in zones 10 and 19. Therefore, in addition to enhance axial solid transport, the installed segmented lifters can be used advantageously to improve axial solid mixing, which will be further discussed in Chapter 5.

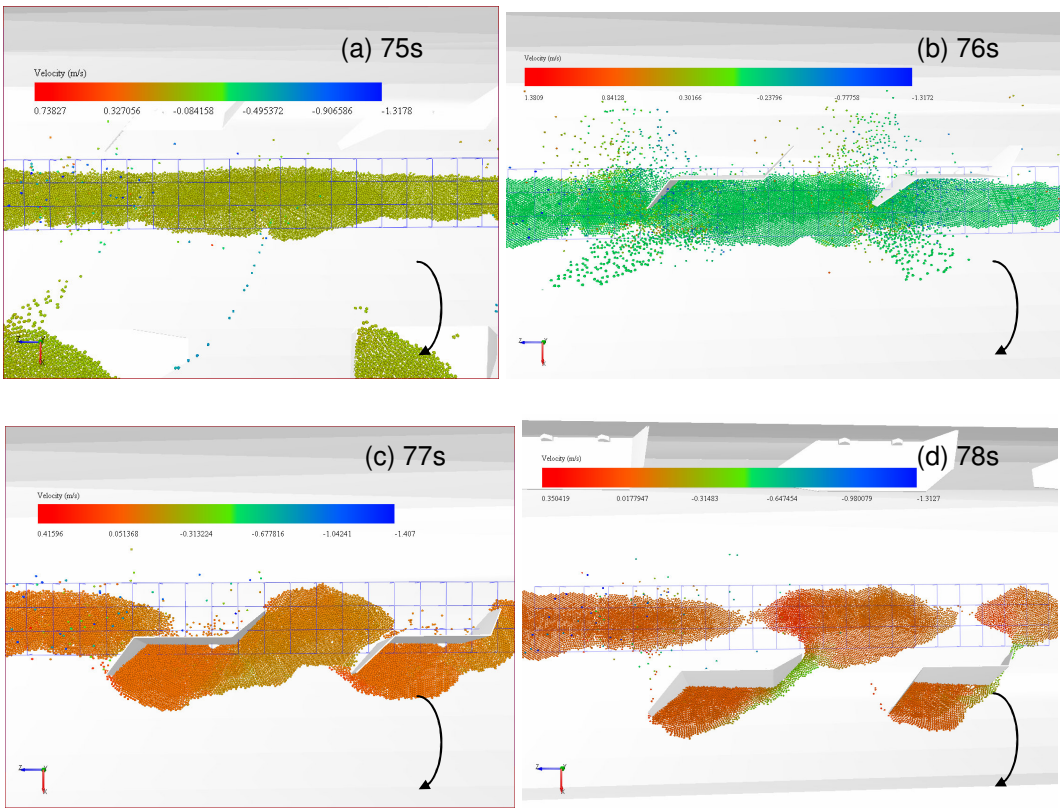

Figure 4.16. Top view snapshots of axial velocity profiles from 75s to 78s

From a design point of view, the axial velocity profiles suggest that the axial motion of bulk solid is predominantly controlled by the folded lifter sections, as evidenced in the –z velocity vectors between zones 10 to 15 at 77 seconds. The DEM simulation confirms in fact that such motion is a result of the physical push of particles towards the kiln discharge end along the bed arch length.

4.3.2 Development of a bed depth prediction model

For horizontal rotating kilns with segmented lifters, our results show that the axial motion of solid through horizontal kilns occurs predominately via the folded lifter sections. The driving force is the physical push of particles towards the kiln discharge end along the bed arc length. This provides a basis to develop a theoretical transport model for predicting bed depths. The model is limited to the underloading regime in open end restriction kilns that give rise to a flat axial bed depth profile as observed experimentally.

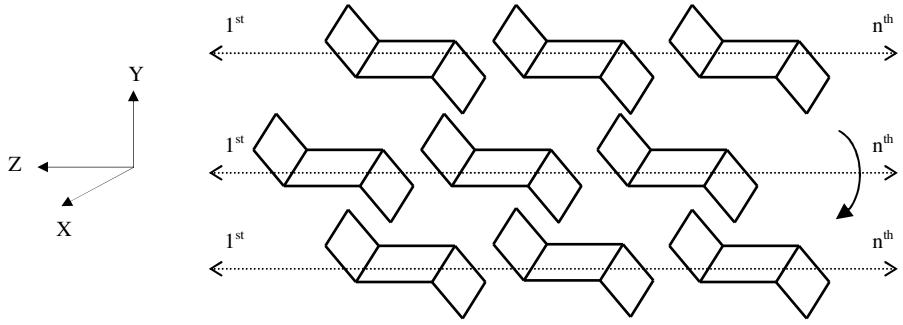

Figure 4.17. Segmented lifter configurations between row

Axial solid motion in horizontal rotating kilns with segmented lifters is a very complex. In Figure 4.17, the particles are transported through the horizontal rotary kiln in a series

of continuous "scooped-pushed to –z direction-lifted-spilled" cycles. Each cycle moves the particles a small distance along the kiln length. The distance is dependent on the solid, kiln designs and operation conditions.

The proposed model seeks to present a relatively simple but physically realistic model. Therefore, some basic assumptions are made, including:

1. Analysis is based on examining the behaviour of bulk particles.
2. All solid motion in the axial direction towards kiln discharge end was due to the force of folded lifter parts along the bed arc length.
3. At the kiln cross-section, the bed surface is a straight chord and inclined to the horizontal plane at its angle of repose (ignoring the difference between static and dynamic).
4. The solid angle of repose is constant along the kiln, independent of the local fill level, the kiln rotational speed, diameter and wall roughness.
5. The modification of axial displacement as a result of feeding plate effect within 540 mm of the kiln feed ends may be neglected.

Consider the motion of granular solid at the bottom of the kiln, the cross-section of an underloaded kiln and the general state of the solid are shown in Figure 4.18.

The bed depth may be estimated directly by performing a mass balance for a section kiln length on the solid entering and exiting the lifters. At given point of time, the particles that will be transported axially are those occupied by the triangular prism shown in Figure 4.19. As mass must be conserved, the rate at which solid enter the kiln m (kg/s) must be equal to the rate at which solid enter the triangular prism of the lifters. Assuming that the kiln rotational speed is n (rps), number of lifters per kiln cross-section for entering and passing the granular bed is N_l, each folded section displacing an axial volume is V_z (m^3/rotation.lifter), bulk density of solid is ρ (kg/m^3), we have feed rate = axial displacement rate,

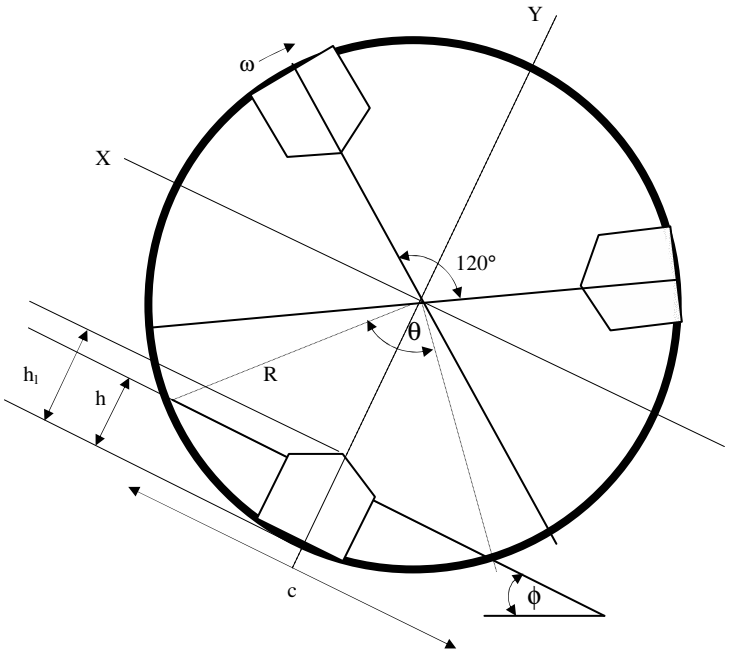

Figure 4.18. Sketch of the kiln cross-section

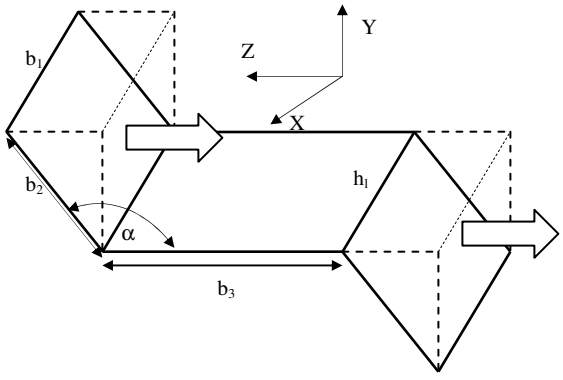

Figure 4.19. Sketch of the lifter structure with two triangular prisms N_f.

$$m = \rho.V_z.n.N_l \quad \text{.....(4.1)}$$

Assuming the bed arc length is L_a (m), the displaced axial volume per folded lifter section along the bed arc length can be simplified as a rectangular prism instead of two triangular prisms (see Figure 4.20). V_z is equal to the product of the number of folded section per lifter N_f, the length of the rectangular $\frac{L_a}{2}$ (m) and perpendicular cross-section area A_z (m^2/folded lifter section):

$$V_z = \frac{L_a}{2}.A_z.N_f \quad \text{.....(4.2)}$$

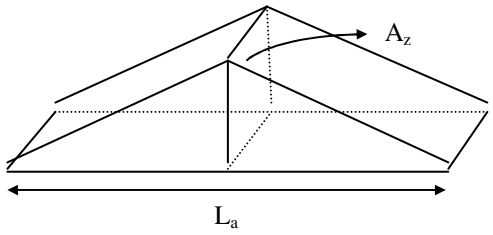

Figure 4.20. Displaced axial volume per folded lifter section along the bed arc length

From Figure 4.18, the bed arc length can be determined by

$$L_a = \frac{\theta°}{360°}.2.\pi.R \quad \text{.....(4.3)}$$

The perpendicular cross-section area A_z to the axial displacement can be approximated as a rectangular geometric shape, which has a height of bed depth h (in case of underloading regime, $h < h_l$) and a width of $b_2.sin(180°-\alpha°)$. We then have

$$A_z = h.b_2.\sin\left(180° - \alpha°\right) \quad \text{.....(4.4)}$$

Considering an arc in a kiln cross-section, the kiln filling angle (subtended by the bed at the kiln axis θ (°), radius R (m) and chord length c (m) can be related by the following geometric relationship, as depicted in Figure 4.18:

$$\sin\left(\frac{\theta°}{2}\right) = \frac{c}{2}.\frac{1}{R} \quad \text{.....(4.5)}$$

The relation between bed depth h (m) in an inclined bed to the horizontal plane at the angle of repose of the granular solid ϕ (°) with chord length c (m) can be determined as follows:

$$\tan\left(\phi°\right) = h.\frac{2}{c} \quad \text{.....(4.6)}$$

From Eqs. (4.5) and (4.6), eliminating c term and simplifying, gives

$$h = R.\tan\left(\phi°\right).\sin\left(\frac{\theta°}{2}\right) \quad \text{.....(4.7)}$$

Rearanging Equations (4.1) – (4.4) and substituting *h* from Equation (4.7) give the final kiln filling angle $\theta(°)$ as

$$\frac{\theta°}{360°}.\sin\left(\frac{\theta°}{2}\right)=\frac{m}{\rho.n.N_l.N_f.b_2.\pi.R^2.\tan(\phi°).\sin(180°-\alpha°)} \quad \text{.....(4.8)}$$

The kiln filling angle θ (°) in Equation (4.8) can be calculated by trial and error. The prediction of kiln filling angle allows for a direct correlation among the bed depth and other solid transport variables via the geometric relationship:

$$h=R-R.\cos\left(\frac{\theta°}{2}\right) \quad \text{.....} \quad (4.9)$$

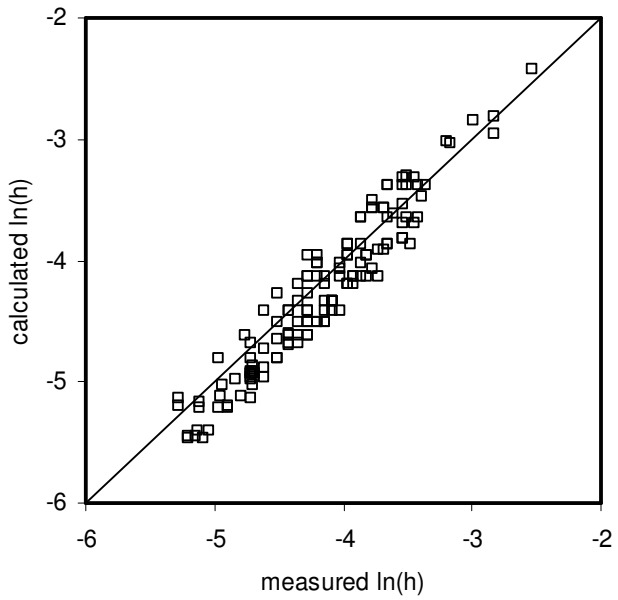

Figure 4.21. Plot of calculated vs. measured bed depths *h* in horizontal rotating kilns with segmented lifters operated in underloading regimes.

The comparisons between the model predicted bed depths and the experimental results are plotted in Figure 4.21. Figure 4.21 clearly shows that the model predictions are in good agreement with experimental data in horizontal rotating kilns when various granular solid under various operating conditions in underloading regimes.

4.3.3 Development of dimensionless empirical correlations

Based on the systematic experiments carried out in this study, a set of dimensionless correlations has been developed. The three solid transport coefficients can be expressed by power-law expressions as follows:

$$f = 10.91\phi^{1.14}\left(d/D\right)^{-0.15}\left(\mathrm{Re}_{\omega}\right)^{-0.90}\left(Fr\right)^{-0.03}\left(h_l/D\right)^{-0.52}\left(L/D\right)^{-0.40} \quad \text{..... (4.10)}$$

$$C_{\tau} = 8.57\phi^{1.14}\left(d/D\right)^{-0.15}\left(\mathrm{Re}_{\omega}\right)^{-0.90}\left(Fr\right)^{-0.03}\left(h_l/D\right)^{-0.52}\left(L/D\right)^{-0.40} \quad \text{..... (4.11)}$$

$$C_{u} = 0.12\phi^{-1.14}\left(d/D\right)^{0.15}\left(\mathrm{Re}_{\omega}\right)^{0.90}\left(Fr\right)^{0.03}\left(h_l/D\right)^{0.52}\left(L/D\right)^{0.40} \quad \text{..... (4.12)}$$

Figure 4.22 clearly illustrates that the predictions of the power-law correlations are in good agreement with the experimental data. The data also shows that ϕ, Re_{ω} and h_l/D have the most significant impacts on solid transport, as each discussed in Section 4.2. Beside, the data indicates that the horizontal kiln with segmented lifters has flexibility to handle solid with a wide range of particle sizes. In presence of lifters, the solid movement is dominantly driven by the folded lifter sections towards the kiln discharge end along the bed arc length, in contrast to kilns without lifters, gravitational forces only

play a minor role. Therefore, *Fr* can be omitted in the correlations. For practical applications, Equations (4.10 – 4.12) can then be simplified as follows:

$$f = 10.91\phi^{1.14}\left(d/D\right)^{-0.15}\left(\mathrm{Re}_{\omega}\right)^{-0.90}\left(h_l/D\right)^{-0.52}\left(L/D\right)^{-0.40} \quad \text{..... (4.10a)}$$

$$C_{\tau} = 8.57\phi^{1.14}\left(d/D\right)^{-0.15}\left(\mathrm{Re}_{\omega}\right)^{-0.90}\left(h_l/D\right)^{-0.52}\left(L/D\right)^{-0.40} \quad \text{..... (4.11a)}$$

$$C_u = 0.12\phi^{-1.14}\left(d/D\right)^{0.15}\left(\mathrm{Re}_{\omega}\right)^{0.90}\left(h_l/D\right)^{0.52}\left(L/D\right)^{0.40} \quad \text{..... (4.12a)}$$

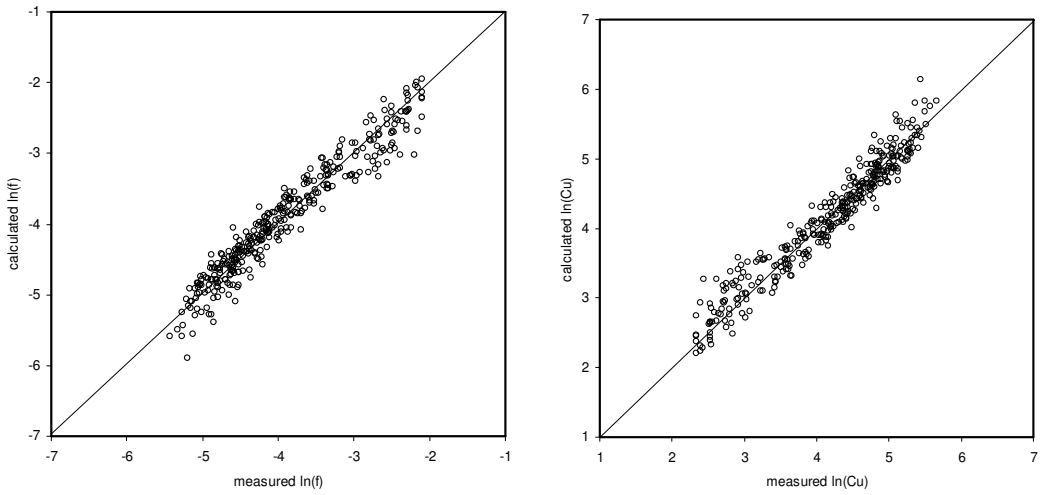

Figure 4.22. Plots of the calculated vs. measured f and C_u

4.3.4 Comparison with selected previous experimental studies

Development of dimensionless correlations in Section 4.3.3 was based on extensive experiments carried out in this study. A thorough literature review was also carried out

to collect experimental data in previous studies to test the applicability of correlations (4.10) – (4.12). A total of seven previous selected independent experimental studies with 328 measurement points collected.

Figure 4.23 shows the dependence of f and C_u on the Re_ω, incorporating the experimental data collected from the previous studies listed in Table 2.2. It can be seen that generally, f follows an inverse power law with Re_ω and C_u increases. This indicates that solid transport in various systems is fundamentally governed by similar mechanisms. Generic dimensionless correlations on solid transport may be developed, although the values of detailed coefficients may depend on kiln designs and operation conditions. One exception is the experimental data by Afacan and Masliyah (1990), which are far outside the general trend. This is believed to be mainly due to the relatively high Fr (0.1 - 1) used in their experiments, leading to the kiln being operated in cataracting mode.

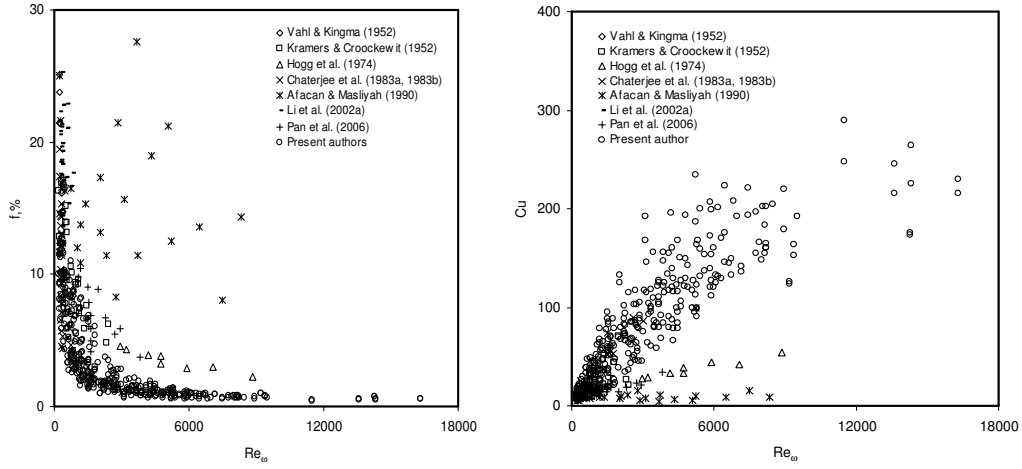

Figure 4.23. The f and C_u in dependence on the Re_ω at different authors.

At a relatively small kiln axis slope without lifters, experiments by Chaterjee et al. (1983a, 1983b), Kramers and Croockewit (1952) and Vahl and Kingma (1952) showed relatively higher f values at the same Re_ω. For rotating kilns without lifters, the axial transport of granular solid mainly occurs in the thin active layer of bed surface, while solid in the passive layer under bed surface only turn around the kiln axis with little axial displacement. This is the phenomena of cascading mode in transversal bed motion described by Henein et al. (1983).

Part of the experimental data by Hogg et al. (1974), Li et al. (2002a) and Pan et al. (2006) also showed higher f values than those of the present study at the same Re_ω. This is most likely due to the differences in the types of lifters and the end constrictions. As this study utilises segmented lifters, the segmented lifters are more effective in enhancing solid transport, leading to a lower f at the same Re_ω. Practically, a high f is required for maintaining certain productivity, but f must not be too large (overloading regime) to affect solid mixing. A lower f also leads to a flat bed depth profile therefore improving load balance and good heat transfer performances.

It should also be noted that in Figure 4.23 (C_u vs Re_ω), experimental data by Hogg et al. (1974), Kramers and Croockewit (1952), Pan et al. (2006) and; Vahl and Kingma (1952) are mostly well below the experimental data obtained in this study. This is mainly due to a high Fr used by Hogg et al. (1974), a small kiln axis slope (<1°) without lifters used by Kramers and Croockewit (1952), types of lifters used by Pan et al. (2006), and a kiln axis slope of 0° without lifters used by Vahl and Kingma (1952).

Table 4.2 summarizes the range of dimensionless numbers used in experiments for the development of correlations in each study. Therefore, the comparisons indicate that extrapolation of the correlations beyond the range could be risky. The developed dimensionless correlations are largely specific to the current lifters.

Table 4.2

Range of input dimensionless terms in various studies on solid transport

Author	Dimensionless groups						
	$\theta.10^2$	ϕ	$d/D.10^3$	Re_ω	Fr	L/D	h_l/D
Vahl & Kingma (1952)	0	0.58	5.45	212 – 858	$4.99.10^{-3}$ – $1.04.10^{-1}$	5.91	n/a
Kramer & Croockewit (1952)	0.87 – 8.73	0.63 – 0.70	4.57 – 5.08	166 - 2400	$6.25.10^{-4}$– $2.25.10^{-2}$	9.04	n/a
Hogg et al. (1974)	0	0.66	4.21	2951 - 8852	$4.31.10^{-1}$	2.61	unspecified
Chaterjee et al. (1983a,b)	1.75-5.24	0.61	10 - 20	217 - 5214	$2.69.10^{-5}$ – $1.21.10^{-4}$	3.33 – 16	n/a
Afacan & Masliyah (1990)	0	0.63	1.04	218 - 8346	$2.45.10^{-3}$ – $9.09.10^{-1}$	5.47	unspecified
Li et al. (2002a)	1.08 – 4.19	0.85	8.33	218 - 694	$6.72.10^{-4}$ – $1.08.10^{-2}$	6	unspecified
Pan et al. (2006)	0	0.52	8.02	1088 - 3809	$1.88.10^{-3}$ – $1.70.10^{-2}$	3.21	unspecified
Present authors	0	0.44 – 0.79	0.81 – 17.50	184 - 16316	$3.01.10^{-4}$ - $5.21.10^{-3}$	5 – 10	0.08-0.16

4.4 Summary

Our experimental data shows that axial bed depth profile strongly depends on the degree of loading and type of lifters. A flat bed depth profile with significantly low total kiln volumetric filling fraction, which is necessary for good heat transfer performance, can be effectively achieved in horizontal rotating kilns with segmented lifters. The effect of helix has insignificant impacts on solid transport performances.

The results presented in Section 4.2 also show that useful dimensionless correlations can be developed for solid transport. The results show that solid transport in horizontal rotating kilns with segmented lifters are dominantly influenced by the static angle of

repose, rotational Reynolds number and lifter height to kiln diameter ratio. Particle size and *Fr* have insignificant impact on solid transport, indicating that the horizontal rotating kilns with segmented lifters are flexible to handle solid with wide size distribution and forms of transverse motion.

The preliminary DEM simulation confirmed that the axial displacement is mainly due to folded lifter sections by pushing towards kiln discharge end along the bed arc length. A simplified theoretical transport model was then developed to predict the average bed depth in rotating kilns operating in the underloading regimes. A set of dimensionless empirical correlations has also been derived to predict solid transport. Such global power-law correlations are universal and physically realistic for practical applications. The predictions are found to be in good agreement with experimental data.

Chapter 5

Solid Mixing

In this chapter, dimensional analysis was performed and a systematic experimental program was then carried out to quantitatively investigate the effect of segmented lifter designs, lifter configurations, helix and design equations on solid mixing, considering various kiln designs, kiln operating conditions and solid physical properties. A dimensionless empirical correlation has then been developed. The validity was tested with previous selected mixing experimental studies.

The solid, kiln design and operating condition parameters can affect the bulk solid mixing variable, namely axial dispersion coefficient D_z in m^2/s. This key solid mixing variable is generally a function of kiln design (kiln length L in m and kiln diameter D in m), kiln operating conditions (feed rate m in kg/s, kiln rotational speed ω in rad/s), solid characteristics (mean particle size d in m, particle bulk density ρ in kg/m^3, particle static angle of repose ϕ in radian), the acceleration of gravity g in m/s^2, lifter geometries (lifter height h_l in m)

Based on Buckingham's Π theorem (Munson et al., 2006), a dimensional analysis has been carried out. The following applicable correlation is developed among a set of dimensionless numbers:

$$Pe = \frac{uL}{D_z} = \Phi_3\left(\phi, \frac{d}{D}, \frac{L}{D}, \frac{h_l}{D}, \frac{\omega^2 D}{g}, \frac{\rho\omega D^2}{m/D}\right)$$

The prediction equation is uL/D_z, known as the Peclet number *Pe*, which is the ratio between convective and molecular transport. The six design equations are ϕ, *d/D*, *L/D*, h_l/D, $\omega^2 D/g$ and $\rho\omega D^2/(m/D)$. The first and second groups denote the solid characteristics. The third and fourth groups denote the geometric ratio of the system. The fifth and sixth groups denote the dynamic ratio of the system. The fifth group is Froude number *Fr*, $\omega^2 D/g$ *or* $\omega^2 R/g$, which is the ratio between inertial and gravitational forces. The sixth group corresponds to the rotational Reynolds number Re_ω, i.e. the ratio between inertial forces and the resistant forces which the solid have to overcome.

5.1 Effect of segmented lifter design, lifter configurations and helix on prediction equation

In this section, a systematic experimental program was carried out using the cold kilns to quantitatively investigate the presence (inclined kiln without lifters) and effect of segmented lifter designs (folded lifter section), lifter configurations (single throughout lifters, number of lifter per row) and helix on solid mixing. All experimental result plots are limited for urea.

5.1.1 Inclined kiln without lifters

There were several previous experimental studies on solid mixing through horizontal (Hehl et al., 1978; Mu & Perlmutter, 1980) and inclined (Hatzilyberis et al., 1999a; Sai et al., 1990; Sudah et al., 2002) rotating kilns without lifters. The details of those studies are summarised in Table 2.3, which indicates the design variables of rotating kilns and their value as well as matrix combinations vary greatly among those studies. Therefore, this study carried out a systematic experimental program to investigate the effect of the

axis kiln slope on solid mixing in a rotating kiln (*L/D* = 7) with and without segmented lifters.

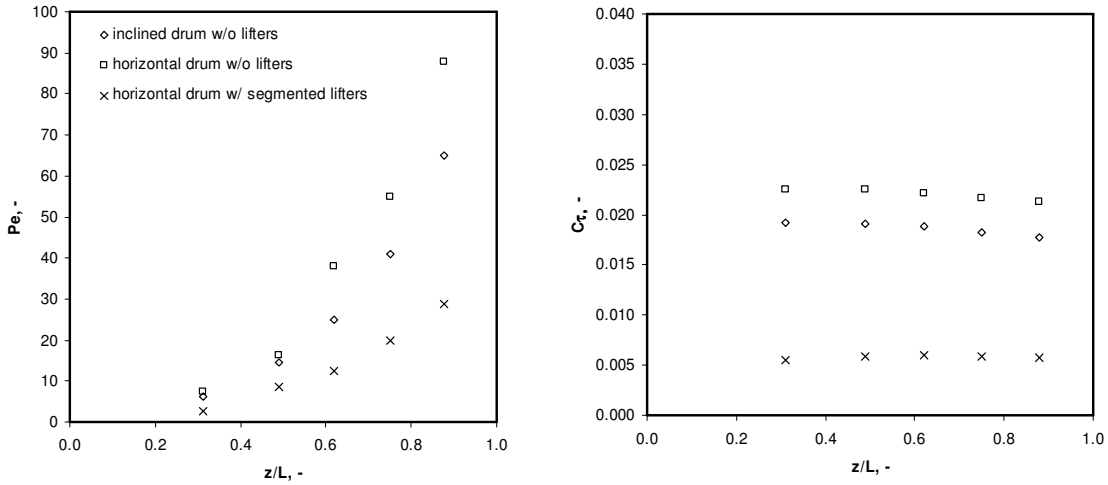

(a) (b)

Figure5.1. The *Pe* and C_τ profiles of urea in a rotary kiln (*L/D* = 7) without and with segmented lifters (h_l/D = 0.16) at Re_ω = 3692: (a) *Pe* vs *z/L* and (b) C_τ vs *z/L*.

Figure 5.1 shows the impact of axis kiln slope without or with segmented lifters on solid mixing of urea (Re_ω = 3692). The *Pe* profile in a horizontal kiln with segmented lifters is lower than the ones without lifters at the same Re_ω with uniform C_τ. The solid mixing in a kiln with segmented lifters is dominantly driven by physical mix via its straight sections along the kiln length.

As axis kiln slope increases from 0° to 0.5° in a rotary kiln without lifters, *Pe* profile decreases with increasing C_τ , as a results of a more inclined bed depth profile and increasing fill level (see discussion in Section 4.1.1). This is understandable because higher axis kiln slope translates into greater forward advance on the chord length and leads to faster solid mixing therefore lower *Pe* profile. The forward advance is based on

the cylinder slope in the axial direction as well as the apparent forward angle of descent resulting from the transverse flow pattern.

5.1.2 Lifter configurations

Solid mixing in rotary kilns is expected to be influenced by the installed lifters. Key parameters to be considered include lifter type and configurations. Figure 5.2 shows the dependence of Pe and C_τ as a function of kiln length of urea at Re_ω = 3692 in underloading regimes. The Pe profile of a kiln with single throughout lifters is located between the inclined kiln without lifters and the horizontal kiln with segmented lifter while C_τ is the highest and has a non-uniform profile.

As discussed in Section 4.1.2, single throughout lifters have more contact surface area with solid bed. In the absence of physical push action towards the kiln discharge end as with segmented lifters, this type of lifters only scoop, lift and spill all solid bed at the same axial kiln positions considering underloading regimes (f < 10%). Therefore those actions result in a Pe profile is slightly lower than the inclined kiln without lifters but higher than the one with segmented lifter. This is due to significantly higher inclined C_τ profile, corresponding to higher fill level with an inclined bed depth profile. Therefore, the presence of single throughout lifters only has minor impact on axial solid mixing.

5.1.3 Folded lifter section

The impact of segmented lifters without folded lifter sections, namely segmented straight lifters, on axial granular solid mixing in horizontal rotating kilns is shown in

Figure 5.3. In addition to width b_3 of segmented lifter in Figure 3.3, segmented straight lifters were extended by 0.055 m for each side to compensate the absence of folded lifter sections. At the same h_l/D ratio of 0.16, it is found that the installation of segmented straight lifters leads to a much lower *Pe* profile along the kiln, with a non-uniform C_τ profile.

With the installation of segmented lifters, in addition to scoop and spill solid bed, a proportion of solid was pushed along the bed arc length and spilled in the negative (toward to kiln discharge end) and positive (toward to kiln feed end) axial kiln directions. Additional axial solid mixing occurs. Solid is transferred quicker and mixing is more intense. However, in absence of the folded section, segmented straight lifters have reduced contact surface area, resulting in a significantly higher non-uniform C_τ profile or fill level. It is doubtless that the usage of folded lifter sections is an effective method to indirectly enhance the axial solid mixing by largely push and spill in the negative axial kiln directions with a uniform C_τ profile.

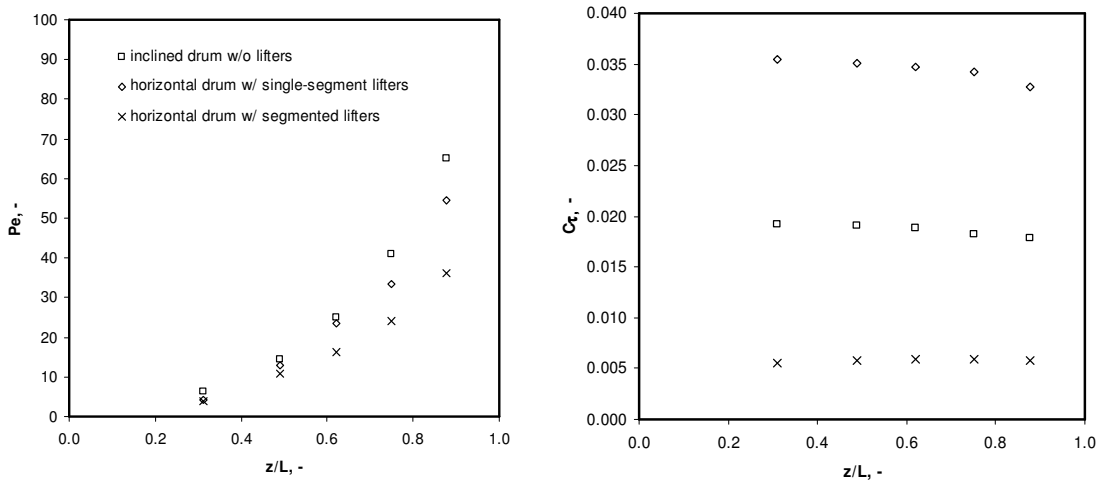

(a) (b)

Figure 5.2. The *Pe* and C_τ profiles of urea in a rotary kiln (*L/D* = 7) without lifters and with single throughout lifters and segmented lifters (h_l/D = 0.16) at Re_ω = 3692: (a) *Pe* vs *z/L* and (b) C_τ vs *z/L*.

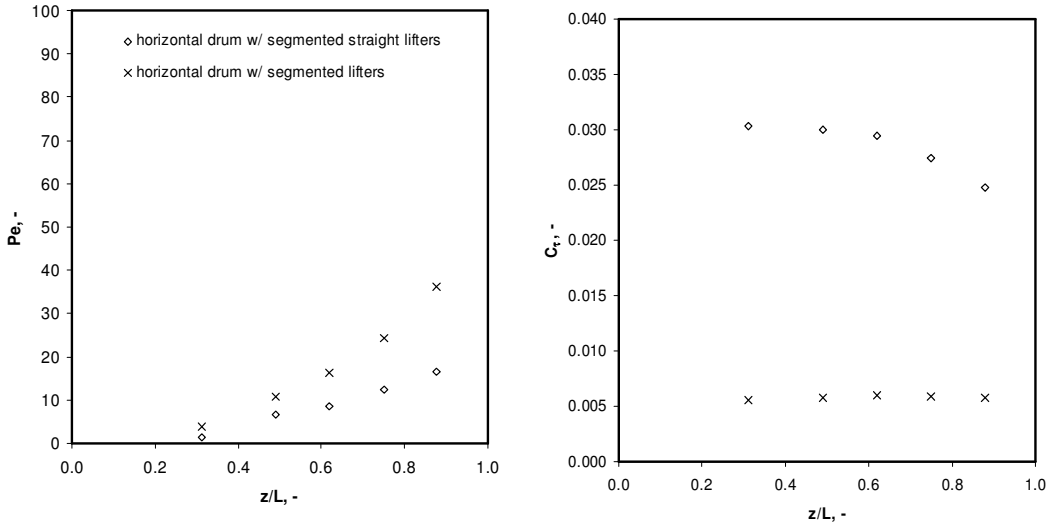

(a) (b)

Figure 5.3. *Pe* and C_τ profiles of urea in a rotary kiln (*L/D* = 7) with and without folded lifter sections (straight) segmented lifters (h_l/D = 0.16) at Re_ω = 3692: (a) *Pe* vs *z/L* and (b) C_τ vs *z/L*.

5.1.4 Number of lifters per row

Figure 5.4 shows the dependence of *Pe* and C_τ as a function of kiln length at (Re_ω = 3692). Two different lifter numbers per row, i.e. four and seven, are considered in a horizontal rotating kiln with segmented lifters. This was achieved by simply removing the second, fourth and sixth lifters in each row of lifters, as shown in Figure. 3.4d.

As the number of lifters per row decreases, the *Pe* and C_τ profiles increase. As discussed in Section 4.1.4, granular solid near lifters will immediately receive a greater forward force relatively to those further away from lifters. The solid further away from lifters are affected only by the resultant forces from granular solid coming from behind due to the inclined bed. Consequently, at certain axial kiln sections without lifters, the granular

solid start to build-up with less mixing, similar to the case in a horizontal kiln without lifters. Therefore, the case of seven lifters per row seems to be sufficient in enhancing both axial solid mixing and transport by consistently push granular solid toward to kiln discharge end.

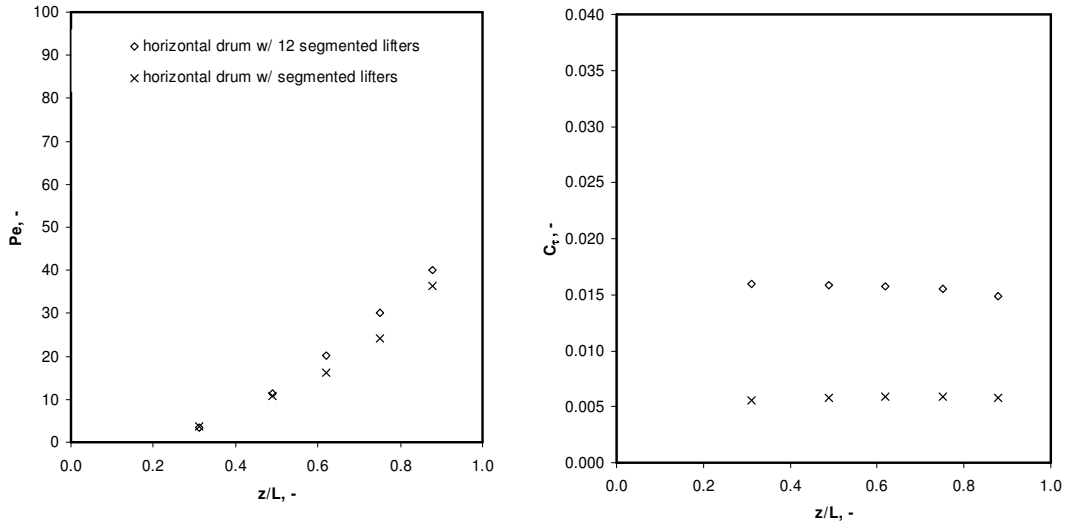

Figure 5.4. The *Pe* and C_τ profiles of urea in a rotary kiln (*L/D* = 7) at two different numbers of lifters per row (h_l/D = 0.16) at Re_ω = 3692: (a) *Pe* vs *z/L* and (b) C_τ vs *z/L*.

5.1.5 Helix

Installation of a helix acts as an additional flow resistance, resulting to a higher *f* particularly at near kiln discharge end (see Section 4.1.5). Figure 5.5 and Figure 5.6 shows the profiles of *Pe* and C_τ of urea in two rotary kilns with and without helix. The *Pe* profiles in both kilns with helix are higher than the ones without helix. The data indicates that the differences increase gradually particularly near drum discharge end (*z/L* > 0.8).

The usage of helix may be an effective method to maintain flat bed depth profiles of solid with poor flowability (see discussion in Section 4.1.6). It may results in a low degree of axial solid mixing particularly in the range at near kiln discharge end where the bed depth profile tends to increase.

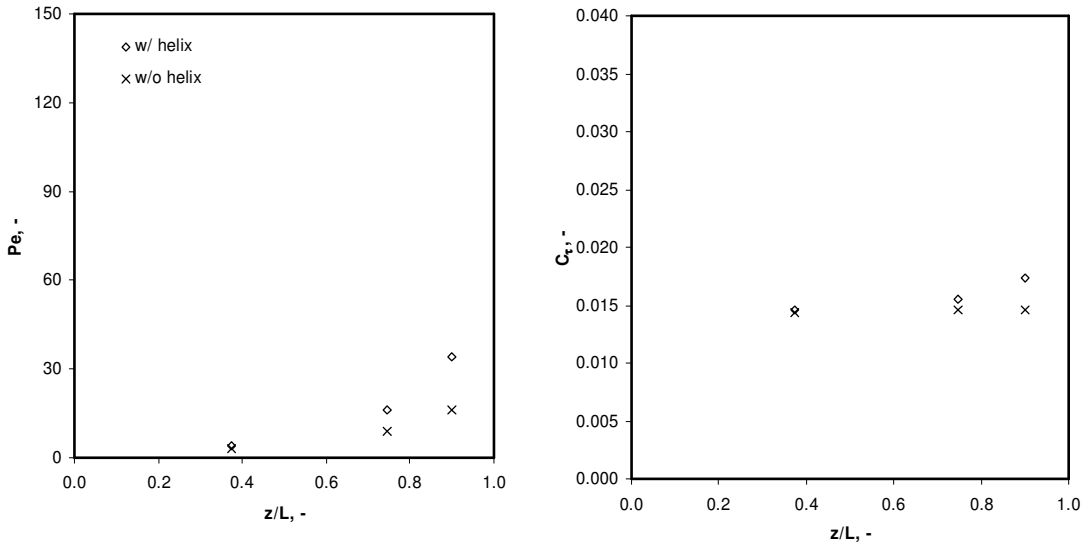

(a) (b)

Figure 5.5. The *Pe* and C_τ profiles of urea in a rotary kiln (*L/D* = 5) with segmented lifters (h_l/D = 0.16) and with or without helix at Re_ω = 2818: (a) *Pe* vs *z/L* and (b) C_τ vs *z/L*.

5.2 Effect of design equations on a prediction equation in a horizontal rotating kiln with segmented lifters

In this section, a systematic experimental program was carried out using the cold kiln to quantitatively investigate the effect of design equations, i.e. dynamic ratio of the system, solid characteristics, geometric ratio of the system, on solid mixing prediction equation, i.e. *Pe*.

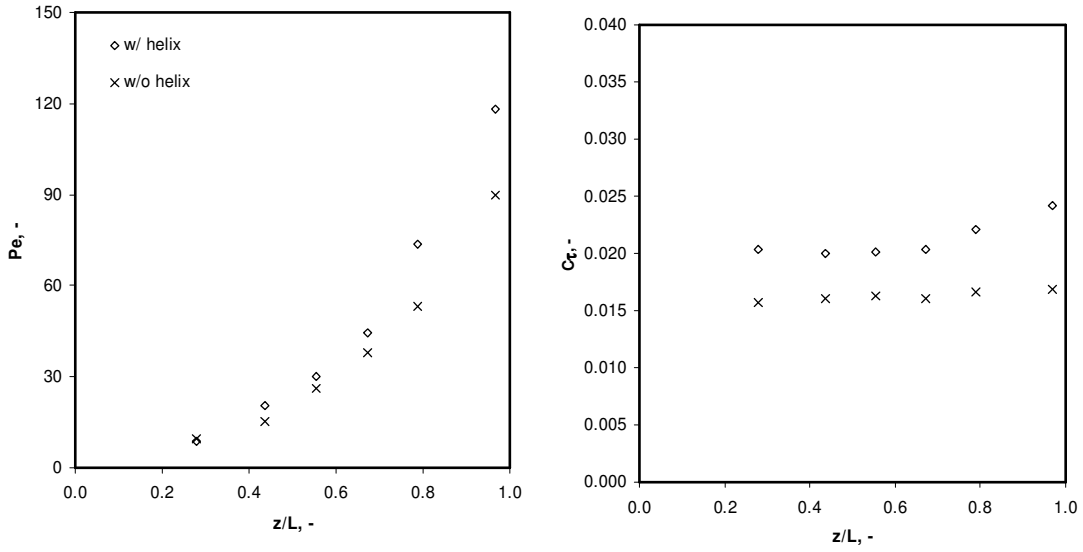

(a) (b)

Figure 5.6. The *Pe* and C_τ profiles of urea in a rotary kiln (*L/D* = 10) with segmented lifters (h_l/D = 0.16) and with or without helix at Re_ω = 1353: (a) *Pe* vs *z/L* and (b) C_τ vs *z/L*.

5.2.1 Dynamic ratios

Figure 5.7 illustrates the dependence of *Pe* in underloading regime (*f* < 10 %) at different Re_ω. Figure 5.7 clearly shows that *Pe* decreases with increasing Re_ω, there are rapid increase in *Pe* for glass bead and sand at Re_ω < ~1500 and ~3000. This expected because a higher Re_ω leading to faster solid mixing therefore lower Pe. As a result of the folded and straight lifter section, higher Re_ω translates into greater inertial force so that lifters have more energy to scoop, mix, push, mix, lift solid into the upper of the kiln until its angle of repose, spill the solid under the influence of gravity and mix with solid bed. The cycle of "scooped-(mixed)-pushed-(mixed)-lifted-spilled-(mixed)" process then repeats itself. Therefore, the segmented lifters employed can largely enhance solid mixing by disturbing the passive layer as Re_ω increases. Figure 5.7 also indicates that *Pe* follows an inverse power law with Re_ω, as discovered in solid transport.

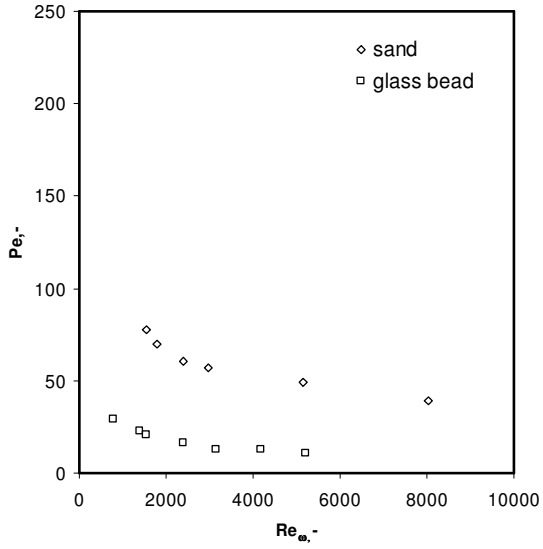

Figure 5.7. The *Pe* as a function of Re_ω at $z/L = 0.8$ in a rotating kiln ($L/D = 7$) with segmented lifters ($h_l/D = 0.16$) using glass bead.

5.2.2 Solid characteristics

Solid mixing in rotary kilns is also expected to be strongly influenced by solid characteristics. Figure 5.8 presents the data for a range of solids which have different characteristics, under the same kiln operating conditions. A higher mixing resistance is expected for granular solid of a smaller d and a higher ϕ when the solid moves towards kiln discharge. Solid of smaller size and higher ϕ have poor flowability and leads to increases in *Pe*. In Figure 5.8, sand has the highest *Pe* compared to other solid. Therefore, a higher Re_ω is required in order to achieve the same *Pe* for granular solid of a higher ϕ and a smaller d. In this case, more energy input is required to drive the kilns.

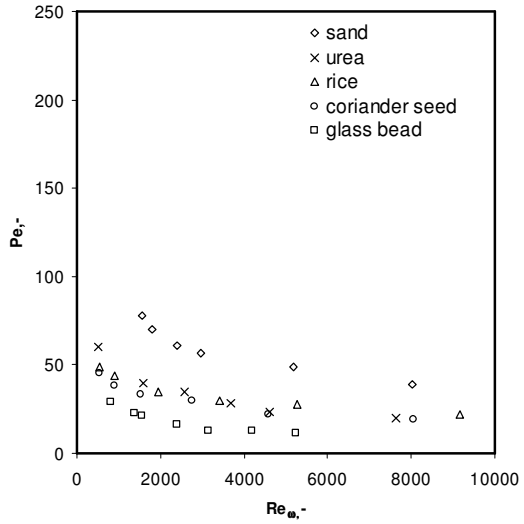

Figure 5.8. The *Pe* as a function of Re_ω at at *z/L* = 0.8 in a rotating kiln (*L/D* = 7) with segmented lifters (h_l/D = 0.16) at various solid. (*d/D* and ϕ for sand, urea, rice, coriander seed, glass bead are $9.8\text{x}10^{-4}$, $5.9\text{x}10^{-3}$, $1.4\text{x}10^{-2}$, $6.9\text{x}10^{-3}$, $3.9\text{x}10^{-3}$ and 32, 35, 30, 35, 25)

5.2.3 Geometric ratios

Figure 5.9 illustrates the dependence of *Pe* on the Re_ω considering segmented lifters with two different h_l/D ratios (0.08 and 0.16). The data in Figure 5.9 indicates that the lifter height significantly affect the axial mixing of solid. Figure 5.9 clearly shows *Pe* decreases with increasing Re_ω. At the same Re_ω, *Pe* is higher for smaller lifters. For smaller lifters, a higher Re_ω is needed to achieve the same *Pe*.

Similar to solid transport, at $f > 3.6\%$, the increasing in *Pe* with decreasing Re_ω is steeper for h_l/D ratio of 0.08 compared to h_l/D ratio of 0.16. As discussed in Section 4.2.3, this may attributed the shift of operation regimes from underloading to design loading and overloading. Flow above the lifters results solid may sometimes bypasses lifters and

resist particle mixing towards kiln discharge end. Therefore the lifters have a greater impact in enhancing axial solid mixing in underloaded kilns compared to overload kilns.

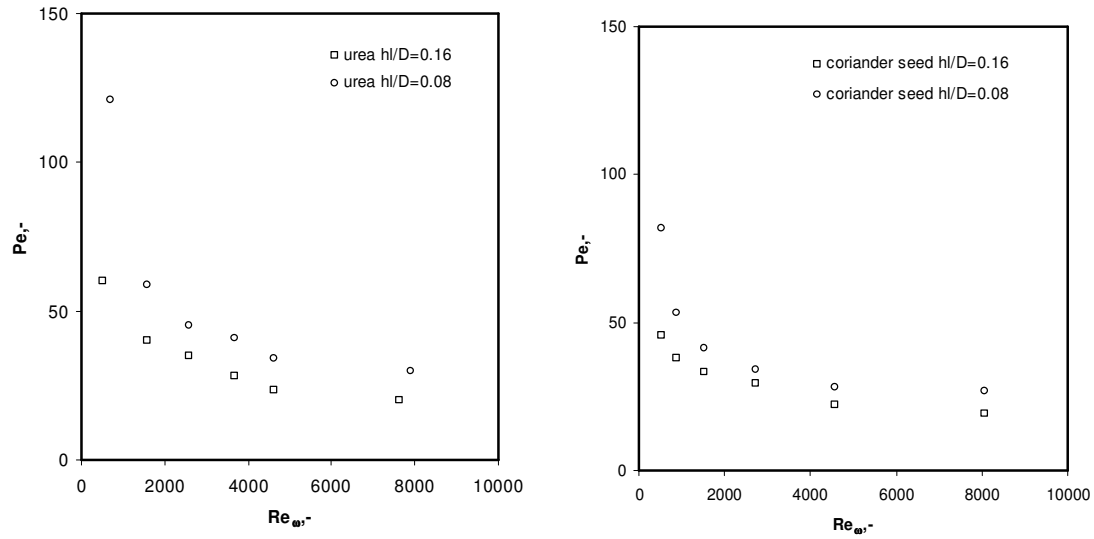

Figure 5.9. The *Pe* as a function of Re_ω at at *z/L* = 0.8 in a rotating kiln (*L/D* = 7) with different segmented lifter heights (0.08 and 0.16): (a) urea and (b) coriander seed.

5.3 Modelling

5.3.1 Development of a dimensionless empirical correlation

Systematic experiments were designed to develop the correlation among dimensionless groups. As experiments were carried out in one kiln with a fixed *L/D*, *L/D* is therefore not included in the current correlation. Applying a multiple linear regression, the *Pe* can be expressed by a power-law expression as follows:

$$Pe = 108.02.\phi^{2.05}\left(d/D\right)^{-0.31}\left(\mathrm{Re}_{\omega}\right)^{-0.36}\left(Fr\right)^{-0.01}\left(h_l/D\right)^{-0.59} \quad \text{..... (5.1)}$$

Equation (5.1) was developed based on *Pe* data at a particular kiln axial distance as shown in Figure 5.10. The dimensionless axial distance of 0.8 was believed to be the most appropriate to represent the overall degree of axial solid mixing. Axial bed section at $z/L > 0.8$ is inappropriate due to the absence of lifters and at $z/L < 0.8$ is inconsistent with the final boundary used at $z/L = 1$ in developing the solid transport correlations (see in Section 4.3.3). Beside, the difference in coefficients for each dimensionless term at different z/L is insignificant.

Figure 5.11 clearly illustrates that the predictions of the power-law correlation are in a good agreement with experimental data, similar to solid transport (see in Section 4.3.3), the data shows that ϕ, Re_{ω} and h_l/D have the most significant impacts on solid mixing, as each discussed in Section 5.2. Similar to solid transport, the data indicates that the horizontal kiln with segmented lifters has flexibility to handle solid with a wide range of particle sizes. Since the solid movement is dominantly driven by folded lifter sections towards the kiln discharge end along the bed arc length and no longer gravitational forces dependent, *Fr* can be omitted in the correlations. For practical applications, Equation (5.1) can then be simplified as follows:

$$Pe = 108.02.\phi^{2.05}\left(d/D\right)^{-0.31}\left(\mathrm{Re}_{\omega}\right)^{-0.36}\left(h_l/D\right)^{-0.59} \quad \text{..... (5.1a)}$$

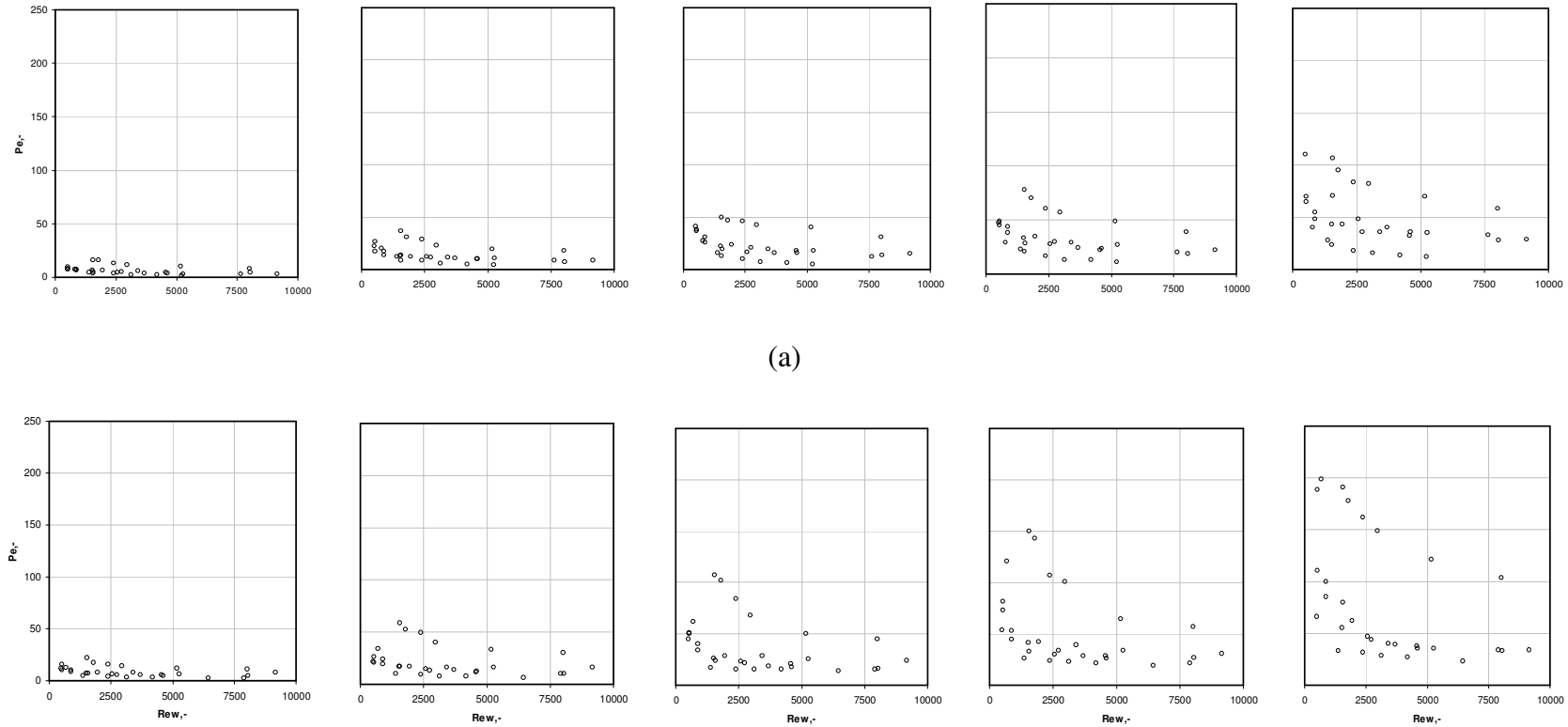

Figure 5.10. The *Pe* as a function of Re_ω in a rotating kiln (*L/D* = 7) at various *z/L* and solid with two different segmented lifter heights: (a) h_l/D = 0.16 and (b) h_l/D = 0.08.

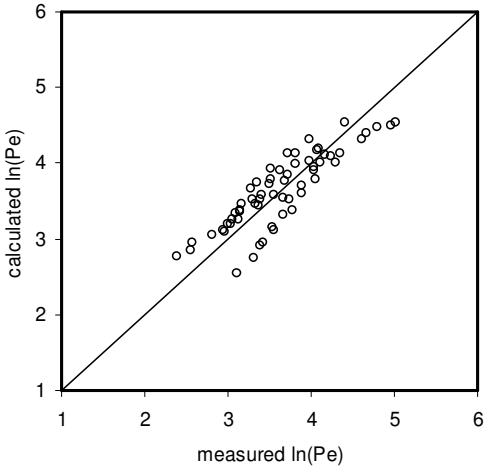

Figure 5.11. Comparison between the calculated vs. measured *Pe* at *z/L* = 0.8.

5.3.2 Comparison with selected previous experimental studies

A thorough literature review was also carried out to collect experimental data in previous studies to test the applicability of correlation (5.1). A total of six previous selected independent experimental studies are selected with 61 measurement points collected at *z/L* = 0.8. Figure 5.12 shows the dependence of *Pe* on the Re_ω, incorporating the experimental data collected from the previous studies listed in Table 2.3. Similar to solid transport, *Pe* follows an inverse power law with Re_ω increases. This indicates that solid mixing in various systems is fundamentally governed by similar mechanisms. Generic dimensionless correlations on solid mixing may be developed, although the values of detailed coefficients may depend on kilns and operation conditions.

There are important findings by directly comparing between *Pe* in Figure 5.12 and corresponding *f* in Figure 5.13, especially the ones reported by Rutgers (1965) and Venkatarman et al. (1986). Their results show similar *Pe* compared to the results of the present study at the same Re_ω. It is most likely due to significantly higher *f* (see discussion in Chapter 4). Rutgers (1965) and Venkatarman et al. (1986) used higher

Froude numbers (3.22 x 10^{-1} - 4.43 x 10^{-1}) and shorter kilns (L/D = 2 - 3). At Re_ω = 439, Wes et al. (1976) found a Pe of 47 at z/L = 0.4 and a higher Pe of 145 at z/L = 1.0, as the same trend observed in Figure 5.10.

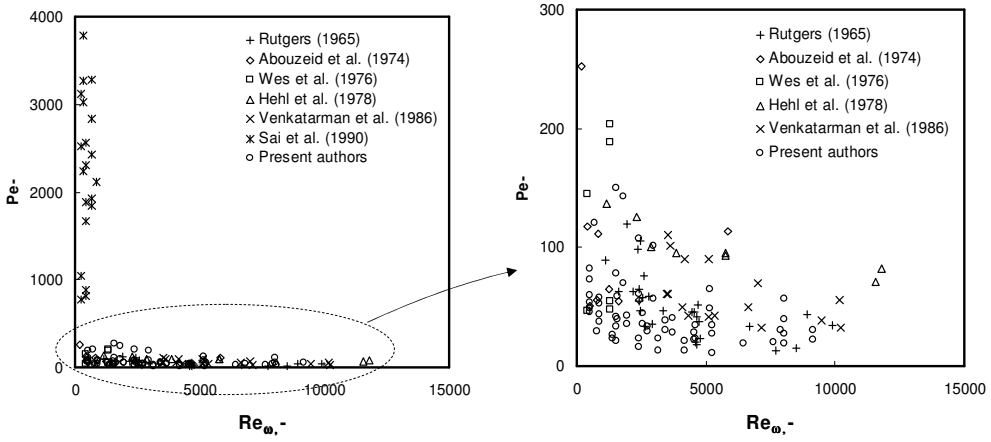

Figure 5.12. The Pe in dependence on the Re_ω at different authors.

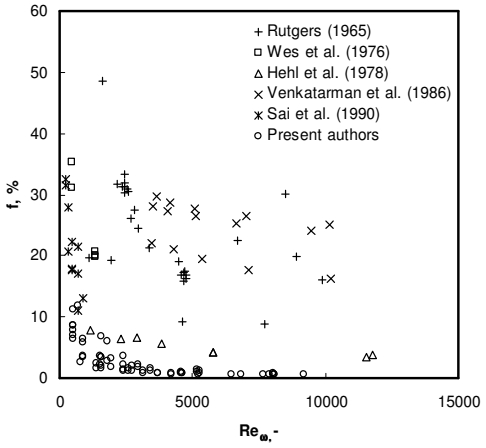

Figure 5.13. The f in dependence on the Re_ω at different authors.

Additionally, at high *f*, the impractical short kilns used by previous investigators (Abouzeid et al., 1974; Hehl et al., 1978; Rutger, 1965; Venkatarman et al., 1986) are believed to be responsible for low *Pe* as identified in Figure 5.12. Furthermore, the *Pe* values by Sai et al. (1990) are very high at relatively low Re_ω. This is believed to be mainly due to the inclined kiln used with very high *L/D* ratio of 40 without lifters used in their experiments.

Table 5.1

Range of input dimensionless group on solid mixing.

Author	Dimensionless groups						
	$\theta.10^2$	ϕ	$d/D.10^3$	Re_ω	Fr	L/D	h_l/D
Rutgers (1965)	0 – 6.98	N/A	6.54 – 43.75	1125 – 9885	$5.70.10^{-3}$ – $8.46.10^{-1}$	3.1	unspecified
Abouzeid et al. (1974)	0 – 5.24	N/A	2.88 – 8.13	186 - 5844	$4.13.10^{-3}$– $6.99.10^{-1}$	3	unspecified
Wes et al. (1976)	0	N/A	0.03-0.17	439 - 1318	$1.34.10^{-3}$– $1.21.10^{-2}$	15	unspecified
Hehl et al. (1978)	0	N/A	0.55	1155 - 11781	$1.40.10^{-4}$ – $1.40.10^{-2}$	2.4	N/A
Venkatarman et al. (1986)	0	N/A	7.87	3471 - 10222	$4.43.10^{-1}$	3	unspecified
Sai et al. (1990)	1.36 – 2.39	0.48	1.29	225 - 881	$8.22.10^{-5}$ – $7.40.10^{-4}$	40	N/A
Present authors	0	0.44 – 0.79	0.81 – 17.50	499 - 9166	$7.68.10^{-4}$ - $8.59.10^{-3}$	7	0.08-0.16

In addition to practical low *f* and flat bed depth profile, as discussed in Chapter 4, the horizontal kiln used in this study utilise segmented lifters achieves low *Pe* numbers in a kiln with a practical low Re_ω and a medium *L/D* ratio. Therefore, compared to most conventional kilns using single throughout lifters; the kiln used in this study is more effective in enhancing axial solid mixing therefore heat transfer performance in rotary kilns.

The comparison also indicates that the developed correlation is largely specific to the current lifters and kiln design. Extrapolation of the correlation beyond the range could be risky.

5.4 Summary

The axial solid mixing was studied systematically using continuous rotating kilns with segmented lifters. Particle mixing dispersion rates were evaluated by Peclet number. Peclet number is found to be strongly dependent on loading and lifter type. The experiment results show that in horizontal rotating kilns, a high degree of axial solid mixing (low *Pe*) with practical low kiln fill level (<10%), which is necessary for good heat transfer performances, can be achieved at practical Re_ω and *L/D* ratio.

Increasing kiln fill level at a low Re_ω in overloading regime significantly increased the Peclet number. Compared to single throughout lifters, segmented lifters has major impact in enhancing axial solid mixing, via the straight lifter section which reduces the passive zone in the bed and significantly decreases the bed fill level. Seven lifters per row were found to be sufficient in enhancing both axial solid mixing and transport. The installation of helix leads to reduce axial solid mixing, particularly in the range near kiln discharge end where bed depth tends to increase. Therefore, in addition to axial solid displacement, the segmented lifters largely enhance axial solid mixing. The usage of segmented lifters, particularly the combination of its folded and straight lifter sections is an effective method to enhance both the axial solid mixing and transport.

Axial solid mixing is also influenced by solid characteristics. A higher Re_ω is required in order to achieve the same *Pe* for granular solid of a higher ϕ and a smaller *d*. The lifter heights h_l also significantly affects by axial solid mixing.

The dimensionless empirical correlation on solid mixing has also been derived on the basis of the experimental results. The angle of repose, rotational Reynolds number and lifter height to kiln diameter ratio, were found to have most significant impacts on Peclet number. However, the developed correlations are largely specific to the current lifters and kiln design.

Chapter 6
Heat Transfer

While the previous two chapters focused on investigations to understand the behaviours of solid transport and mixing, this chapter is devoted to developing a heat transfer model for a hot kiln with segmented lifters. The model is developed to predict axial temperature profiles and determine the rate limiting steps among the heat transfer modes. The present model incorporates the developed axial solid transport and mixing correlations, and takes into account the suitable heat transfer modes as well as relevant reaction kinetic parameters of the solid. The input data of the model was obtained by own experiments or from the literature. The model is validated by our own experimental data.

6.1 Development of integrated mechanisms

Despite the inclusion of many physical phenomena in the model, certain assumptions and strategies were made to simplify the task and refine the scope. The assumptions and strategies are listed below:

1. Discrete solid particles were assumed to be pseudo fluids.
2. The particles were assumed to be spherical and were characterized by the mean size (diameter).
3. The bed and gas elements were assumed to be distinct, well mixed and isothermal within a control volume.
4. The temperature of falling is assumed to be same as bed temperature.
5. The gas phase was simply considered as a plug flow model.

6. Radiation heat transfer for both inside and outside the kiln was neglected due to maximum operating temperature below 1073°K (Barr et al., 1989; Gorog et al., 1981, 1982).
7. Temperature-dependent variables in the correlations are calculated from the average temperatures.
8. Direct-contact convection between the gas and the outer rotating kiln wall is approximated using a method proposed by Tscheng and Watkinson (1979) has been used.

6.1.1 Heat transfer modes

The basic heat transfer coefficients have been determined using the reliable empirical correlations proposed by previous authors as shown in Table 6.1. The heat transfer coefficients for each mode, as discussed later in Section 6.1.2, were calculated using combining these relevant coefficients.

Table 6.1
Correlations of various basic heat transfer coefficients ($W/m^2.K$) (definitions of symbols can be found in the nomenclature).

Symbol	Equation	Reference
h_{ew-g}, h_{eb-g}	$h_{ew-g} = 1.54 \frac{k_g}{D_H} \mathrm{Re}_g^{0.575} \mathrm{Re}_\omega^{-0.292}$ $h_{eb-g} = 0.46 \frac{k_g}{D_H} \mathrm{Re}_g^{0.535} \mathrm{Re}_\omega^{0.104}$ $\mathrm{Re}_g = \frac{u_g D_H}{v_g} = \frac{\rho_g u_g D_H}{\mu_g} \; (1600 < \mathrm{Re}_g < 7800)$	Tscheng and Watkinson (1979)

	$\mathrm{Re}_{\omega} = \frac{D_H{}^2 \omega}{v_g} = \frac{\rho_g \omega D_H{}^2}{\mu_g} \; (20 < \mathrm{Re}_{\omega} < 800)$ $D_H = 0.5 D_{iw} (2\pi - \theta + \sin\theta) / (\pi - \theta/2 + \sin\theta/2)$	
h_{f-ow}	$h_{f-ow} = 1.54 \frac{k_f}{D_{H,f-ow}} \mathrm{Re}_{f-ow}{}^{0.575} \mathrm{Re}_{\omega,f-ow}{}^{-0.292}$ $\mathrm{Re}_{f-ow} = \frac{u_f D_{H,f-ow}}{v_f} = \frac{\rho_f u_f D_{H,f-ow}}{\mu_f} \; (1600 < \mathrm{Re}_f < 7800)$ $\mathrm{Re}_{\omega,f-ow} = \frac{D_{H,f-ow}{}^2 \omega}{v_f} = \frac{\rho_f \omega D_{H,f-ow}{}^2}{\mu_f} \; (20 < \mathrm{Re}_{\omega} < 800)$ $D_{H,f-ow} = D_{ii} - D_{ow}$	Tscheng and Watkinson (1979)
h_{f-ii}	$h_{f-ii} = \frac{k_f}{D_{H,f-ii}} (0.023 \mathrm{Re}_{f-ii}{}^{4/5} \mathrm{Pr}_{f-ii}{}^{1/3})$ $\mathrm{Re}_{f-ii} = \frac{u_f D_{H,f-ii}}{v_f} = \frac{\rho_f u_f D_{H,f-ii}}{\mu_f} \; (10^4 < \mathrm{Re}_{f-ii} < 10^5)$ $\mathrm{Pr}_{f-ii} = \frac{\mu_f c_{pf}}{k_f} \; (0.5 < \mathrm{Pr}_{f-ii} < 160)$ $D_{H,f-ii} = D_{ii} - D_{ow}$	Incropera (2007)
h_{cw-cb}	$h_{cw-cb} = \left(\chi d_p / k_g + 0.5 / \sqrt{2 k_b \rho_b c_{pb} n / \phi} \right)^{-1}$ $(0.096 < \chi < 0.198)$	Li et al. (2005)
h_{oc-a}	$h_{oc-a} = \frac{k_a}{D_{oc}} \left(0.6 + \frac{0.386 (Gr \, \mathrm{Pr}_{oc-a})^{1/6}}{\left(1 + (0.559/\mathrm{Pr}_{oc-a})^{9/16}\right)^{8/27}} \right)^2$	Churchill and Chu (1975)

	$10^{-4} < Gr\,\mathrm{Pr}_{oc-a} < 10^{12}$ $Gr = \frac{g\rho_a{}^2\beta_a(T_{oc}-T_a)D_{oc}{}^3}{\mu_a{}^2} = \frac{g\beta_a(T_{oc}-T_a)D_{oc}{}^3}{\nu_a{}^2}$ $\mathrm{Pr}_{oc-a} = \frac{\mu_a c_{pa}}{k_a}$	
h_{fp-g}	$h_{fp-g} = \frac{k_g}{d_p}\left(2 + \frac{0.589\left(Gr_{fp-g}\,\mathrm{Pr}_{fp-g}\right)^{1/4}}{\left(1+\left(0.469/\mathrm{Pr}_{fp-g}\right)^{9/16}\right)^{4/9}}\right)$ $Gr_{fp-g} = \frac{g\rho_g{}^2\beta_g(T_b-T_g)D_H{}^3}{\mu_g{}^2} = \frac{g\beta_g(T_b-T_g)D_H{}^3}{\nu_g{}^2}$ $\mathrm{Pr}_{fp-g} = c_{pg}\frac{\mu_g}{k_g}\,(\mathrm{Pr} > 0.7)$	Churchill (1983)

6.1.2 Reaction rate model

This model represents the complex coal pyrolysis reactions by a single endothermic reaction based on simple reaction stoichiometry as

Volatile in solid phase → Volatile in gas phase + Char (+ ΔH kJ/kg volatile)

The global pyrolysis reaction kinetic parameters of the low-rank coal were determined based on previous methods proposed in the field of heat transfer analysis (Ceylan et al., 1999; Ciuryla et al., 1979; Guldogan et al., 1999; Kastanaki et al., 2002; Lappas & Vasalos, 1989; Lappas et al., 1990; Sadhukhan et al., 2008; Sutcu, 2007; Suuberg et al., 1978, Vamvuka et al., 2003). All lumped volatile components were modelled follow the Arrhenius law ($k = Ae^{-E_a/RT_b}$) for a 1st – order reaction.

The maximum pyrolysis temperature and heating rate were 773-1273°K and 283-313°K/min. The pre-exponential factor or frequency factor A and the activation energy E_a were found to be 0.2-0.6 s^{-1} and 46-197 kJ/mol.

6.1.3 Energy and mass balances

Figure 6.1 shows a schematic of a horizontal indirectly-heated rotary kiln. A cold material of $T_{b,0}$ enters the kiln at $x = 0$ and has to be heated to $T_{b,L}$. The counter current flue gas of $T_{f,L}$ enters at $x = L$ and is cooled to $T_{f,0}$. The kiln is partially filled with solid particles with a cross-sectional area of A_b.

A one-dimensional model can be derived by considering a transverse slice (Figure 1.1) which divides the section into separate control volumes of freeboard gas, solid bed and flue gas. Under steady state conditions, governed by the energy conservation law, for any control volume, we have:

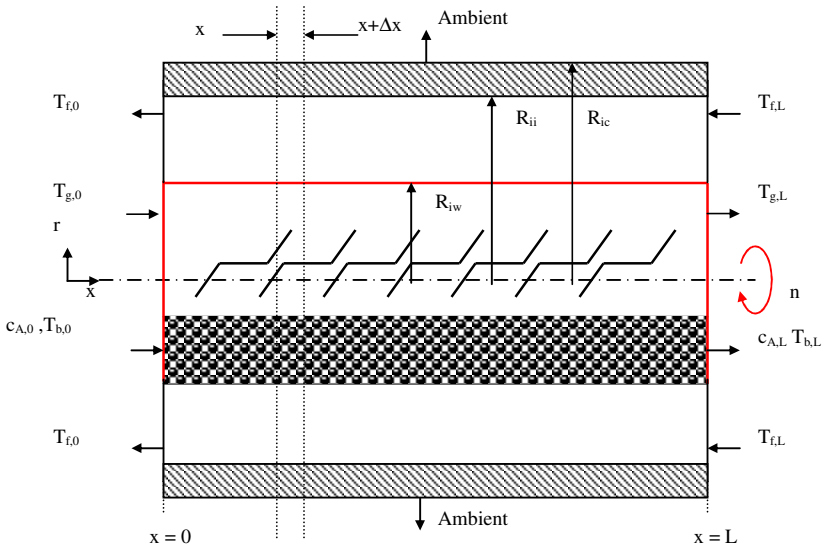

Figure 6.1 A schematic diagram of a horizontal indirectly-heated rotary kiln with segmented lifters. (Do not scale)

Freeboard gas phase :

$$m_g c_{pg} \frac{dT_g}{dx} = Q_{ew-g} + Q_{eb-g} + Q_{fp-g} \quad \text{..... (6.1)}$$

Bed phase :

$$m_b c_{pb} \frac{dT_b}{dx} = Q_{eb-g} + Q_{cw-cb} + Q_{fp-g} + \Delta H.\rho_b.A_b.r_A \quad \text{..... (6.2)}$$

Flue gas phase :

$$m_f c_{pf} \frac{dT_f}{dx} = Q_{f-a} + Q_{f-iw} \quad \text{..... (6.3)}$$

As the net energy accumulation within the wall can be neglected, we have,

Wall :

$$Q_{f-iw} = Q_{ew-g} + Q_{cw-cb} \quad \text{..... (6.4)}$$

Considering heat transfer coefficients in Table 6.1, Eqs (6.1-6.4) can be regarded as:

$$m_g c_{pg} \frac{dT_g}{dx} = h_{ew-g} A_{ew} \left(T_w - T_g\right) + h_{eb-g} A_{eb} \left(T_b - T_g\right) + h_{fp-g} A_{fp} \left(T_b - T_g\right) \quad \text{..... (6.5)}$$

$$m_b c_{pb} \frac{dT_b}{dx} = h_{eb-g} A_{eb} \left(T_b - T_g\right) + h_{cw-cb} A_{cw} \left(T_w - T_b\right) + h_{fp-g} A_{fp} \left(T_b - T_g\right) + \Delta H.\rho_b.A_b.r_A$$

..... (6.6)

$$m_f c_{pf} \frac{dT_f}{dx} = h_{f-a} A_{oc} \left(T_f - T_a\right) + h_{f-iw} A_{iw} \left(T_f - T_w\right) \quad (6.7)$$

$$h_{f-iw} A_{iw} \left(T_f - T_w\right) = h_{ew-g} A_{ew} \left(T_w - T_g\right) + h_{cw-cb} A_{cw} \left(T_w - T_b\right) \quad (6.8)$$

The heat loss from flue gas to the ambient Q_{f-a} includes four heat transfer resistances: the forced convection resistance between the flue gas and inner insulation $\left(1/h_{f-ii}\right)$, the conduction resistance between the inner insulation and inner casing $\left(1/h_{ii-ic}\right)$, the conduction resistance between inner casing and outer casing $\left(1/h_{ic-oc}\right)$; and the free convection resistance between the outer casing and ambient $\left(1/h_{oc-a}\right)$. The total resistance of heat transfer can be written as:

$$h_{f-a} = \left(1/h_{f-ii} + 1/h_{ii-ic} + 1/h_{ic-oc} + 1/h_{oc-a}\right)^{-1} \quad (6.9)$$

The total heat transfer coefficient between flue gas and inner wall h_{f-iw} can be expressed as:

$$h_{f-iw} = \left(1/h_{f-ow} + 1/h_{ow-iw}\right)^{-1} \quad (6.10)$$

The three conduction resistances can be calculated by:

$$1/h_{ii-ic} = \frac{D_{ic}}{2k_i} \ln\left(\frac{D_{ic}}{D_{ii}}\right) \quad (6.11)$$

$$1/h_{ic-oc} = \frac{D_{oc}}{2k_w}\ln\left(\frac{D_{oc}}{D_{ic}}\right) \quad \text{..... (6.12)}$$

$$1/h_{ow-iw} = \frac{D_{iw}}{2k_w}\ln\left(\frac{D_{iw}}{D_{ow}}\right) \quad \text{..... (6.13)}$$

Chapter 5 has shown that ideal plug flow may not be realized in a rotary kiln with segmented lifters. A solid bed model is needed to consider the deviations from an ideal plug flow. The surface tracer concentration measurements show a reasonable amount of axial dispersion as travels through the kiln. The dispersed steady state plug-flow mass balance to account for a reacting species *A* (gaseous in bed phase) given in Equation (6.14) allows for this spreading phenomenon (Levenspiel, 1999). The dispersion term is described by a second-order derivative in the axial direction.

$$u_b \frac{dc_A}{dz} - (-r_A) - D_z \frac{d^2c_A}{dz^2} = 0 \quad \text{..... (6.14)}$$

The concentration of species *A* along the kiln is c_A in kg volatile/kg coal, the axial flow velocity of the solid is u in m/s, the axial dispersion coefficient is D_z in m^2/s and the axial distance along the kiln length is z in m.

Written in a dimensionless form, this equation is seen to depend on dimensionless groups u_bL/D (= *Pe*), *x/L* (= z) and a parameter *a* as $a = \sqrt{1 + 4kD_z/u_b^2}$. The solution of Equation (6.14) subjects to boundary conditions of Wehner and Wilhelm (1956) for species *A* gives

$$\frac{c_A}{c_{A0}} = 1 - X_A = 2\exp\left(Pe\frac{x}{2L}\right)\frac{(1+a)\exp\left[Pe\frac{a}{2}\left(1-\frac{x}{L}\right)\right] - (1-a)\exp\left[Pe\frac{a}{2}\left(\frac{x}{L}-1\right)\right]}{(1+a)^2\exp\left(Pe\frac{a}{2}\right) - (1-a)^2\exp\left(-Pe\frac{a}{2}\right)} \quad \text{..... (6.15)}$$

An examination of the above ordinary differential equations (ODEs), Equations (6.5 – 6.7), show that they are nonlinear. Since it was unlikely that an analytical solution could be found for these equations, these ODEs were solved numerically by the Runge-Kutta-Fehlberg (RKF) technique (Forsythe et al., 1977) combined with the explicit equations and inlet conditions of the freeboard gas, bulk solid, flue gas and volatile in solid phase. The information flow diagram for the integrated heat transfer model is depicted in Figure 6.2.

The overall heat transfer efficiency η is calculated as:

$$\eta = 100\frac{U\Delta T_{LM}}{(Q_{f-iw} + Q_{f-a})} \quad \text{..... (6.16)}$$

The overall heat transfer coefficient from flue gas to solid bed U and the log mean temperature difference ΔT_{LM} are given as:

$$U = \left[\left(\frac{1}{h_{f-iw}A_{eb}}\right) + \left(\frac{1}{h_{ow-iw}A_{ow}}\right) + \left(\frac{1}{h_{cw-cb}A_{cw}}\right)\right]^{-1} \quad \text{..... (6.17)}$$

$$\Delta T_{LM} = \frac{(T_{f,L} - T_{b,L}) - (T_{f,0} - T_{b,0})}{\ln\left(\frac{T_{f,L} - T_{b,L}}{T_{f,0} - T_{b,0}}\right)} \quad \text{..... (6.18)}$$

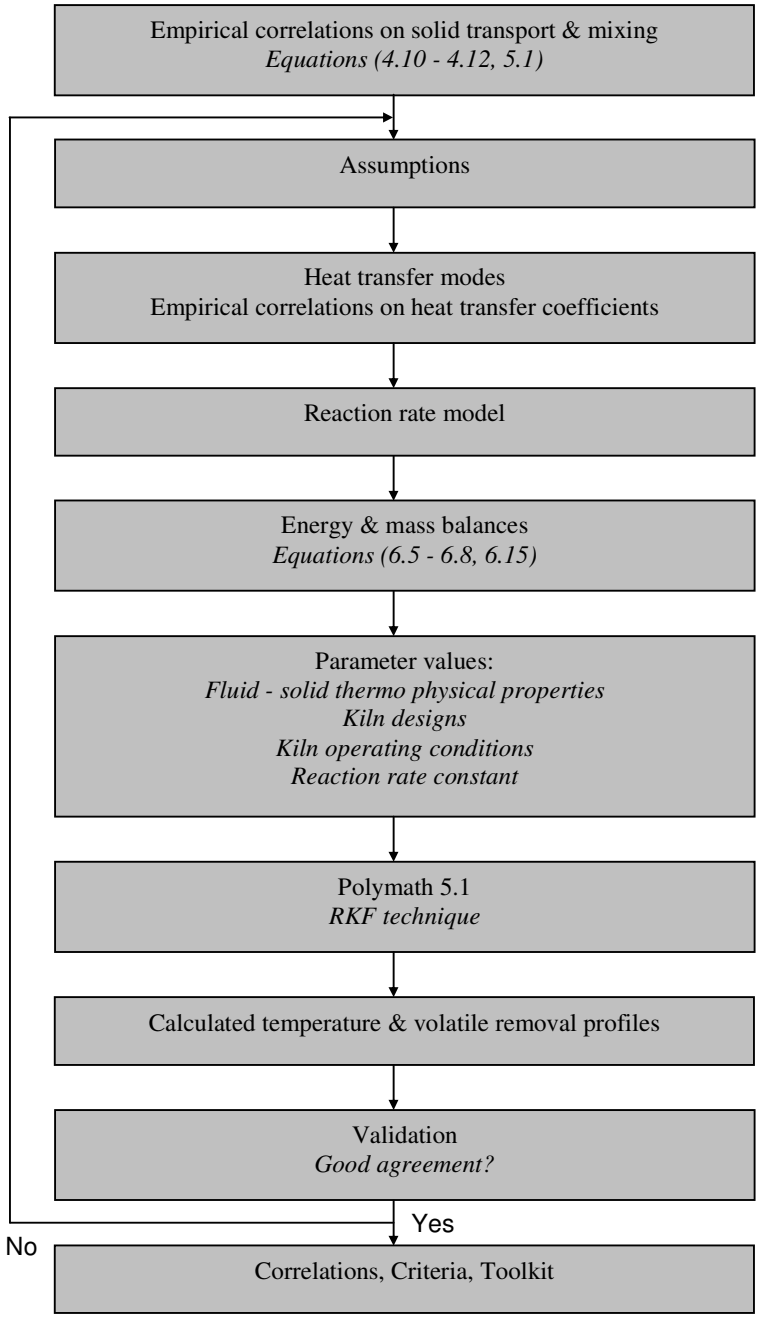

Figure 6.2. Flow diagram of the heat transfer model.

6.1.4 Validation

In the present work, two sets of data from the hot kiln experiments are used for model validation. The experiment conditions of the pilot hot kiln and relevant thermo-physical properties of the flue gas, freeboard gas and solid, are summarized in Table 6.2. Both Figures 6.3 and 6.4 display the comparison of the measured temperatures profiles and volatile species removal with those predicted by the current one-dimensional model.

It can be seen that the calculated data are in reasonably agreement with the experimental data. It is apparent that the actual temperatures of the flue gas and inner kiln wall are slightly higher that the predicted results at the middle section.

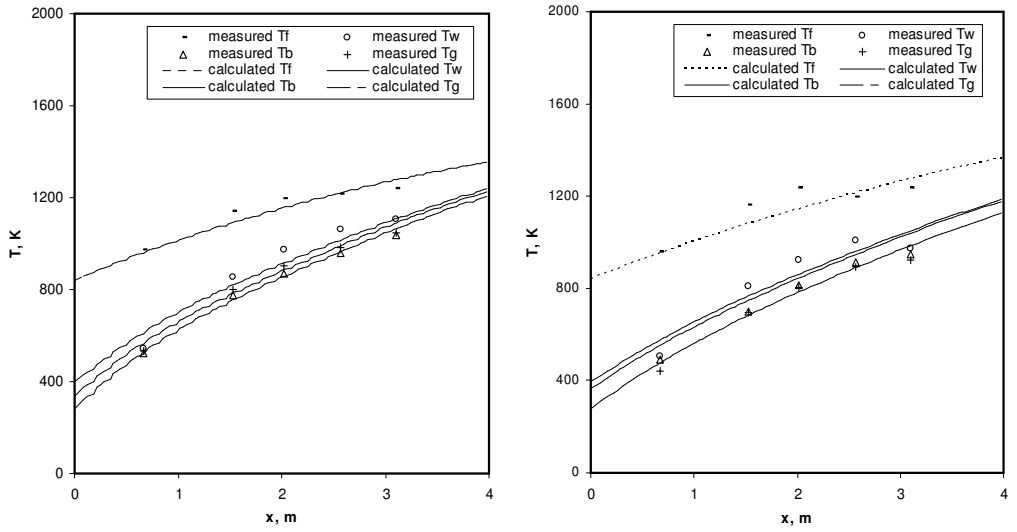

(a) (b)

Figure 6.3. Comparison of predicted axial temperature profiles by the one-dimensional model and experimental data: (a) m_b = 260 kg/h, m_f = 260 kg/h and (b) m_b = 365 kg/h, m_f = 234 kg/h

Table 6.2.

Parameter values used during the simulations (definitions of symbols can be found in the nomenclature).

Symbol	Value/equation	Unit	Reference
L	3.980	m	Design
D_{iw}	0.498	m	Design
D_{ow}	0.510	m	Design
D_{ii}	1.200	m	Design
D_{ic}, D_{oi}	1.350	m	Design
D_{oc}	1.362	m	Design
$D_{H,f\text{-}ow}$, $D_{H,f\text{-}ii}$	$D_{ii} - D_{ow}$	m	Based on system geometry
D_H	0.422	m	Based on system geometry
A_{iw}	πD_{iw}	$m^2.m^{-1}$	Based on system geometry
A_{ow}	πD_{ow}	$m^2.m^{-1}$	Based on system geometry
A_{ii}	πD_{ii}	$m^2.m^{-1}$	Based on system geometry
A_{ic}, A_{oi}	πD_{ic}	$m^2.m^{-1}$	Based on system geometry
A_{oc}	πD_{oc}	$m^2.m^{-1}$	Based on system geometry
A_{ew}	$\pi D_{iw} - A_{cw} + 4h_l + 2t_l$	$m^2.m^{-1}$	Based on system geometry
A_{eb}	$2\sqrt{R_{iw}^2 - (R_{iw} - h)^2}$	$m^2.m^{-1}$	Based on system geometry
A_{cw}	$R_{iw}\theta + 2h_l + t_l$	$m^2.m^{-1}$	Based on system geometry
A_{fp}	R_{iw}	$m^2.m^{-1}$	Based on system geometry
A_{kiln}	$0.25\pi D_{iw}^{\ 2}$	m^2	Based on system geometry
A_b	$f.A_{kiln}$	m^2	Based on system geometry
A_g	$A_{kiln} - A_b$	m^2	Based on system geometry
A_f	$0.25\pi\left(D_{ii}^{\ 2} - D_{ow}^{\ 2}\right)$	m^2	Based on system geometry
h_l	0.08	m	Design
t_l	0.006	m	Design
k_g	0.06	$W.m^{-1}.K^{-1}$	Li et al (2005)
k_f, k_a	0.03	$W.m^{-1}.K^{-1}$	Incropera & Dewitt (2002) at T_{oc}
k_b	0.4	$W.m^{-1}.K^{-1}$	Badzioch et al (1964)
k_i	0.17	$W.m^{-1}.K^{-1}$	CeraTex (n.d.)
k_w	60	$W.m^{-1}.K^{-1}$	Perron & Bui (1990)

ρ_g	0.857	kg.m^{-3}	Li et al. (2005)
ρ_f, ρ_a	1	kg.m^{-3}	Incropera & Dewitt (2002) at T_{oc}
ρ_b	600	kg.m^{-3}	Measured
μ_g	8.57 x 10^{-7}	kg.m^{-1}.s^{-1}	Calculated ($\mu_g = \rho_g . \nu_g$)
μ_a, μ_f	2.1 x 10^{-5}	kg.m^{-1}.s^{-1}	Incropera & Dewitt (2002) at T_{oc}
ν_g	1 x 10^{-5}	m^2.s	Li et al. (2005)
ν_a, ν_f	2.1 x 10^{-5}	m^2.s	Incropera & Dewitt (2002) at T_{oc}
$c_{p,g}$	2920	J.kg^{-1}.K^{-1}	Design
$c_{p,a}$	1009	J.kg^{-1}.K^{-1}	Incropera & Dewitt (2002) at T_{oc}
$c_{p,f}$	1209	J.kg^{-1}.K^{-1}	Design
$c_{p,b}$	1150	J.kg^{-1}.K^{-1}	Agroskin et al. (1970)
u_g	0.20 – 0.26	m.s^{-1}	Calculated ($m_g/\rho_g A_g$)
u_f	0.07 - 0.08	m.s^{-1}	Calculated ($m_f/\rho_f A_f$)
u_b	Equation (4.12)	m.s^{-1}	Present author
d_p	0.03	m	Measured
ϕ	0.79	rad	Measured
χ	0.1	-	Li et al. (2005)
g	9.80665	m.s^{-2}	-
R	8.314472	J.mol^{-1}K^{-1}	-
π	3.142857143	-	-
T_{oc}	353	K	Measured
T_a	293	K	Design
n	2	rpm	Design
m_g	0.4 m_b	kg.h^{-1}	Design
m_b	260 - 325	kg.h^{-1}	Measured
m_f	(0.2 - 0.5) $m_g + m_{air}$	kg.h^{-1}	Design
m_{air}	208	kg.h^{-1}	Design
ΔH	3 x 10^5	J/kg volatile	Patisson et al. (2000)
A	0.6	s^{-1}	see in Section 6.1.2
E_a	5.225 x 10^4	J/mol	see in Section 6.1.2
f	Equation (4.10)	-	Present author
θ	$f = (\theta - \sin(\theta))/2\pi$	rad	Based on system geometry
h	$R_{iw} - R_{iw}\cos(\theta/2)$	m	Based on system geometry
H	$0.25\pi D_{iw}{}^2 L \rho_b f$	kg	Based on system geometry
τ	Equation (4.11)	s	Present author
Pe	Equation (5.3-1)	-	Present author
ew-g	34.1- 40.5	W.m^2.K^{-1}	calculated (see in Table 6.1)

g-eb	191.8 – 221.7	$W.m^2.K^{-1}$	calculated (see in Table 6.1)
f-ow	19.4 - 24.0	$W.m^2.K^{-1}$	calculated (see in Table 6.1)
f-ii	0.7 - 0.9	$W.m^2.K^{-1}$	calculated (see in Table 6.1)
oc-a	4.6	$W.m^2.K^{-1}$	calculated (see in Table 6.1)
cw-cb	176.4 – 177.1	$W.m^2.K^{-1}$	calculated (see in Table 6.1)
g-fp	367.3 – 480.6	$W.m^2.K^{-1}$	calculated (see in Table 6.1)
ii-ic	2.1	$W.m^2.K^{-1}$	calculated (see in Table 6.1)
ic-oc	9955.9	$W.m^2.K^{-1}$	calculated (see in Table 6.1)
ow-iw	9881.9	$W.m^2.K^{-1}$	calculated (see in Table 6.1)
f-iw	19.4 - 24.0	$W.m^2.K^{-1}$	calculated (see in Table 6.1)
f-a	0.5 - 0.6	$W.m^2.K^{-1}$	calculated (see in Table 6.1)

As shown in Figures 6.3a and 6.3b, the bed temperature at a lower coal feed rate increased more rapidly along the kiln. The temperature difference between solid bed and flue gas is also smaller. It can be explained in terms of the role of solid transport and mixing played in the heat transfer process.

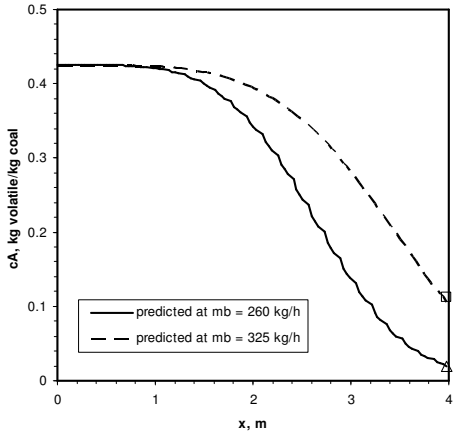

Figure 6.4. Predicted volatile species concentration profiles and its comparison with experimental data (Δ = measured at m_b = 260 kg/h, □ = measured at m_b = 325 kg/h)

Based on Equations (4.10) and (5.1), it should be noted that the kiln fill levels and Peclet numbers *Pe* increased from 14 % to 17 % and from 71 to 77, corresponding to

rotational Reynolds numbers Re_ω decreased from 215 to 172, respectively. Based on Equations (6.16 – 6.18), the overall heat transfer efficiency η increases significantly from 51 % to 80 % with the overall heat transfer coefficient U slightly increases from 31 to 35 W/m^2.K due to 50 % less of recycled off-gas, from 52 to 26 kg/h. This corresponds to an increase in the concentration of the solid product from to 2.0 % to 10.5 % as shown in Figure 6.4 and slightly decreases in the mean residence time slightly decreased from 15 to 14.6 minutes. The increase in the volatile content of the solid product is mainly due to reducing bed temperature as a result of increasing flow rate.

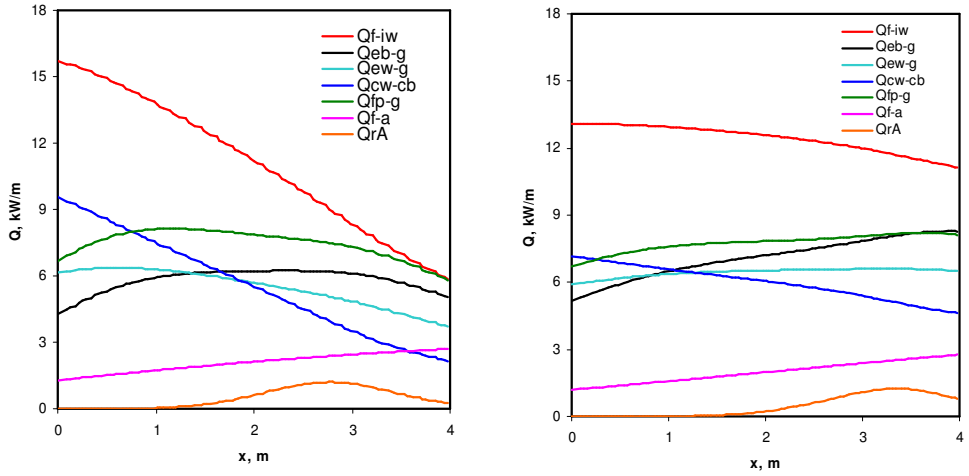

Figure 6.5. Net heat fluxes outside and inside kiln from different modes of transfer: (a) m_b = 260 kg/h and (b) m_b = 365 kg/h.

Calculations have then been carried out to assess the net heat fluxes and the contribution of different heat transfer modes to overall heat transfer process, as shown in Figure 6.5. Figure 6.5 shows that net input to the bed $Q_{cw\text{-}cb}$ for a low coal feed rate declined more rapidly (by 76.8% from 9.5 to 2.2 kW/m) along the kiln than that of a high coal feed rate (by 36.1% from 7.2 to 4.6 kW/m). At a low coal feed rate (Re_ω = 215), the kiln operation achieves a higher degree of axial solid transport and mixing, leading to an enhanced heat transfer to the bed from inner kiln wall. The

wall, bed and freeboard gas temperatures increased along the kiln length rapidly as shown in Figure 6.3a. The profile of $Q_{f\text{-}iw}$ is similar to that of $Q_{cw\text{-}cb}$. While heat loss from the flue gas to the ambient $Q_{f\text{-}a}$ gradually increased along the axial location. $Q_{f\text{-}a}$ at both feed rates has reached 2.7 kW/m at the kiln outlet.

Figure 6.6 shows the contribution of different heat transfer modes (Q_{rA}, $Q_{ew\text{-}g}$, $Q_{cw\text{-}cb}$, $Q_{eb\text{-}g}$, and $Q_{fp\text{-}g}$), as a fraction to the total heat flux inside the kiln. Heat transfer from the covered wall to covered bed ($Q_{cw\text{-}cb}$) plays a key role in overall heat transfer into the bed. The proportions of $Q_{cw\text{-}cb}$ reduce gradually because the difference between the temperatures of the solid bed and inner kiln wall decreases along the kiln length. In the initial zone (kiln feed end), the net input to the bed $Q_{cw\text{-}cb}$ is lower than the lower at a higher coal feed rate. This is likely due to the non-uniformity solid load along the kiln, especially in the initial zone as discussed in Chapter 4. This leads to a decreased bed depth, therefore heat transfer rate along the kiln length.

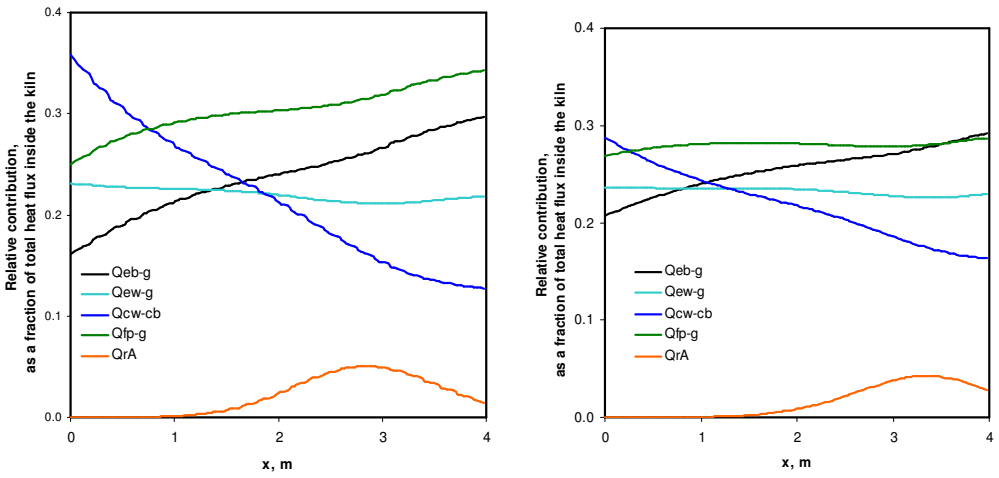

(a) (b)

Figure 6.6. Contribution of various heat transfer modes inside the kiln: (a) m_b = 260 kg/h and (b) m_b = 365 kg/h.

The heat required for a chemical reaction was found to make the smallest contribution (< 5 %) to the overall heat transfer inside the kiln. For heat transfer to freeboard gas, in comparison to the heat transfer from exposed inner wall ($Q_{ew\text{-}g}$) and exposed bed ($Q_{eb\text{-}g}$), the heat transfer from falling particles ($Q_{fp\text{-}g}$) makes the biggest contribution to the net heat input to the freeboard gas. Along the kiln length, $Q_{fp\text{-}g}$ retains at steady value of 8 kW/m at a high coal feed rate (see Figure 6.6b), corresponding to a gradual increase in the bed and freeboard gas temperatures as shown in Figure 6.3b. As discussed in Chapters 4 and 5, at a higher Re_{ω}, lifters have more energy in enhancing both axial solid transport and mixing by scooping, pushing, lifting and spilling solid. This leads to an increase in $Q_{fp\text{-}g}$ along the kiln.

The predicted $Q_{ew\text{-}g}$ profiles at the low and high coal feed rates are at steady values of 5.5 and 6.4 kW/m along the kiln, respectively. This is mainly due to a 25% increase in the freeboard gas produced at a higher coal feed rate.

Heat transfer from exposed bed ($Q_{eb\text{-}g}$) increases coal feed rate, particularly in the initial zone. This is mainly the 5% increase in the average heat transfer area A_{eb}, from 0.397 to 0.417 m^2/m kiln length. In fact, heat transfer area proportion in the initial zone was believed to be the highest due to an inclined bed depth profile.

As discussed in Chapters 4 and 5, overloading kilns have an inclined bed depth profile, corresponding to an increasing axial solid velocity and a decreasing residence time along the kiln and poor axial solid mixing. The heat transfer non-uniformity along the kiln length is fundamentally related to solid transport and mixing therefore must be considered in the design stage. This indicates that heat transfer from the covered wall to the covered bed is the limiting heat transfer step.

6.2 Summary

An integrated axial heat transfer model has been developed and applied to the process of low-rank coal pyrolysis in a pilot-scale indirectly heated rotary kiln at two different coal feed rates, with consideration for the effect of segmented lifters which

has not been considered by any axial heat transfer model to date. The reasonable agreement between the present model predictions and experimental data was achieved on the effect of feed rates.

The model has provided further insights into the solid transport and mixing processes occurring within the bed affecting the heat transfer behaviours. The overall heat transfer efficiency can be significantly increased by 57 % by lowering Re_ω from 215 to 172 and using 50 % less amount of recycled off gas. However, the volatile species in coal at the kiln end significantly increased from 2.0 % to 10.5 % as coal feed rate increased, corresponding to lower Re_ω. This is due to the kiln was operated in overloading regime leading to an inclined bed depth profile and poor axial mixing performances. Among the heat transfer modes, it is clear that heat transfer from the covered inner kiln wall to the covered bed, which is fundamentally dependent on solid transport and mixing in the kiln bed, is the limiting step of the overall heat transfer inside the kiln. Typical values of overall heat transfer coefficient are also estimated to be 31 - 35 $W/m^2.K$.

Chapter 7
Conclusions and Recommendations

This chapter concludes the present study by highlighting the main research findings. The present research has led to the discovery of new knowledge on solid transport, solid mixing and heat transfer mechanisms in an indirectly rotary kiln with lifters of various designs and configurations. The research has developed new dimensionless correlations on solid transport, solid mixing as well as a steady-state axial heat transfer model for the kiln with segmented lifters.

7.1 Conclusions

The key findings from the present study are as follows:

1. This study has investigated the effect of segmented lifters on axial solid transport and solid mixing in horizontal rotary kilns and revealed the fundamental mechanisms leading to such effect. It is found that the axial bed depth profile, total kiln volumetric filling fraction and Peclet numbers are strongly dependent on solid loading, lifter design and lifter configurations.

2. A flat bed depth profile and enhanced axial solid mixing can be effectively achieved in horizontal rotating kilns with segmented lifters, particularly those with a design combining both folded and straight sections. The effect of helix has insignificant impacts on solid transport and mixing performances.

3. The preliminary Discrete Element Method (DEM) confirmed that the axial displacement is mainly due to folded lifter sections, which push the solids towards kiln discharge end along the bed arc length.

4. A simplified theoretical model has been developed to predict the average depth in horizontal rotating kilns with segmented lifter, operating in the underloading regimes. The predictions are in good agreement with experimental data.

5. A set of useful dimensionless empirical correlations on solid transport and solid mixing have been developed. Such global power-law correlations are validated by our experimental data. The results indicate that

   - solid transport and mixing in horizontal rotating kilns with segmented lifters are dominantly influenced by the static angle of repose, rotational Reynolds number and lifter height to kiln diameter ratio.
   - *Fr* has an insignificant impact on solid transport and mixing, indicating that in horizontal rotating kilns with segmented lifters, solid transport and mixing is dominantly driven by lifters, rather than gravity force in kilns without lifters.
   - horizontal rotating kilns with segmented lifters are flexible to handle solid with wide size distribution.

6. A steady-state axial heat transfer model, validated by experimental data, has been developed for an indirectly heated horizontal rotary kiln with segmented lifters. The model incorporates the solid transport and solid mixing correlations developed in this study. The model predicts the temperature profiles of the freeboard gas, solid bed, inner kiln wall and flue gas. It is found that the limiting step is the heat transfer from covered inner kiln wall to covered bed, which is strongly influenced by solid transport and solid mixing.

7.2 Recommendations

Although the overall objectives of the present study have been achieved, there are still considerable scopes for future research. The recommendations for future study are listed as follows:

1. In the present study, a wide variety of solid have been used which limited to monosize dry granular solid, a systematic investigation on axial solid transport and mixing considering dry granular solid with a realistic particle size distribution can be part of future study.

2. The current study considers configuration of 3 rows lifters. Future study should extend to investigate the effect of the number of segmented lifter rows, since big lifters are not favourable in commercial kilns.

3. Theoretical model on solid transport developed is limited to underloading regimes. Future study should consider modelling in overloading regimes.

4. Future work should also consider comprehensive DEM simulations in order to compare the model predictions with experimental data on solid mixing.

5. In practical applications, the heat transfer in the rotary kilns involves a strong coupling among discrete particle flow and continuum gas. Future work should consider coupled DEM - CFD simulations for better prediction.

6. Future work should also extend the solid mixing correlation to include the kiln length to kiln diameter ratio.

7. The steady state axial heat transfer model lays a foundation for the continuing effort in developing an overall process system model for various applications. Future modelling work should incorporate the combustion model of burner.

Nomenclature

A	[m^2]	cross-sectional area
A	[$m^2.m^{-1}$]	heat transfer area per kiln length
A	[s^{-1}]	pre-exponential / frequency factor
A_z	[m^2.folded lifter section^{-1}]	perpendicular cross-section area
b_1	[m]	height of folded lifter parts
b_2	[m]	width of folded lifter parts
b_3	[m]	lifter width
C	[-]	tracer concentration
C	[-]	solid transport coefficient
c	[m]	chord length of the top face of the bed
c_A	[kg volatile. kg coal^{-1}]	concentration of species A
C_D	[-]	drag coefficient
c_p	[$J.kg^{-1}.K^{-1}$]	heat capacity
D	[m]	kiln diameter
d	[m]	particle size
D_z	[$m^2.s^{-1}$]	axial dispersion coefficient
E	[s^{-1}]	exit age distribution
Ea	[$J.mol^{-1}$]	activation energy
f	[-]	total kiln volumetric filling fraction
Fr	[-]	Froude number
$\vec{F}_{total,i}$	[N]	total force acting on particle i
g, $\vec{g}$	[$m.s^{-2}$]	acceleration of gravity
Gr	[-]	Grashof number
h	[$W.m^{-2}.K^{-1}$]	heat transfer coefficient
h	[m]	bed depth
H	[kg]	total solid hold-up
h_l	[m]	lifter or helix height

i	[-]	nth data
k	[$W.m^{-1}.K^{-1}$]	heat transfer conductivity
k	[s^{-1}]	rate constant
L	[m]	total kiln length
L_a	[m]	arch length of the bed
m	[$kg.s^{-1}$, $kg.h^{-1}$]	feed rate
m_i	[kg]	mass of particle i
n	[rps, rpm]	kiln rotational speed
N_f	[-]	number of folded section per lifter
N_l	[-]	number of lifter per kiln cross-section
P	[m]	wetted perimeter
Pe	[-]	Peclet number
Pr	[-]	Prandtl number
Q	[$m^3.s^{-1}$]	volumetric flow rate of solid
Q	[$W.m^{-1}$]	net heat transfer rate
R	[m]	kiln or kiln radius
R	[$J.K^{-1}.mol^{-1}$]	gas constant (=8.314472)
R^2	[-]	correlation coefficient
Re	[-]	Reynolds number
Re_ω	[-]	(gas, solid) rotational Reynolds number
r_A	[kg volatile. kg $coal^{-1}.s^{-1}$]	reaction rate of species A
T	[K]	temperature
t	[s]	time
t_l	[m]	lifter thickness
u	[$m.s^{-1}$]	axial fluid or solid velocity
U	[$W.m^{-1}.K^{-1}$]	overall heat transfer coefficient
u_{local}	[$m.s^{-1}$]	local axial solid velocity
$\vec{u}_i$	[$m.s^{-1}$]	velocity of particle i
V_z	[$m^3.rotation^{-1}.lifter^{-1}$]	displaced axial volume
z, x	[m]	axial distance
X_A	[-]	conversion of species A

Greek letters

χ	[-]	thickness of gas film
β	[K^{-1}]	volumetric heat transfer expansion coefficient (β =1/T)
η	[%]	overall heat transfer efficiency
ρ	[$kg.m^{-3}$]	density
ν	[$m^{-2}.s^{-1}$]	kinematic viscosity ($\nu=\mu/\rho$)
μ	[$N.s.m^{-2}$]	dynamic viscosity
α	[$m^{-2}.s^{-1}$]	heat transfer diffusivity
α	[degree]	folded lifter angle,
Δ	[-]	interval
ΔH	[J.kg volatile^{-1}]	overall heat of pyrolysis
ΔT_{LM}	[K]	log mean temperature difference
θ	[degree, rad]	filling angle
θ	[degree, rad]	kiln axis slope
ϕ	[degree, rad]	static angle of repose
ω	[$rad.s^{-1}$]	kiln rotational speed
π	[-]	phi (=22/7)
τ , $\bar{t}$	[s]	mean residence time
σ^2	[-]	variance
σ_θ^2	[-]	dimensionless standard deviation
σ_r^2	[-]	relative error variance
σ	[-]	standard deviation

$$\sigma = \sqrt{\sum_{i=1}^{N}\left[\left|\frac{y_{calc,i}-y_{\exp,i}}{y_{\exp,i}}\right| - AARE\right]^2 /(N-1)}$$

Average absolute relative error,

$$AARE = \frac{1}{N}\sum_{i=1}^{N}\left|\frac{\left(y_{calc,i}-y_{\exp,i}\right)}{y_{\exp,i}}\right|$$

Subscript

a	ambient
b	bed
cb	covered bed
cw	covered inner kiln wall
eb	exposed bed
ew	exposed inner kiln wall
f	flue gas
fp	falling particles
g	freeboard gas
H	hydraulic
i	insulation
ic	inner casing
ii	inner insulation
iw,w	inner kiln wall
oc	outer casing
ow	outer kiln wall
p	particle
t	terminal velocity

References

Abouzeid, A.-Z. , T.S. Mika, K.V. Sastry, and D.W. Fuerstenau. 1974. The influence of operating variables on the residence time distribution for material transport in a continuous rotary kiln. *Powder Technology* 10: 273– 288.

Abouzeid, A.-Z.M., and D.W. Fuerstenau. 1980. Scale-up of particulate hold-up in rotary kilns. *Powder Technology* 25: 65-70.

Abouzeid, A.-Z.M., D.W. Fuerstenau, and K.V.S. Sastry. 1980. Transport behavior of particulate solid in rotary kilns: scale-up of residence time distribution using the axial dispersion model. *Powder Technology* 27: 241-250.

Adler, R.J., and R.B. Hovorka. 1961. *Proceedings of the Second Joint Automatic Control Conference 1961: A finite-stage model for highly asymmetric residence time distributions.*

Afacan, A., and J.H. Masliyah. 1990. Solid hold-up in rotary kilns. *Powder Technology* 61: 179–184.

Agroskin, A.A., E.I. Goneczarow, L.A. Makeev and W.P. Jakunin. 1970. Heat transfer capacity and heat of pyrolysis of Donbass coal. *Koki Chimija* (in Russian) 5: 8-13.

Alonso, M., M. Satoh, and K. Miyanami. 1991. Optimum combination of size ratio, density ratio and concentration to minimize free surface segregation, *Powder Technology* 68: 145-152.

Androutsopoulos, G.P., K.S. Hatzilyberis, N.A. Theofilou, D.S. Agalianos, C.G. Chronis, V.N. Kapassakalis, A.G. Karsakos, A.N. Katsaros, C.P. Stamatakis, and C.L. Zissis. 2003. Gasification of Greek lignite in an indirect heat (alloheat transfer) rotary kiln gasifier. *Chemical Engineering Communications* 190(9): 1200-1232.

Austin, L.G., K. Shoji, R. Hogg, J. Carlson, and R.L.C. Flemmer. 1978. Flow rates of dry powders in inclined rotating cylinders under open-end discharge conditions. *Powder Technology* 20: 219-225.

Badzioch, S., D.R. Gregory, and M.A. Field. 1964. Investigation of the Temperature Variation of the Heat transfer Conductivity and Heat transfer Diffusivity of Coal. *Fuel* 43: 267.

Barr, P.V., J.K. Brimacombe, and A.P. Watkinson. 1989. A heat-transfer model for the rotary kiln: Part II. Development of the cross-section model. *Metallurgical and Materials Transaction* 20B: 403–419.

Brimacombe, J.K., and A.P. Watkinson. 1978. Heat transfer in a direct-fired rotary kiln: I. Pilot plant and experimentation. *Metallurgical and Materials Transaction* 9B: 201–208.

CeraTex, n.d. *Chemical and Physical Data*. http://www,ceramicfiber.net (accessed February 20, 2009).

Ceylan, K., H. Karaca, Y. Onal. 1999. Thermogravimetric analysis of pretreated Turkish lignites. *Fuel* 78: 1109-1116.

Chaterjee, A., A.V. Sathe, and P.K. Mukhopadhyay. 1983b. Flow of materials in rotary kilns used for sponge iron manufacture: Part II. Effect of kiln geometry. *Metallurgical and Materials Transaction* 14B: 383-392.

Chaterjee, A., P.K. Mukhopadhyay, M.P. Srivastava, and A.V. Sathe. 1983a. Flow of materials in rotary kilns used for sponge iron manufacture: Part I. Effect of some operational variables. *Metallurgical and Materials Transaction* 14B: 375-382.

Churchill, S.W., and H.H.S. Chu. 1975. Correlation equations for laminar and turbulent free convection from a horizontal cylinder. *International Journal of Heat and Mass Transfer* 18:1049-1053.

Churchill, S.W. 1983. Free convection around immersed bodies. In *Heat exchanger design handbook*, ed. E.U. Schlunder, New York: Hemisphere Publishing Corp.

Ciuryla, V.T., R.F. Weimer, D.A. Bivans, and S.A. Motika. 1979. Ambient-pressure thermogravimetric characterization of four different coals and their chars. *Fuel* 58: 748-754.

Clement, E., J. Rajchenbach, and J. Duran. 1995. Mixing of granular material in a bidimensional rotating kiln, *Europhysic Letter* 30: 7-12.

Dauman, B., and H. Nirschl. 2008. Assessment of the mixing efficiency of solid mixtures by mean of image analysis. *Powder Technology* 182: 415-423.

Davis, R.A. 1996. Mathematical model of magnetite oxidation in a rotary kiln furnace. *The Canadian Journal of Chemical Engineering* 74: 1004-1009.

Davis, R.A., and D.J. Englund. 2003. Model and Simulation of a Ported Kiln for Iron Oxide Pellet Induration. *The Canadian Journal of Chemical Engineering* 81: 86-93.

Dinesh, L., and P.S.T. Sai. 2004. A model for residence time distribution of solid in rotary kiln. *The Canadian Journal of Chemical Engineering* 82: 392-398.

Ding ,Y.L., R.N. Forster, J.K. Seville, and D.J. Parker. 2001. Some aspects of heat transfer in rolling mode rotating kilns operated at low to medium temperatures. *Powder Technology* 121: 168–181.

Ding, Y.L., R.N. Forster, J.P.K. Seville, and D.J. Parker. 2001. Scaling relationships for rotating kilns. *Chemical Engineering Science* 56: 3737-3750.

Ferron, J.R., and D.K. Singh. 1991. Rotary kiln transport processes. *AIChE Journal* 37(5): 747-758.

Forsythe, G.E., M.A. Malcolm, and C.B. Moler. 1977. *Computer Methods for Mathematical Computation,* Englewood Cliffs: Prentice-Hall.

Georgallis, M., P. Nowak, M. Salcudean, and I.S. Gartshore. 2005. Modelling the rotary lime kiln. *The Canadian Journal of Chemical Engineering* 83: 212-223.

Ghoshdastidar, P.S., G.Bhargava, and R.P. Chhabra. 2002. Computer simulation of heat transfer during drying and preheating of wet iron ore in a rotary kiln. *Drying Technology* 20(1): 19-35.

Gorog, J.P., J.K. Brimacombe, and T.N. Adams. 1981. Radiative heat transfer in rotary kilns, *Metallurgical and Materials Transaction* 12B: 55–70.

Gorog, J.P., T.N. Adams, and J.K. Brimacombe. 1982. Regenerative heat transfer in rotary kilns, *Metallurgical and Materials Transaction* 13B: 153–163.

Guldogan, Y., T. Durusoy, and T.O. Bozdemir. 1999. Pyrolysis kinetics of blends of Tuncbilek lignite with Denizili peat. *Themochimica Acta* 332: 75-81.

Gupta, S.D., D.V. Khakhar, and S.K. Bhatia. 1991. Axial transport of granular solid in horizontal rotating cylinders. Part 1: Theory. *Powder Technology* 67: 145–151.

Gyenis, J., Zs. Ulbert, J. Szepvolgyi, and Y. Tsuji. 1999. Discrete particle simulation of flow regimes in bulk solid mixing and conveying. *Powder Technology* 104: 248-257.

Hatzilyberis, K.S. and G.P. Androutsopoulos. 1999a. An RTD study for the flow of lignite particles through a pilot rotary dryer. Part II: Bare kiln case. *Drying Technology* 17(4): 745-757.

Hatzilyberis, K.S. and G.P. Androutsopoulos. 1999b. An RTD study for the flow of lignite particles through a pilot rotary dryer. Part II: Flighted kiln case. *Drying Technology* 17(4): 759-774.

Hatzilyberis, K.S. and G.P. Androutsopoulos. 2006. Lignite chemical conversion in an indirect heat rotary kiln gasifier. *Heat transfer Science* 10(3): 181-197.

Hehl, M., H. Kroger, H. Helmrich, and K. Schugerl. 1978. Longitudinal mixing in horizontal rotary kiln reactors. *Powder Technology* 20: 29-37.

Henein, H., J.K. Brimacombe, and A.P. Watkinson. 1983. Experimental study of transverse bed motion in rotary kilns. *Metallurgical and Materials Transaction* 14B: 191-205.

Hirosue, H. 1989. Influences of particles falling from flights on volumetric heat transfer coefficient in rotary dryers and coolers. *Powder Technology* 59; 125-128.

Hirosue, H., and A.S. Mujumdar. 1993. Effect of particle cascade from flights on heat transfer and pressure drop in rotary dryers and coolers. *Drying Technology* 11(1):195-207.

Hirosue, H., and H. Shinohara. 1976 b. Behaviour of particles and pressure drop in rotary dryers and coolers. *Memoirs Faculty of Engineering, Kyushu University* 36(2):173-187.

Hirosue, H., and H. Shinohara. 1976a. Volumetric heat transfer coefficient in rotary dryers and cooler. *Heat Transfer: Japanese Research* 5(4): 59-66

Hogg, R., K. Shoji, and L.G. Austin. 1974. Axial transport of dry powders in horizontal rotating cylinders. *Powder Technology* 9: 99-106.

Incropera, F.P., and D.P. Dewitt. 2007. *Fundamentals of heat and mass transfer*, 5th ed., New York: John Wiley & Sons.

Kamke,F.A., and J.B. Wilson. 1986. Computer simulation of a rotary dryer. Part II: Heat and mass transfer. *AIChE Journal* 32(2): 269-275.

Karra, V.K., and D.W. Fuerstenau, D.W. 1977. Material transport in a continuous rotating kiln. Effect of discharge plate geomety. *Powder Technology* 16: 23-28.

Karra, V.K., and D.W. Fuerstenau. 1978. Scale-up of the axial profile of material hold-up in horizontal rotating cylinders. *Powder Technology* 19: 265-269.

Kastanaki, E., D. Vamvuka, P. Grammelis, and E. Kakaras. 2002. Thermogravimetric studies of the behaviour of lignite-biomass blends during devolatilization. *Fuel Processing Technology* 77-78: 159-166.

Khakhar, D.V., J.J. McCarthy, T. Shinbrot, and J.M. Ottino. 1997. Transverse flow and mixing of granular materials in a rotating cylinder. *Physic Fluids* 9: 3600-3614.

Klose, W., and W. Wiest. 1999. Experiments and mathematical modeling of maize pyrolysis in a rotary kiln. *Fuel* 78: 65-72.

Kohav, T., J.T. Richardson, and D. Luss. 1995. Axial dispersion of solid particles in a continuous rotary kiln. *AIChE Journal* 41(11): 2465–2475.

Kramers, H., and P. Croockewit. 1952. The passage of granular solid through inclined rotary kilns. *Chemical Engineering Science* 1: 259-265.

Kroger, H., M. Hehl, H. Helmrich, and K. Schugerl. 1979. Decomposition of powders in horizontal rotary kiln reactors. *Powder Technology* 22: 1-10.

Lappas, A.A., and I.A. Vasalos. 1989. Evaluation and kinetic modelling of Greek lignites. *Fuel* 68: 1243-1247.

Lappas, A.A., D. Papavasiliou, K. Batos, and I.A. Vasalos. 1990. Product distribution and kinetic predictions of Greek lignite pyrolysis. *Fuel* 69: 1304-1308.

Laurent, B.F.C. 2006. Scaling factors in granular flow – analysis of experimental and simulation results. *Chemical Engineering Science* 61: 4138-4146.

Lebas, E., F. Hanrot, D. Ablitzer, and J.L. Houzelot. 1995. Experimental study of residence time, particle movement and bed depth profile in rotary kilns. *Canadian Journal of Chemical Engineering*, 73: 173-180.

Lehmberg, J., M. Hehl, and K. Schugerl. 1977. Transverse mixing and heat transfer in horizontal rotary kiln reactors, *Powder Technology* 18: 149-163.

Levenspiel, O. 1999. *Chemical reaction engineering*, 3rd ed., New York: Wiley.

Li, S.-Q, J.-H. Yan, R.-D. Li, Y. Chi, and K.-F. Cen. 2002a. Axial transport and residence time of MSW in rotary kilns. Part I: Experimental. *Powder Technology* 126: 217-227.

Li, S.-Q., L.-B Ma, W. Wan, and Q. Yao. 2005. A mathematical model of heat transfer in a rotary kiln thermo-reactor. *Chemical Engineering Technology* 28(12): 1480-1489.

Li, S.-Q., Y. Chi, R.-D. Li, J.-H. Yan, and K.-F. Cen. 2002b. Axial transport and residence time of MSW in rotary kilns. Part II: Theoretical and optimal analyses. *Powder Technology* 126: 228-240.

Lybaert, P. 1987. Wall-particles heat transfer in rotating heat exchangers. *International Journal of Heat and Mass Transfer* 30(8): 1663-1672.

Marias, F. 2003. A model of a rotary kiln incinerator including processes occurring within the solid and the gaseous phases. *Computer and Chemical Engineering* 27:813-825.

Marias, F., H. Roustan, and A. Pichat. 2005. Modelling of a rotary kiln for the pyrolysis of aluminium waste. *Chemical Engineering Science* 60: 4609-4622.

Martin, M.A., S.O. Leandro, S.F. Adriana. 2001. Modeling and simulation of petroleum coke calcination in rotary kilns. *Fuel* 80: 1611-1622.

Matchett, A.J., and C.G.J. Baker. 1987. Particle residence times in cascading rotary dryers. Part I: Derivation of the two-stream model. *Journal of Separation and Process Technology* 8: 11-17.

Matchett, A.J., and C.G.J. Baker. 1988. Particle residence times in cascading rotary dryers. Part II: Application of the two-stream model to experimental and industrial data. *Journal of Separation and Process Technology* 9: 5-13.

Matchett, A.J., and M.S. Sheikh. 1990. An improved model of particle motion in cascading rotary dryers. *Transactions of the Institution of Chemical Engineers* 68A: 139-148.

Mellmann, J. 2001. The transverse motion of solid in rotating cylinders forms of motion and transition behavior. *Powder Technology* 118: 251-270.

Metcalfe, G., J.M. Ottino, J.J. McCarthy, and T. Shinbrot. 1995. Avalanche mixing of granular solid. *Nature* 374: 39-41

Mindlin, R.D. 1949. Compliance of elastic bodies in contact. *Journal of Applied Mechanics* 16: 259-268.

Mitchell, D.A., A. Tongta, D.M. Stuart, and N. Krieger. 2002. The potential for establishment of axial temperature profiles during solid-state fermentation in rotating kiln bioreactors. *Biotechnology and Bioengineering* 80(1): 114-122.

Moriyama, A., and T. Suga. 1974. Axial dispersion and residence time distribution of spherical particles in rotary kilns. *Tetsu-to-Hague* 60(9): 1283-1288.

Mu, J., and D. Perlmutter. 1980. The mixing of granular solid in a rotary cylinder. *AIChE Journal* 26(6) : 928-934.

Mujumdar, K.S., K.V. Ganesh, S.B. Kulkarni, and V.V. Ranade. 2007. Rotary cement kiln simulator (RoCKS): Integrated modelling of pre-heater, calciner, kiln and clinker cooler. *Chemical Engineering Science* 62: 2590-2607.

Mujumdar, K.S. and V.V. Ranade. 2006. Simulation of rotary cement kilns using a one-dimensional model. *Trans IChemE, Part A, Chemical Engineering Research and Design* 84(A3): 165-177.

Mujumdar, K.S., A. Arora, and V.V. Ranade. 2006. Modeling of rotary cement kilns: applications to reduction in energy consumption. *Industrial and Engineering Chemistry Research* 45: 2315-2330.

Munson, B.R., D.F. Young, and T.H. Okiishi. 2006. *Fundamentals of Fluid Mechanics*. 5th ed. Brisbane: John Wiley & Sons.

Ortiz, O.A., G.I. Suarez, and A. Nelson. 2005. Dynamic simulation of a pilot rotary kiln for charcoal activation. *Computers and Chemical Engineering* 29: 1837-1848.

Palmer, G., and T. Howes. 1998. *Proceedings of the 30th IEEE Cement Industry Technical Conference, Quebec, May 24-26, 1998: Heat transfer in rotary kilns.*

Pan, J.-P., T.-J. Wang, J.-J. Yao, and Y. Jin. 2006. Granule transport and mean residence time in horizontal kiln with inclined flights. *Powder Technology* 162: 50-58.

Pandey, P., Y. Song, F. Kayihan, and R. Turton. 2006. Simulation of particle movement in a pan coating device using discrete element modelling and its comparison with video-imaging experiments. *Powder Technology* 161: 79-88.

Patisson, F., E. Lebas, F. Hanrot, D. Ablitzer, and J.-L. Houzelot. 2000. Coal pyrolysis in a rotary kiln: Part II. Overall model of the furnace. *Metallurgical and Materials Transaction* 31B: 391-402.

Perron, J. and R.T. Bui. 1990. Rotary cylinders: solid transport prediction by dimensional and rheological analysis. *The Canadian Journal of Chemical Engineering* 68: 61-68.

Ramakrishna, V. and P.S.T. Sai. 1999. Mathematical modelling of pneumatic char injection in a direct reduction rotary kiln. *Metallurgical and Materials Transaction* 30B: 969-977.

Ranz, W.E., and W.R. Marshall 1952a. Evaporation from drops. Part I. *Chemical Engineering Progress* 48(3): 141-146

Ranz, W.E., and W.R. Marshall 1952b. Evaporation from drops. Part II. *Chemical Engineering Progress* 48(3): 173-180

Riquelme, G., and R. Benavides. 1991. Analysis and simulation of a rotary dryer the effect of flight and gas mixing. In *Drying'91*, ed. A.S. Mujumdar, 228-236. Amsterdam: Elsevier Science Publishers.

Rogers, R.S.C., and R.P. Gardner. 1979. A Monte Carlo method for simulating dispersion and transport through horizontal rotating cylinders. *Powder Technology* 23: 159-167.

Russ, J.C. 2002. *The image processing handbook*, 4th ed., Boca Raton: CRC Press.

Rutgers, R. 1965. Longitudinal mixing of granular material flowing through a rotating cylinder. Part II: Experimental. *Chemical Engineering Science* 20: 1089-1100.

Sadhukan, A.K., P. Gupta, T. Goyal, and R.K. Saha. 2008. Modelling of pyrolysis of coal-biomass blends using thermogravimetric analysis. *Bioresource Technology* 99: 8022-8026.

Saeman, W.C. 1951. Passage of solid through rotary kilns. *Chemical Engineering Progress* 47(10): 508-514.

Sai, P.S.T., G.D. Surender, A.D. Damodaran, V. Suresh, Z.G. Philip, and K. Sankaran. 1990. Residence time distribution and material flow studies in a rotary kiln. *Metallurgical and Materials Transaction* 21B: 1005-1011.

Sai, P.S.T., G.D. Surender, and A.D. Damodaran. 1992. Prediction of axial velocity profiles and solid hold-up in a rotary kiln. *The Canadian Journal of Chemical Engineering* 70: 438-443.

Sammouda, H., C. Royere, A. Belghith, and M. Maalej. 1999. Heat transfer in a rotating furnace of a solar sand-boiler at a 100 kW heat transfer concentration system. *Renewable Energy* 17: 21-47.

Santomaso, A., M. Olivi, and P. Canu. 2005. Mixing kinetics of granular materials in kilns operated in rolling and cataracting regime. *Powder Technology* 152: 41-51.

Sass, S. 1967. Simulation of the heat-transfer phenomena in a rotary kiln. *Industrial & Engineering Chemistry Process Design and Development* 6: 532–535.

SEED. n.d. *Building a Hele-Shaw Cell*. http://www.seed.slb.com (accessed June 30, 2006).

Sherritt, R.G., J. Chaouki, A.K. Mehrotra, and L.A. Behie. 2003. Axial dispersion in three-dimensional mixing of particles in a rotating kiln reactor. *Chemical Engineering Science* 58: 401-405.

Sherritt, R.G., L.A. Behie, and A.K. Mehrotra. 1996. The movement of solid in flighted rotating kilns. In *Mixed-flow hydrodynamics: advances in engineering fluid mechanics*, ed. N.P. Cheremisinoff, 421-441. Texas: Gulf Pub.

Sherritt, R.G., R. Caple, L.A. Behie, and A.K. Mehrotra. 1993. The movement of solid through flighted rotating kilns. Part I: Model formulation. *The Canadian Journal of Chemical Engineering* 71 (6): 337– 346.

Sherritt, R.G., R. Caple, L.A. Behie, and A.K. Mehrotra. 1994. The movement of solid through flighted rotating kilns. Part II: Solid-gas interaction and model validation. *The Canadian Journal of Chemical Engineering* 72 (2): 240– 248.

Speight, J.P. 2005. *Handbook of Coal Analysis*, John Wiley & Sons.

Spurling, R.J. 2000. Granular flow in an inclined rotating cylinder: steady state and transients. PhD diss., University of Cambridge.

Sudah, O.S., A.W. Chester, J.A. Kowalski, J.W. Beeckman, and F.J. Muzzio. 2002, Quantitative characterization of mixing processes in rotary calciners. *Powder Technology* 126: 166-173.

Sullivan, J.D., C.G. Maier, and O.C. Ralson. 1927. U.S. Bureau of Mines Technical Paper. No. 384.

Sutcu, H. 2007. Pyrolysis by thermogravimetric analysis of blends of peat with coals of different characteristics and biomass. *Journal of the Chinese Institute of Chemical Engineers* 38: 245-249.

Suuberg, E.M., W.A. Peters, J.B. Howard. 1978. Product composition and kinetics of lignite pyrolysis. *Industrial & Engineering Chemistry Process Design and Development* 17(1): 37-46.

Sze, M.W. 1995. Reduction of ilmenite with coal in a rotary kiln. MEng thesis, Curtin University of Technology.

Tscheng, S.H., and A.P. Watkinson. 1979. Convective heat transfer in a rotary kiln, *The Canadian Journal of Chemical Engineering* 57: 433–443.

Uhl, V.W., and J.B. Gray. 1967. *Mixing: theory and practice*, New York: Academic Press.

Vahl, L., and W.G. Kingma. 1952. Transport of solid through horizontal rotary cylinders. *Chemical Engineering Science* 1: 253-258.

Vamvuka, D., E. Kakaras, E. Kastanaki, and P. Grammelis. 2003. Pyrolysis characteristics and kinetics of biomass residuals mixtures with lignite. *Fuel* 82: 1949-1960.

Van Puyvelde, D.R., B.R. Young, M.A. Wilson, and S.J. Schmidt. 1999. Experimental determination of transverse mixing kinetics in a rolling kiln by image analysis. *Powder Technology* 106: 183-191.

Venkataraman, K.S., and D.W. Fuerstenau. 1986. Effect of lifter shape and configuration on material transport. Part I: In rotating kilns. *Powder Technology* 46: 23-32.

Wachters, L.H.J., and H. Kramers. 1964. *Proceedings of the Third European Symposium in Chemical Reaction Engineering*, ed. J. Hoogschagen, New York: Pergamon Press.

Watkinson, A.P., and J.K. Brimacombe. 1978. Heat transfer in a direct-fired rotary kiln: II. Heat flow results and their interpretation. *Metallurgical and Materials Transaction* 9B: 209-219.

Watkinson, A.P., and J.K. Brimacombe. 1982. Limestone calcinations in a rotary kiln. *Metallurgical and Materials Transaction* 13B: 369-378.

Wehner, J.F., and R.H. Wilhelm. 1956. Boundary conditions of flow reactor. *Chemical Engineering Science* 6(89): 89-93.

Wes, G.W.J., A.A.H. Drinkenburg, and S. Stemerding. 1976. Heat transfer in a horizontal rotary kiln reactor. *Powder Technology* 13: 185-192.

Wes, G.W.J., A.A.H. Drinkenburg, and S. Stemerding. 1976. Solid mixing and residence time distribution in a horizontal rotary kiln reactor. *Powder Technology* 13: 177–184.

Whitaker, S. 1972. Forced convection heat transfer correlations for flow in pipes, past flat plates, single cylinders, single spheres, and for flow in packed beds and tube bundles. *AIChE Journal* 18: 361-371.

Wild, M. 1994. A theoretical and experimental study of heat transfer in rotary kilns. MEng thesis, Curtin University of Technology.

Zhang, Y., P.V. Barr, and T.R. Meadowcroft. 2008. Continuous scarp melting in a short rotary furnace. *Minerals Engineering* 21: 178-189.